UiT The Arctic University of Norway

Faculty of Health Sciences, Institute of Medical Biology, Translational Cancer Research group

Establishment of an advanced flow cytometry protocol for analyzing immune cell subsets from lung cancer patients

A methodological study establishing and validating a protocol to study the presence of functional lymphocytes subtypes in blood from non-small cell lung cancer (NSCLC) patients

Sweet Yibio Beyene

Main Supervisor: Associate Professor Sigve Andersen

Master's thesis in Biomedicine – MBI-3911 – August 2022

Table of Contents

Acknowledgement

The work presented in this thesis was conducted at the Translational Cancer Research group, University of Tromsø.

First and foremost, I would like to thank my supervisor *Associate Professor Sigve Andersen* and my co-supervisor *Professor Lill-Tove Rasmussen Busund* for giving me the opportunity to work on this project.

I would like to extend my eternal gratitude to my supervisor *Associate Professor Sigve Andersen* for sharing his wide knowledge, encouragement and detailed feedback which helped make this thesis readable. It was an outstanding experience to be allowed to make mistakes while also having you around to answer questions. Additionally, I would also like to thank *Dr. Ilona Halva Urbarova* and *Professor Inigo Zubiavrre Martinez* for their guidance and help with the process of writing and completing this thesis.

I give special thanks to *Dr. Maria Therese Ahlen, Dr. Rodrigo Berzaghi and Roy Andre Lyså*, for teaching me all I need to know about flow cytometry and always being there when I needed help.

More personally, I want to express my profound love and gratitude to my mother (*Abrhet*), father (*Yibio*), brothers (*Yonatan, Abel, Esayas and Thomas*) and friends for their love and encouragement. Last, I want to thank my partner, *Marcus*, for his unfailing support and continuous love and encouragement.

This would have not been possible without all of you, thank you!

Tromsø, August 2022
Sweet Yibio Beyene

Abstract

Lymphocytes are known for their role in tumor promotion and tumor suppression. T cell infiltration of the tumor microenvironment has been linked to a better prognosis and outcome in various malignancies. CD8+ T cells can eliminate cancer cells by causing them to lyse, while CD4+ T cells can be both tumor promoting and tumor suppressing. However, the prognostic impact of functional lymphocyte subtypes in non-small cell lung cancer (NSCLC) is not completely known. Therefore, the aim of this thesis was to establish a multiparametric flow cytometry protocol to explore the presence of functional lymphocyte subtypes in peripheral blood mononuclear cells from healthy donors and validate it for use in blood and tissue samples from NSCLC patients. Furthermore, the effects of cryopreservation on sample quality and lymphocyte subtype distribution were also explored.

Our study showed that the presence of selected lymphocyte subtypes can be explored in blood from NSCLC patients. However, it also showed that cryopreservation had an effect on the distribution of some lymphocyte subtypes. The blood samples that were analyzed using the CD8+ T cell subtypes panel showed a quantitative decrease of cells after cryopreservation. Similar observations were made for blood samples analyzed using the expanded lymphocyte panel. Statistical analysis showed that these differences may be attributable to the effects of cryopreservation. However, due to small sample sizes we were unable to determine whether the differences were statistically significance.

Having established this protocol, our future aim is to analyze more NSCLC patient samples, both from blood and tissue.

Keywords: CD8+ T cells, CD4+ T cells, flow cytometry, prognosis, Tregs, B cells, NK cells

Abbreviations

SCLC – small cell lung cancer

NSCLC – non-small cell lung cancer

EGFR – epidermal growth factor receptor

KRAS – Kristen rat sarcoma virus

ALK – anaplastic lymphoma kinas

CT – computed tomography

TNM staging – primary tumor (T), invasion of nearby lymph nodes (N) and metastasis

IASLC – International Association for the Study of Lung Cancer

TME – Tumor microenvironment

NK cells – natural killer cells

TAMs – tumor associated macrophages

CAFs – cancer-associated fibroblasts

TILs – tumor-infiltrating lymphocytes

DC – dendritic cells

CD – cluster of differentiation

B cells – B lymphocytes

T cells – T lymphocytes

TCR – T cell receptors

T_N – naïve T cells

T_{SCM} – stem-cell like memory T cells

T_{CM} – central memory T cells

T_{EM} – effector memory T cells

T_{EMRA} – terminally differentiated effector memory T cells re-expressing CD45RA

T_{RM} – tissue resident memory T cells

Th1 – T helper 1

Th2 – T helper 2

Th17 – T helper 17

T_{regs} – regulatory T cells

Tfh – T follicular helper cells (Tfh)

T_{dys} – dysfunctional T cells

T_{DT} – terminally differentiated dysfunctional T cells

T_{bys} – bystander T cells

FACS – fluorescence activated cell sorting

FSC – forward scatter

SSC – side scatter

PMT – photomultiplier tube

PBMCs – Peripheral blood mononuclear cells

LUAD – Lung adenocarcinoma

DPBS – Dulbecco Phosphate Buffered Saline

RT – room temperature

DMSO – dimethyl sulfoxide

FBS – fetal bovine serum

CS&T – cytometer setup and tracking

1 Introduction

1.1 Cancer

The proliferation and differentiation of healthy cells is tightly regulated by strict control mechanisms. However, when rapid and uncontrolled cellular proliferation occurs, a disease called cancer can be developed. Cancer is characterized by unrestricted growth, sustained angiogenesis and evasion of apoptosis [1]. Cancer develops and progresses due to abnormalities and modifications in cellular DNA. This leads to the activation of oncogenes and/or loss of tumor suppressor genes.

The transformation of healthy cells into cancer cells is termed carcinogenesis. Carcinogenesis is a multistep process involving genetic mutations, deregulated growth, and eventually metastatic dissemination [1], [2]. Carcinogenesis consists of three main stages; initiation, promotion, and progression. During the initiation stage, genetic alterations occur in genes of the regulatory pathways that control cellular proliferation, survival, and differentiation. During the second stage, promotion, mutated cells avoid destruction by the immune system while expanding in number and resisting apoptosis. The final stage of carcinogenesis is progression. During this stage, cancer cells gain multiple types of chromosomal alterations, promoting the development of malignant characteristics, such as increased capacity for invasion and metastatic growth [1], [3].

1.2 Lung cancer

Cancer is a leading cause of mortality worldwide, with lung cancer accounting for ~18% of all cancer deaths in 2020 [4]. In Norway, lung cancer accounts for the majority of cancer-related mortalities [5]. However, recent data shows a decrease in incidence and an improved 5-year survival rate for men [6].

Lung cancer is divided into two main groups: (I) small cell lung cancer (SCLC) and (II) non-small cell lung cancer (NSCLC). SCLC accounts for about 15% of lung cancer cases, while NSCLC accounts for the remaining 85% [7]. SCLC is a form of lung cancer and is characterized by its aggressive growth. The biggest group of people affected by lung cancer are heavy smokers, linking tobacco use as a major risk factor [8], [9]. Contrary to NSCLC, SCLC is almost always developed by the inactivation of the tumor suppressors p53 and RB [8].

1.2.1 Non-small cell lung cancer

NSCLC is characterized by somatic mutations in genes that drive tumor progression, including *epidermal growth factor receptor (EGFR), Kristen rat sarcoma virus (KRAS), anaplastic lymphoma kinase (ALK)* [10], [11]. NSCLC can be divided into three main histological subtypes: (I) squamous cell carcinoma, (II) adenocarcinoma and (III) large cell carcinoma, with the most common type being adenocarcinoma [10], [12]. Squamous cell carcinoma and adenocarcinoma are often treated similarly. However, due to the gene mutations that are oncogenic drivers in adenocarcinoma, determining the lung cancer subtype using histological and genetic analysis are crucial for selecting appropriate treatment strategy [13], [14].

1.2.1.1 Diagnosis and prognosis

Detection and surgical resection at early stages of the disease give the best long-term survival for NSCLC patients, although many still experience recurrence [15]. Unfortunately, lung cancer is often diagnosed at advanced stages, where treatment options are limited. In order to detect lung cancer early, it is therefore important to conduct targeted screenings of high-risk groups. The screening can be conducted by administering low-dose computed tomography (LDCT) or regular chest x-ray [13]. A recent randomized control trial (NELSON-study [16]) screened more than 15,000 high-risk individuals between the ages 50-74 resulting in a significant reduction in lung cancer mortality. These positive results have since led to the introduction of routine screenings of high-risk individuals in several countries. Additionally, a project that will introduce early screening programs in Norway has received funding in an attempt to improve early detection [17]. Lung cancer symptoms typically present themselves once the disease has reached advanced stages and can often be mistaken for other symptoms and recurring infections associated with a history of smoking. This causes a delay in the lung cancer diagnosis and treatment which increases the mortality rate [13].

The ministry of health's national plan of action for patients suspected of having lung cancer is to ensure early diagnosis and careful classification to provide an appropriate treatment [13]. Patients are examined to determine the presence of metastasis, since this can impact diagnosis and prognosis. Following a positive LDCT or chest x-ray, a biopsy is collected for histological and cytological examination to determine the lung cancer stage. All lung cancer patients who after initial diagnostic assessment are potential candidates for intended curative treatment are examined by PET-CT to exclude inoperable metastasis. The lung cancer is then classified according to the size of the primary tumor (T), the invasion of nearby lymph nodes (N) and

metastasis (M) - (TNM) staging. The 5-year survival rate for lung cancer patients decreases with increasing stage. According to the revised TNM stage grouping by the International Association for the Study of Lung Cancer (IASLC), the overall survival for patients in clinical stage I (IA1) is 92%, since this stage indicates containment of the cancer within the lungs. Meanwhile, the overall survival for patients in clinical stage IV (IVB) is 0% due to cancerous spread outside of the chest [18].

1.2.2 Tumor microenvironment

The tumor microenvironment (TME) includes cellular and non-cellular components giving support to tumor cells. These components are necessary for tumor progression, but the composition of the TME may vary from one type of cancer to another and between patients with the same tumor type. The predominant cellular components recruited to the TME are immune cells such as lymphocytes, tumor associated macrophages (TAMs), cancer-associated fibroblasts (CAFs) and endothelial cells in the form of blood vessels. There is also an abundant level of secreted products from the cellular components, such as growth factors, chemokines, cytokines, and extracellular matrix proteins [2], [19].

During the early stages of tumorigenesis, the TME plays a significant role in suppressing the development of malignant clones. However, at a certain timepoint, many cancer cells start developing resistance and reprogram the cells of the TME to promote their malignant progression and survival [2], [19]. Figure 1 shows some of the cell populations that make up the TME in solid tumors [20].

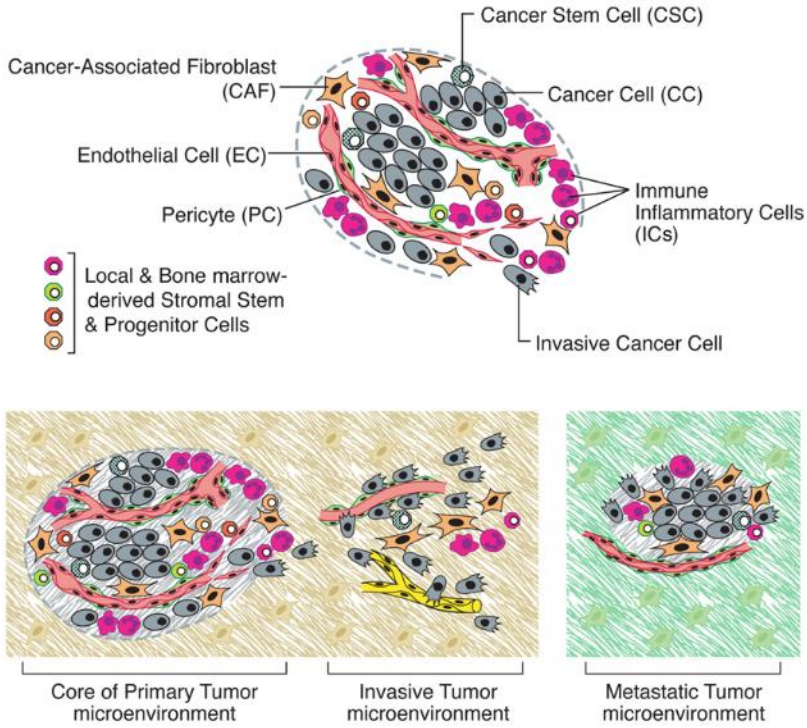

Figure 1. Cells of the tumor microenvironment (TME). *The top part of this figure shows some the distinct cell types that make up most solid tumors. These distinct cell types promote tumor growth and progression. The immune inflammatory cells include both tumor-promoting and tumor-killing subtypes. The lower part illustrates how the TME changes as tumors start to invade normal tissue and metastasize. Figure acquired from [19]. Permission obtained through CCC Marketplace™.*

The TME of NSCLC, similarly to other cancers, consists of a heterogeneous mixture of cells supported by an aberrant vascular network. As such, the oxygen tension and nutritional levels within the TME often varies between different regions [19]. Other important components of the NSCLC TME include the adaptive and innate immune systems, where studies have shown that the density of tumor-infiltrating lymphocytes (TILs), such as CD8+ T cells and CD4+ T cells have a prognostic impact [21], [22].

1.3 Immune system

The immune system's main task is maintaining homeostasis by protecting the body against foreign pathogens, facilitating tissue repair and providing tumor immune surveillance. However, the immune system has also been implicated in disease and cancer promotion [23].

1.3.1 Roles of innate and adaptive immunity

The immune system is comprised of two main components: (I) the innate and (II) the adaptive immune systems. The innate immune system is the body's first line of defense and serves three

main functions: acting as a barrier to pathogens in the form of mucous membranes and the skin, activating the adaptive immune system, and recruiting immune cells to sites of infection. The cells involved in the innate immune system are dendritic cells (DC), NK cells, NK T cells, macrophages, mast cells, neutrophils, basophils, and eosinophils. The innate immune system is always present, and therefore also referred to as the native immune system [23]–[25].

Contrary to the innate immune system, the adaptive immune system is acquired as a response to foreign pathogens and infections by providing a more specialized protection against them. The adaptive immune system can respond pathogens and fights infections that may have developed resistance to the innate immune responses. Cells involved in the adaptive immune response are mainly B lymphocytes (B cells), T lymphocytes (T cells) and antigen-presenting cells (APCs). The adaptive immune system requires a longer time to respond compared to the innate immune system, since lymphocytes must be primed and differentiated into effector cells in order to fight the infection. Furthermore, after the body is first exposed to a foreign antigen, some lymphocytes will differentiate into memory cells, which can respond faster to a second exposure to the same antigen [23]–[25].

1.3.2 Role of the immune system in cancer

One of the principal roles of the immune system is to hinder tumor progression and facilitate tumoral destruction in a process called tumor immune surveillance. However, despite this critical role of the immune system, people still develop cancer. In fact, the ability of cancer cells to avoid destruction by the immune system is one of the hallmarks of cancer [2]. The process by which tumor cells avoid destruction by the immune system is called cancer immunoediting and consists of three stages: (I) elimination, (II) equilibrium and (III) escape [26]. During the elimination phase the immune system attempts to eliminate tumor cells that have escaped tumor suppressors. The tumor cells that manage to escape the elimination stage continue to the equilibrium stage. In this stage, tumor cell growth is limited, since the immune system holds the tumor in a state of functional dormancy. However, the tumor cells are edited in this stage and eventually continue to the escape stage where they proliferate unrestricted [26]. The role of immune surveillance in cancer prevention is further emphasized by the fact that immunocompromised patients experience an increase of virus induced cancers. This clearly illustrates that the immune system can limit the formation of some tumors [2].

1.3.3 Lymphocytes

Lymphocytes are the intermediaries of the adaptive immune system. Approximately one trillion lymphocytes can be found in a healthy human adult, and although they are similar in shape, they can be classified based on their function and their expression of surface proteins called cluster of differentiation (CD). Surface proteins can be used to distinguish between different categories of lymphocytes and their subtypes. Additionally, surface proteins are also used to determine lymphocyte differentiation stage. Lymphocytes develop in the bone marrow, but are frequently categorized based on where they mature, with B cells maturing in the bone marrow and T cells maturing in the thymus. T cells can be further categorized into three main subtypes: CD4+ T cells, CD8+ T cells, and regulatory T cells (T_{regs}) [23] (Figure 2).

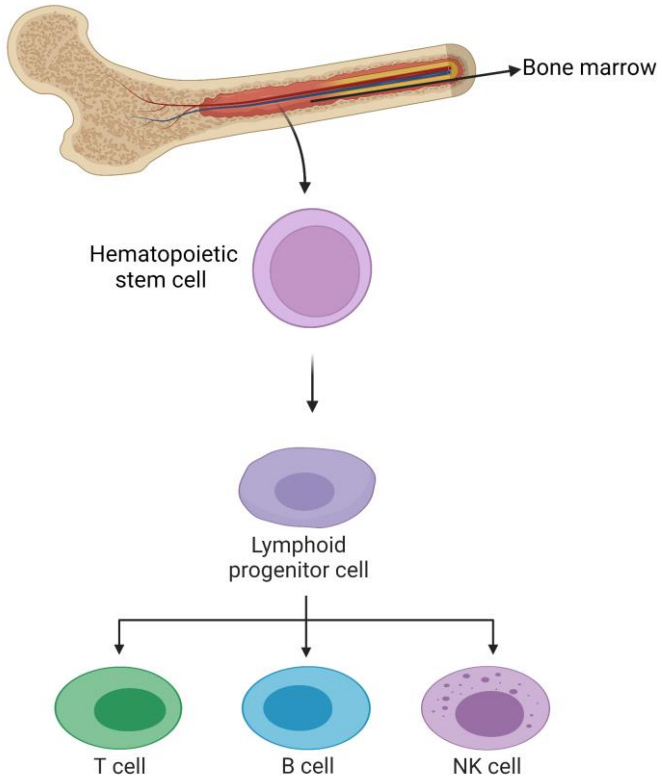

Figure 2. Lymphocyte lineage. *This figure shows some of the immune cells derived from hematopoietic cells (HSCs). HSCs differentiate into lymphoid and myeloid (not shown) progenitors that further branch out to more specific cells associated with adaptive and innate immunity. This figure was created with BioRender.com*

B cells arise from pluripotent stem cells, which go through several stages before developing into immature B cells in the bone marrow. Once mature, B cells exit the bone and migrate to secondary lymphoid organs. B cells express B cell receptors (BCRs), through which they can bind foreign antigens, and start proliferating and differentiating into antibody-secreting effector

cells [23]. Meanwhile, progenitors of T cells migrate to the thymus from the bone marrow for maturation. In the thymus, these immature T cells start expressing T cell receptors (TCRs) and the surface markers CD4 or CD8 and can be released from the thymus as mature CD4+ T cells and CD8+ T cells, respectively. Prior to their encounter with an antigen, these T cells are collectively referred to as naïve T cells. However, once introduced to a foreign antigen, these cells proliferate and differentiate into effector cells to mount an immune response. CD8+ effector T cells are capable of directly eliminating foreign antigens, while CD4+ effector T cells do so indirectly by producing cytokines that activate B cells and other cells that are part of the innate immune system. Naïve T cells can also differentiate into memory cells after differentiating into effector cells upon recognizing antigens. Memory cells are inactive, but upon re-exposure to the same antigen can trigger a more rapid immune response [23].

1.3.3.1 Role of T lymphocytes in cancer progression

CD8+ T cells are known for their ability to recognize and eliminate cancer cells [27]. CD8+ T cells can directly kill cancer cells by recognizing peptides present on their surface through TCRs. CD8+ T cells cause cancer cells to lyse by secreting cytotoxic enzymes and cytokines [28], [29].

The role of CD4+ T cells in tumors can be both tumor promoting and tumor suppressing. For instance, CD4+ T cells can promote tumor growth indirectly by deregulating the action of CD8+ T cells. Conversely, CD4+ cells can also activate CD8+ T cells to facilitate elimination of cancer cells [30]. Based on their cytokine secretion and functionality, CD4+ T cells can be classified into T helper 1 (Th1), T helper 2 (Th2), T helper 17 (Th17), Tregs and T follicular helper cells (Tfh) [30].

As mentioned earlier, T cell infiltration of the TME has been linked to better prognosis and outcome in various malignancies, including melanomas, colorectal cancers, and ovarian cancers [31], [32]. Studies have also shown that the levels of TILs can be used as markers to predict outcome [32], [33]. Furthermore, the outcome can also depend on the types of TILs. Quite consistently, infiltration of CD8+ T cells is associated with good prognosis in most cancers [34], with the exception of renal cell carcinomas [35]. Contrary to this, the role of CD4+ T cells in prognosis seems to be less clear and will vary depending on the type of cancer, the composition of TME, and the cancer stage [33]. This is probably due to the broad range of functional subtypes of CD4+ T cells, which include Th1, Th2, Th17, Tregs and Tfh. Broadly, Th1 is associated with a good prognosis, Th2 is associated with a poor prognosis, while the

levels of Tregs present in the TME can have a mixed impact on prognosis of NSCLC patients [36]. Tregs are immune suppressors and their enrichment is linked to worse outcome [27] [33]. In NSCLC, CD8+ T cells are associated with a good prognosis. However, there are conflicting reports regarding the effect of CD4+ T cells on prognosis of patients with NSCLC [36].

NK cells have a role in targeting cancer cells that downregulate their surface antigens to avoid detection by CD8+ T cells. NKT cells, while being similar to NK cells, use TCRs to recognize peptide fragments presented on the surface of cancer cells [27]. B cells also have a significant role in cancer immunology, where they prevent tumor development by producing tumor-specific antibodies and promote the elimination of tumor cells by NK cells [27].

1.3.3.2 Functional subtypes of lymphocytes in lung cancer

As mentioned in section 1.3.3.1, the role of lymphocytes in cancer can vary based on the immune cell subtype. Therefore, it is difficult to predetermine which lymphocyte subtypes are the most relevant and impactful for NSCLC, as the prognostic value has only been explored for some subtypes. The functional lymphocyte subtypes in this thesis had been predetermined by the research group based on the main lineage identification, and research publications available prior to 2021. To explore some of the immune cells that could potentially have a prognostic value, two panels were set up. The first panel (CD8+ subtype panel) encompasses CD8+ T cells and its subtypes according to their status of differentiation (lineage) and function (Figure 3). The immune cells in this panel included naïve T cells (T_N), stem-cell like memory T cells (T_{SCM}), central memory T cells (T_{CM}), effector memory T cells (T_{EM}), terminally differentiated effector memory T cells re-expressing CD45RA (T_{EMRA}), tissue resident memory T cells (T_{RM}), dysfunctional T cells (T_{dys}), terminally differentiated dysfunctional T cells (T_{DT}) and bystander T cells (T_{bys}) [37]–[39]. T_{dys} are recognized for their proliferation defects and lack of inflammatory cytokine production [31]. These features are characterized by an increase in the expression of an inhibitory receptor PD1. Dysfunctional CD8+ T cells can also be divided into terminally differentiated dysfunctional CD8+ T cells (T_{DT}) [31]. T_{bys} refers to cells that do not express CD39; an ATPase that mediates immunosuppression [40], [41]. CD8+ T cells that are tumor-specific highly express CD39, which means that T_{bys} cells are not stimulated by cancer antigens [42].

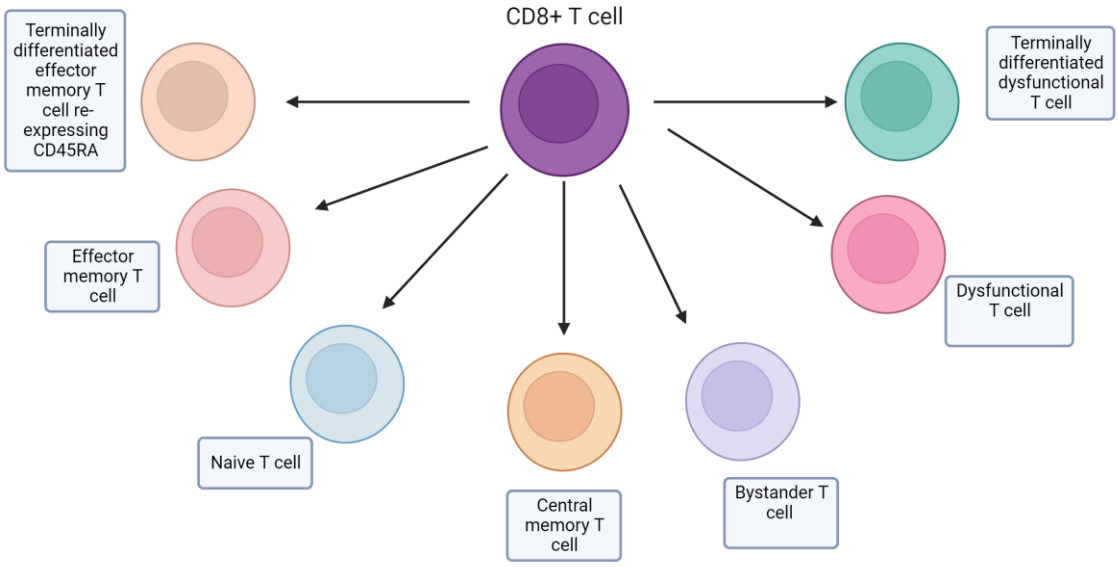

Figure 3. CD8+ T cells and subtypes. *CD8+T cells can differentiate into naïve T cells (T_N), central memory T cells (T_{CM}), effector memory T cells (T_{EM}), terminally differentiated effector memory T cells re-expressing CD45RA (T_{EMRA}), dysfunctional T cells (T_{dys}), terminally differentiated dysfunctional T cells (T_{DT}) and bystander T cells (T_{bys}). These are some of the CD8+ T cells explored in this thesis. This figure was created with BioRender.com*

The second panel (expanded lymphocyte panel) was primarily designed to get a more complete picture of lymphocyte distribution in peripheral blood. This panel included CD4+ T cells and the phenotypes T_N, memory T cells and T_{regs}, B cells (B_N) and memory B cells (B_M), NK cells and NK T cells [38], [43].

The immune cells included in the first- and second panel have a role in cancer immunology and represent some of the cells of the immunological environment in NSCLC. The surface markers that help to distinguish these subtypes and their state of differentiation are listed in section 1.3.3.3.

1.3.3.3 Lymphocyte subtype markers

All immune cells present CD surface proteins that help in their identification. For instance, all T cells express CD3, while it is absent on B cells and myeloid cells. Based on whether they are CD4+ T cells or CD8+ T cells, they express in addition to CD3 either CD4 or CD8, respectively. All CD8+ T cells express CD3 and CD8 and based on cell subtype they can express more surface markers. The surface markers used to explore the distribution of CD8+ lymphocyte subsets are listed in Table 1.

Table 1. Surface markers used in the first panel (CD8+ subtype panel). *All T lymphocyte cells express the surface marker CD3 on their surface. In addition to CD3, they can express several other surface markers that can be used to determine the type and differentiation status. The populations of interest for the CD8+ subtype panel are shown along with the surface markers they express. The surface markers are assigned either + or - depending on their presence or absence on the surface of the subtype, respectively.*

Marker	T_N	T_{SCM}	T_{EM}	T_{CM}	T_{EMRA}	T_{RM}	T_{bys}	T_{dys}	T_{DT}
CD3	+	+	+	+	+	+	+	+	+
CD8	+	+	+	+	+	+	+	+	+
CD45RA	+	+	-	-	+	+/-*			
CCR7	+	+	-	+	-	+			
CD57			+/-*		+/-*			-	+
CD279 (PD-1)		+/-*					+/-*	+++**	+++**
CD39							-		
CD103						+			
CD95	-	+							

T_N = naïve T cells, T_{SCM} = stem cell like memory T cell, T_{CM} = central memory T cell, T_{EM} = effector memory, T_{EMRA} = terminally differentiated effector memory cells re-expressing CD45RA, T_{RM} = tissue resident memory T cell, T_{bys} = Bystander T cells, T_{dys} = Dysfunctional T cells, T_{DT} = Terminally differentiated dysfunctional T cell.
*Can be expressed/absent from population
**Highly expressed

In addition to the CD8+ lymphocytes, we also wanted to explore the distribution of other immune cells mentioned in section 1.3.3.2. CD4+ T cells and their subtypes can be characterized using the markers CD4 and CD45RA. CD4+ naïve and memory T cells can be identified using CD45RA as naïve cells are CD4+CD45RA+ and memory cells are CD4+CD45RA-. The memory cells can further be divided into the subtypes resting and activated using the activation markers CD25 and CD69. The subtype Tregs can also be distinguished from the other subtypes using the markers CD25 and CD127 as Tregs are CD4+CD25+CD127lo/-. NK cells and NKT cells can be determined using the markers CD3 and CD56. NK cells are not T cells and therefore do not express CD3. They are CD3-CD56+, while NKT cells are CD3+CD56+. Similarly as for, the CD4 memory T cells, the activation marker CD69 can be used to divide NK cells into activated (CD3-CD56+CD69+) and resting (CD3-CD56+CD69-). Finally, the B cells can be distinguished using the markers CD19 and CD27 as B naïve cells are CD19+CD27- and B memory cells are CD19+CD27+ [27], [44]. An overview of the surface markers used to explore the populations in the expanded lymphocyte panel is presented in Table 2.

Table 2. Surface markers used in the second panel (expanded lymphocyte panel). *Lymphocyte subtypes can be distinguished from each other based on their surface markers. CD4+ T cell subtypess are all positive for the markers CD3 and CD4, CD4+ memory T cells are in addition negative for CD45RA. However, resting memory (M.res) and activated memory (M.act) CD4+ T cells can be distinguished from one another based on their expression of CD25. CD4+ activated memory T cells are positive for CD25. Regulatory T cells (Tregs) are positive for both CD3 and CD4 as well as CD25 while negative or have low expression of CD127. B lymphocytes are positive for the surface marker CD19. Naïve B cells are negative for CD27, but memory B cells are positive for CD27. Both natural killer (NK) cells and NK T cells express the surface marker CD56. NK cells do not express the T cell marker CD3, and are therefore negative for it. Activated NK cells are also positive for CD69, while resting NK cells are negative for CD69.*

	CD4+ T cells				B cells				
Marker	**T_N**	**M.res**	**M.act**	**T_{regs}**	**B_N**	**B_M**	**NK rest**	**NK act**	**NKT**
CD3	+	+	+	+			-	-	+
CD19					+	+			
CD127				Lo/-					
CD25			+	+					
CD56							+	+	+
CD45RA	+	-	-						
CD27					-	+			
CD4	+	+	+	+					
CD69		-	+					+	

T_N = naïve T cells, **M.res** = resting memory T cells, **M.act** = activated memory T cells, **T_{regs}** = regulatory T cells, **B_N** = naïve B cells, **B_M** = memory B cells, **NK rest** = resting natural killer cells, **NK act** = activated natural killer cells, **NK T** = **n**atural killer T cells. *Lo/- can be very low expressed and absent from the population

In order to explore the presence of these subtypes, fluorophore conjugated antibodies/ fluorescent-labelled antibodies that bind specifically to these surface markers can be used. The appropriate fluorophores for each surface marker were selected in collaboration with Miltenyi Biotec (Germany), and are listed in the method section. A technique called flow cytometric immunophenotyping can then be used to identify and distinguish between these lymphocyte subtypes.

1.4 Flow cytometry

Flow cytometry is a laser-based method used to identify single cells or particles within a heterogenous cell population suspended in fluid. The first flow cytometer developed was only capable of distinguishing cells based on their size. Today, however, flow cytometers are capable

of distinguishing cells based on multiple parameters, allowing researchers to explore and characterize individual cells based their size, granularity, and protein markers [45]. Using flow cytometry one can detect cell antigens, cellular components and the differentiation status of individual cells by using fluorescently-labelled monoclonal antibodies or dyes [45]. Flow cytometers can also be used to study intracellular proteins; however cells need to be fixated and permeabilized prior to staining with intracellular markers. As the experiments in this thesis only include the use of surface markers, this topic will not be further elaborated.

Flow cytometry-based immunophenotyping has become an instrumental tool in disease diagnosis and classification. Immunophenotyping is the analysis of a heterogenous cell population using markers (e.g., antibodies) to identify and quantify the population of interest [45]. Flow cytometers are categorized into two types: (I) cell sorting, also called fluorescence activated cell sorters (FACS, e.g. FACSAria^{TM}), and (II) the non-sorting (e.g. LSRFortessa^{TM}). Both types operate on the same basic principle, which is passing a sample one cell at a time through a laser beam and capturing the light scattered from the cells/particles struck by the light. However, as the name suggests, the FACS flow cytometer can also identify labelled cells and separate them from a heterogenous cell population (cell sorting) [45].

All flow cytometers consist of four different parts: (1) a fluidic system, (2) an optical system, (3) an electronic network, and (4) a computer (Figure 4). When conducting a flow cytometry-based immunophenotyping, a single-cell heterogenous suspension with the markers/dyes of interest is prepared. The sample is then loaded into the machine and with the help of the fluidics system, sheath fluid (diluent phosphate buffer saline (PBS)) in addition to pressurized lines direct the cells to the focused light from the laser beams. The optical system centers the light source on the cells, which then scatter light that is detected by the emission detectors (filters and mirrors). The filters and mirrors direct the light signal to the electronic network, which converts the light signal into a digital/electronic signal that is proportional to the intensity of the light signal. The electronic signal is then registered by a computer, which allows us to analyze the data in form of dot plots as shown in Figure 4, or even histograms and contour plots [45], [46].

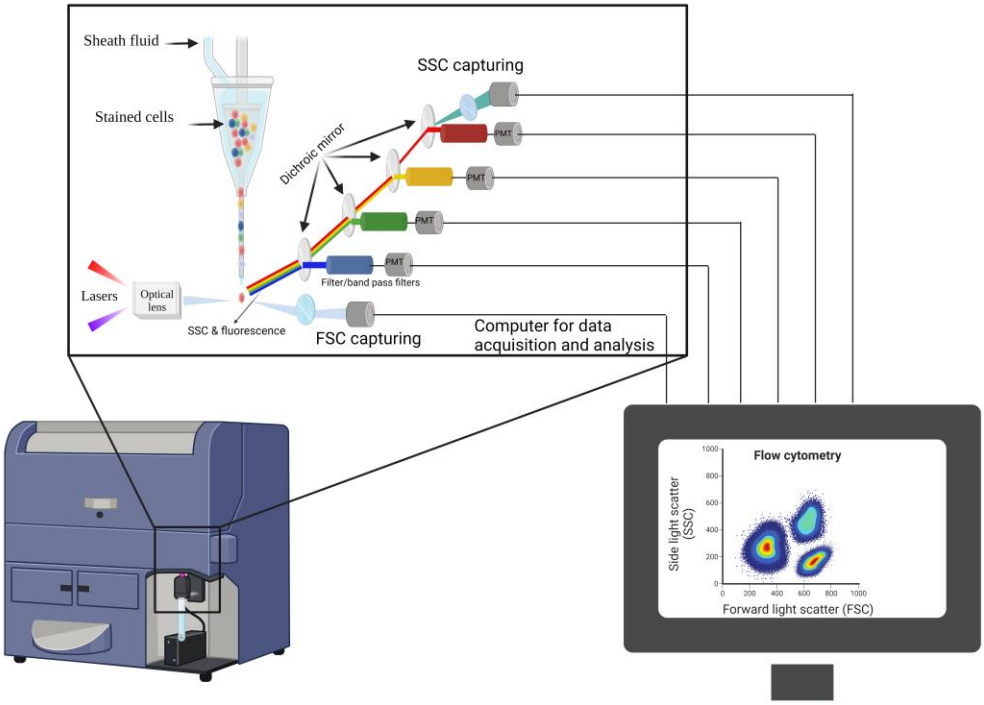

Figure 4. Flow cytometer overview. *A simple overview of how a cell suspension is aligned in order to pass the laser beam one cell at a time by the sheath fluid. Light from the laser beam goes through optical lens and hits the cell causing it to emit fluorescence and scatter light. This signal is then filtered by the Dichroic mirror and captured by the photomultiplier tube (PMT). The signals captured are then converted into electrons that create an electrical current. The electrical current signal is then converted into digital signal data, which is displayed as plots or histograms on the computer. This figure was created with BioRender.com*

The light scattered by cells is measured by two optical detectors: (I) forward scatter (FSC), which is proportional to cell size, and (II) side scatter (SSC), which is reflective of cell granularity or complexity (Figure 5). In addition to light scattering, cells also emit fluorescence, which can be cellular autofluorescence or fluorescence from the markers/dyes added to them. All cells have autofluorescence that they emit when they are hit with light.

When setting up an immunophenotyping experiment with multiple parameters, such as multiple antibody-conjugated fluorescent labels, there are several factors that must be considered, including spectral overlap, dye spillover and compensation [27], [45], [47]. Based on which cell or differentiation state one wishes to examine, fluorochrome-conjugated antibodies specific to the antigens/surface markers present on the cell of interest can be obtained commercially. As cells can express several antigens, it is possible to use multiple antibodies conjugated to different fluorochromes that are specific to them in order to identify the cell type or differentiation/activation status.

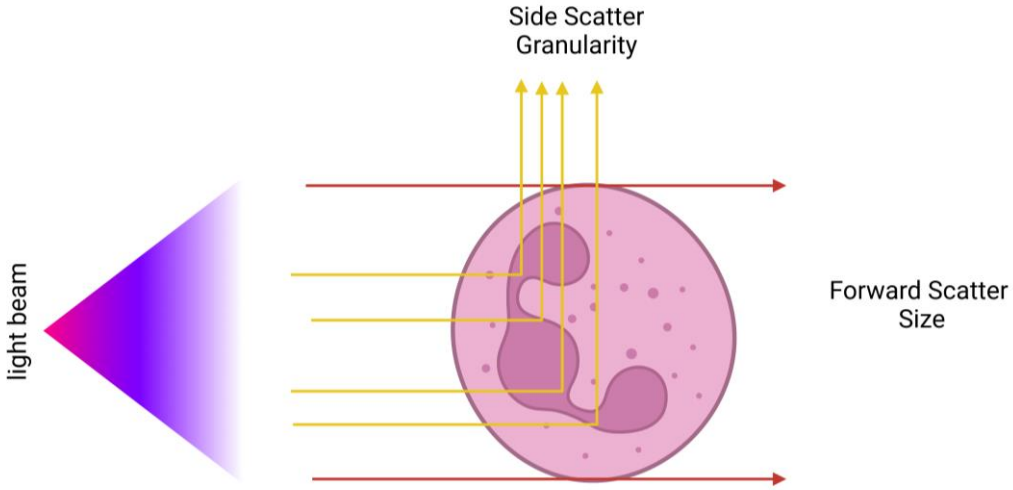

Figure 5. Light scatter. *An illustration of how light scatters after striking a particle/cell. When the light scatter strikes the cell, forward light scatter reflects the size of the cell while the light that hits the granularities in the cell get scattered at a 90 degree angle reflecting the cells complexity. This figure was created with BioRender.com*

After a sample with labelled cells is loaded onto the flow cytometer, the detectors register the fluorescence emitted in addition to the light scattering. These signals can then later be analyzed and the cell type determined based on the size, complexity and antigen/surface markers. When running experiments with multiple parameters, the flow cytometer sensitivity can be adjusted by changing the photomultiplier tube (PMT) voltage. Specifically, increasing or decreasing the PMT value may ensure better separation between autofluorescence (negative signal) and fluorescence emitted from the fluorochromes (positive signal) [47]. Flow cytometers are equipped with several detectors, lasers and filters that can distinguish between the various fluorescent signals. However, some fluorochromes have a wide emission spectrum and can spill over into another detector or overlap with other fluorochromes resulting in false positive signals (Figure 6). This issue can be minimized by setting up compensation. Compensation is a process by which the overlapping part of a fluorophore´s signal is subtracted from the signal of another. Compensation is set up by preparing a sample containing either cells or particles. The particles/cells that emit the same autofluorescence as the sample being analyzed, can also bind the same fluorophore-conjugated marker. A single stained sample is prepared for every fluorophore used in the experiment. It is important that a highly expressed antigen/surface marker is not matched with an extremely bright fluorophore as this can cause overlap between the fluorophores [27].

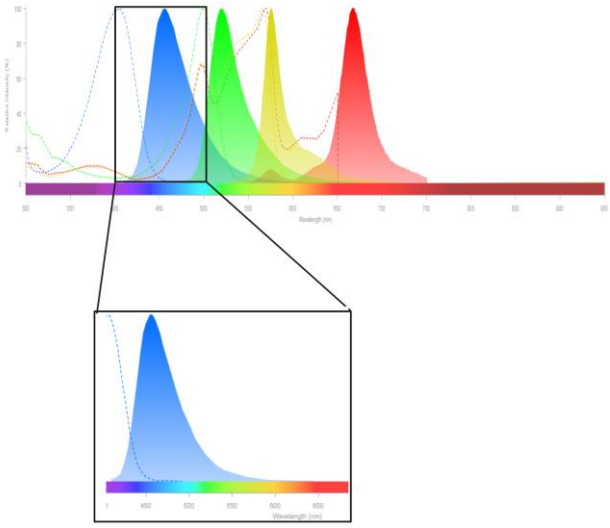

Figure 6. Fluorophore spectral viewer. *This is a view of the emission from some fluorophores used in combination. The zoomed image of the blue fluorophore shows how its emission spectrum has spilled over into the green fluorophore. This figure is created with Biorender.com and Thermofisher Fluorescence SpectraViewer*

2 Aim of the study

This study is a part of a larger study where we pose the following research questions: (I) What is the abundance of various lymphocyte subtypes present in blood and/or tumor tissue at the time of resection in NSCLC patients? (II) Are there correlations between lymphocyte subtype distribution in blood and tissue? (III) What is the prognostic impact of the various lymphocyte subtypes in NSCLC?

The aim of this study was to establish and validate a multiparametric flow cytometry method to analyze the presence of functional subtypes of lymphocytes in blood from resectable NSCLC patients. We therefore sought to optimize protocols using two panels of antibodies containing different surface markers: one for the analysis of CD8+ subtypes and the other for the analysis of expanded lymphocyte subtypes.

To achieve our aim, we formalized the following objectives:

- Isolation of peripheral blood mononuclear cells (PBMCs) from healthy donors
- Establishing the optimal antibody concentration needed by titrating the panel antibodies
- Configuration of the multiparametric antibody panels for analysis by flow cytometry
- Compensating for the spectral overlap between the fluorophore-conjugated antibodies in the panels
- Validating the established protocol for use on PBMCs from resected NSCLC patients
- Assessing how cryopreservation affects the different lymphocyte subtypes

3 Materials and methods

3.1 Ethics

The use of human samples for this study was approved by the Regional Committee (REK) for Medical Ethics (REK#:2016/2054) and the Data Protection Officer at UNN HF. Resectable NSCLC patients have given a broad written consent, which thereby include exploration of their blood samples for immune cell composition. Blood samples in form of buffy coats from healthy anonymous donors were obtained from the blood bank at the University Hospital of Northern Norway (UNN).

3.2 Study population

The blood from five anonymous healthy donors was used to establish and optimize the protocol. Blood from healthy donors was also used to establish a baseline, which will serve at a later stage as a control for profiling of lymphocyte subsets in blood samples from resectable non-small cell lung cancer (NSCLC) patients. The included patients are all included in the TNM-I study (Clinical trials identifier; NCT03299478), for whom there are available viable lymphocytes from blood.

In order to validate the protocol for the use in NSCLC patient samples, we included four randomly selected patient samples out of the 60 available in the TNM-I study. The patient characteristics are presented in Table 3.

Table 3 Characteristics of resected NSCLC patients included in the pilot for validation. *This table shows the age, smoking history, cancer stage, histological classification, total leukocyte and total lymphocyte count at the time of resection.*

ID	Sex	Age	Smoking status (Packyears*)	P-stage	Histology	Total leukocyte count (10^9/l)	Total lymphocyte count (10^9/l)
30	F	85	Previous (16.5)	1A3	LUAD	6.7	1.5
40	M	82	Previous (18)	2A	LUAD	14.4	1.3
58	F	74	Current (19.8)	1A1	LUAD	5.4	1.4
95	M	49	Previous (6)	1A2	LUAD	7.8	1.3

Abbreviations: F= Female, M= Male, P-stage= pathological stage, LUAD= Lung Adenocarcinoma

* Pack years: the amount of cigarettes smoked per day multiplied by the number of years the person has smoked

3.3 Isolation of peripheral blood mononuclear cells

Peripheral blood mononuclear cells (PBMCs) were isolated from leukocyte-enriched blood (buffy coat) from five different healthy donors using Lymphoprep™ (Norway, Serumwerk Bernburg) [48].

3.3.1 General principles

Lymphoprep is a separation medium with a density of 1.077g/ml composed of Sodium diatrizoate, polysaccharide and water. Lymphoprep exploits the difference in cell density to separate PBMCs from other blood components. PBMCs such as lymphocytes, monocytes and platelets have a lower density than the gradient separation medium. The polysaccharide component of the separation medium causes erythrocytes and granulocytes to aggregate, leading them to sediment and pellet at the bottom of the conical tube following centrifugation leaving PBMCs in the plasma: lymphoprep interface (Figure 7C) [48][49].

3.3.2 General procedures

The leukocyte-enriched blood of approximately 50 mL was diluted 1:1 with Dulbecco's Phosphate Buffered Saline (DPBS) (Sigma-Aldrich, MO, USA) in a T75 flask. 25 mL of the diluted blood was carefully layered in 50 mL conical tubes containing 15 mL of the density gradient Lymphoprep™. The tubes were subsequently centrifuged for 30 minutes at 800 x g using a centrifuge setup with low acceleration and low break as to not disrupt the gradient at room temperature (RT). Figure 7 is an illustrative drawing of the PBMC isolation steps. After centrifugation, the PBMC layer shown in Figure 7C was collected using a Pasteur pipette with as little plasma and Lymphoprep™ as possible. The PBMCs were pipetted into an empty 50 mL conical tube, and they were washed twice by adding 25-30 mL cold- DPBS (Figure 7D) and centrifuged for 10 minutes at 350 x g at 4°C. To ensure that all residual erythrocytes are removed from the PBMC pools, 1-3 mL Red Blood Cell Lysis Buffer (Roche Diagnostics, Mannheim, Germany) was added to the PBMC pellet and incubated at RT for 5 minutes. Subsequently, the PBMCs were washed by adding DPBS and centrifuging at 350 x g for 10 minutes at 4°C. The supernatant was discarded, and the pellet resuspended in DPBS until further processing.

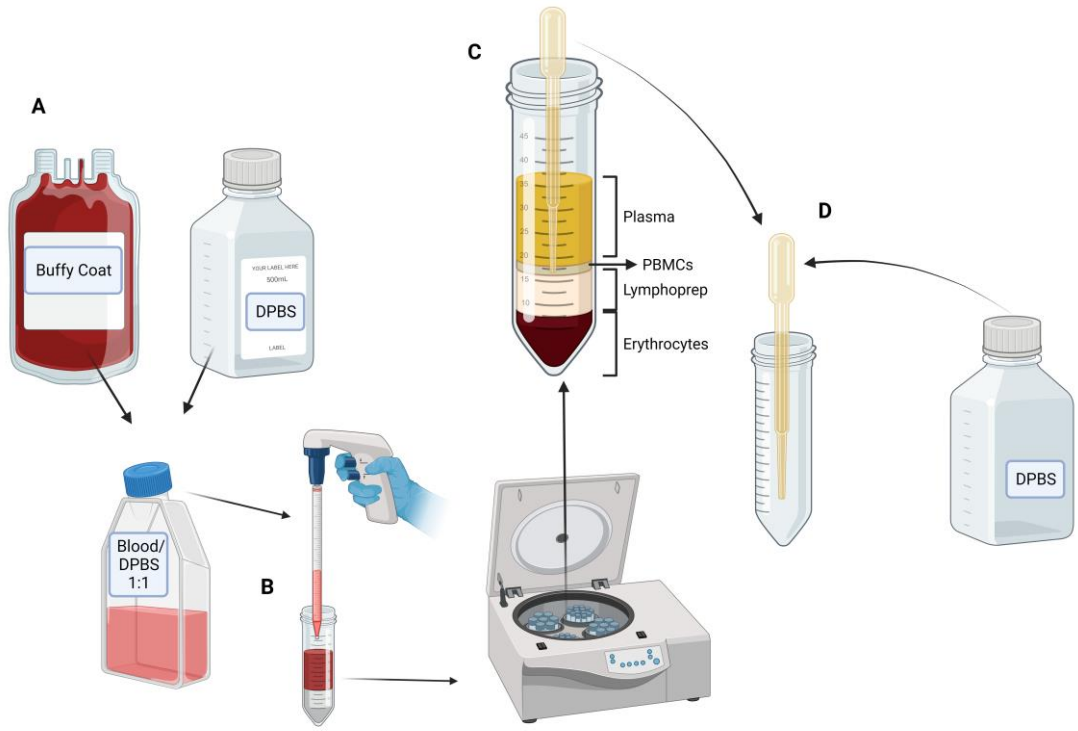

***Figure 7**. **Illustrative image of PBMC isolation procedure.** A. The contents of the buffy coat were emptied in a T75 flask along with an equivalent amount of DPBS (1:1). B. A conical tube was filled with 15 mL Lymphoprep, diluted blood was carefully layered on top, and the tube centrifuged. C. The figure shows gradient distribution of erythrocytes at the bottom, PBMCs at the plasma: lymphoprep interface and plasma on top D. Using a Pasteur pipette, the PBMCs were carefully allocated into a new conical tube along with DPBS. Figure created using Biorender.com*

3.4 Cell counting and viability assessment

A 50 mL buffy coat contains between 200 million to 1 billion PBMCs, and to assess the quantity and quality of the PBMCs that were isolated in section 3.3.2, Neubauer cell counting chamber and Trypan blue (Sigma-Aldrich, UK) were used. This is a crucial step before conducting any experiment using cells, especially regarding data reproducibility. Trypan blue is a viability stain that is only taken up by cells with compromised membranes, staining their cytoplasm blue [50]. Therefore, this stain is used to quantify live cells by labeling dead cells exclusively.

3.4.1 General procedure

10 µl of the PBMCs suspension (section 3.3.2) was allocated into an eppendorf tube and diluted in 990 µl of DPBS. From this dilution, 10 µl were allocated into a new eppendorf tube along with 10 µl 0.4% Trypan blue. The cell and Trypan blue mixture was homogenized by resuspending it gently using pipette before 10 µl of the mixture was transferred onto the counting chamber using a pipette (Figure 8). Viable PBMCs were then counted within 2

minutes of adding Trypan blue, only considering cells that were inside the four large squares on the counting chamber. The calculation was conducted using the equations shown in Table 4.

Table 4. Equations. *These equations were used when calculating the quantity of viable cells and the volume from the cell suspension needed to achieve the desired cell concentration*

Eq.1 Cell count	$\frac{(sum\ cells\ counted\ in\ large\ squares\ in\ burker's chamber)}{nr\ of\ squares\ counted} x\ 10^4$
Eq.2 Total cell number in solution	$(Cell\ count)\ x(Volume\ of\ cell\ suspension)$
Eq.3 Volume cell suspension needed	$v1 = \frac{final\ concentration\ x\ final\ volume}{initial\ concentration}$
Eq.4 Volume of medium needed	$(Final\ volume - volume\ of\ cell\ suspension\ needed)$

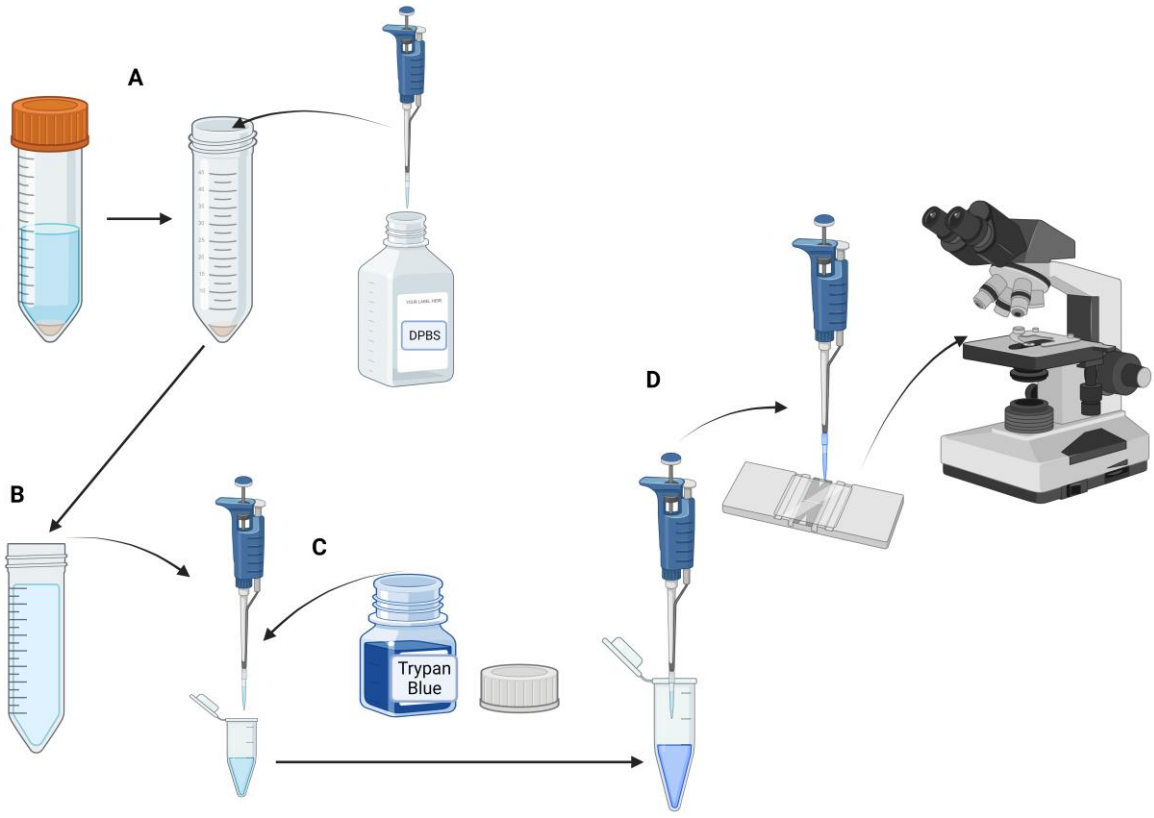

Figure 8. Illustrative image of PBMCs quality and quantity assessment. *A-B: The isolated PBMC suspension is diluted and from the dilution 10 µl is allocated into an eppendorf tube with 10 µl of Trypan blue. C-D: The cell and Trypan blue mixture is homogenized and 10 µl of the mixture is pipetted onto the counting chamber. The cells are then counted using a light microscope. Figure created using Biorender.com*

3.5 Cryopreservation and thawing of PBMCs

As aforementioned, a 50 mL buffy coat bag contains between 200 million and 1 billion PBMCs. One of the aims of this study was to assess what effects cryopreservation had on lymphocyte subtypes, since the 60 NSCLC patient samples in the TNM-I study were cryopreserved. To do that, the protocol was evaluated on fresh and frozen PBMCs from healthy donors.

3.5.1 General principles

Cryopreservation is a technic used to store and preserve cells for future use, as it is not always possible to use freshly isolated PBMCs. When cells are exposed to low temperatures and extracellular fluid starts to freeze, osmosis occurs in order to restore the imbalance. However, this causes the cell to shrink significantly and die. To solve this problem, a cryoprotectant such as dimethyl sulfoxide (DMSO) (Sigma, MO, USA) is used when freezing down cells for storage. When DMSO is added, it helps prevent the outflux of intracellular fluid by preventing crystallization. Despite its positive use, DMSO is toxic to cells and is therefore only used at concentrations not exceeding 10% [49]. The prolonged exposure of PBMCs to DMSO can also be harmful, and this is especially important to remember during the thawing process of cryo-preserved cells. For this reason, it is important to eliminate DMSO as soon as possible following the thawing of the cells.

3.5.2 General procedure

Following PBMC isolation, cell concentration and viability assessment, the necessary volume of PBMCs for fresh sample analysis was allocated into a separate tube while the remaining PBMCs were cryopreserved for future use. The freezing medium was prepared by diluting DMSO in 90% Fetal Bovine Serum (FBS) (Biochrom, Germany). The PBMCs were resuspended in the freezing medium and transferred into cryotubes at a concentration of $5x10^6$ cells/mL. As mentioned earlier DMSO can be toxic to cells, so once the medium was added the cells in the cryotubes, the cryotubes were placed in a freezing container and then placed in the freezer at -70 °C for 24 hours. After 24 hours, the tubes were transferred into the liquid nitrogen tank before the cryotubes were transferred into the nitrogen tank for long-term storage.

When running an analysis on the frozen PBMCs, a cryovial was retrieved from the nitrogen tank and transferred to the working station on ice. The cryovial was then thawed rapidly by hand while making sure to constantly swirl the vial, to prevent both thermal and DMSO concentration gradient. Once the vial was thawed, the cells were then transferred dropwise using a Pasteur pipette into a 50 mL conical tube with 30-40 mL MACS buffer to dilute and

later eliminate the cryoprotectant agent. MACS buffer is a mix of MACS BSA Stock Solution (Miltenyi Biotec, Germany) diluted 1:20 with autoMACS Rinsing Solution (Miltenyi Biotec, Germany). The cells were then quantified, and the viability was assessed before seeding out the cells for staining and analysis.

3.6 Flow cytometry

When analyzing single cells using flow cytometry, in addition to measuring FSC and SSC, a single-cells suspension can be stained using fluorescently-labelled antibodies to differentiate between the different subtypes. For this study, a non-sorting flow cytometer LSRFortessa™ (Becton, Dickinson & Company, USA)(serial no. H647794E6059) (Figure 9A) was used. Figure 9B shows the fluorescence-activated cell sorting (FACS) AriaIII (Becton, Dickinson & Company, USA) flow cytometer which allows the sorting and collection of the different subtypes from a heterogenous cell population.

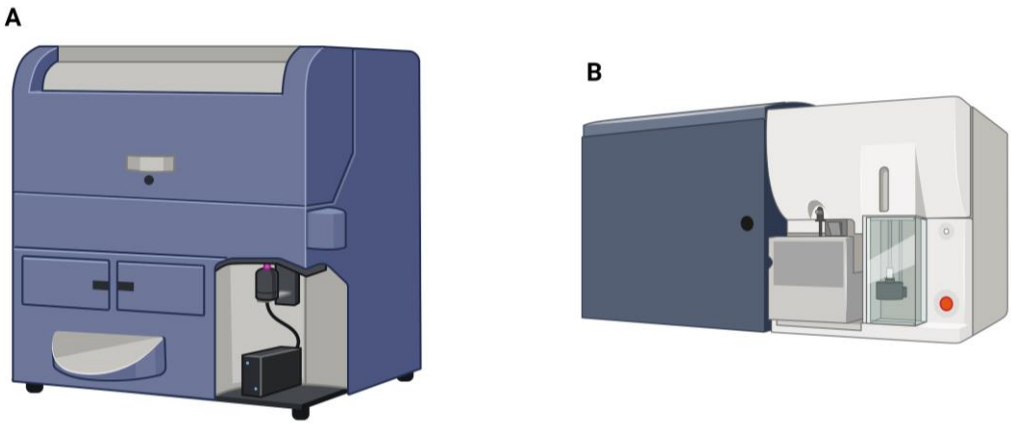

Figure 9. ***Flow cytometers.*** *A. An image of the LSRFortessa ™ used in this study. B. An image of the FACS AriaIII, the cell sorting flow cytometer. Both machines are available at the Advanced Microscopy Core Facility (AMCF), UiT. Figure was created with Biorender.com*

3.6.1 General principles

The flow cytometer LSRFortessa ™ was used to immunophenotype the PBMCs since there was no need to sort the cell suspension. The main components of LSRFortessa ™ are: (I) the fluidics systems which transports the cells from the cell suspension through the instrument, (II) the optical system, which includes the lasers and lenses. The lenses focus the laser beam whose light is spread as light scatter, which strikes the particles, and (III) signal detection, where the

scattered light is detected as the cells pass the laser beam in the fluid. The signals are turned into voltages by photodetectors. There are two detectors (I) photodiodes, which detect FSC and (II) photomultiplier, which then detect SSC and fluorescence. This is then visualized through the computer connected to the flow cytometer [51].

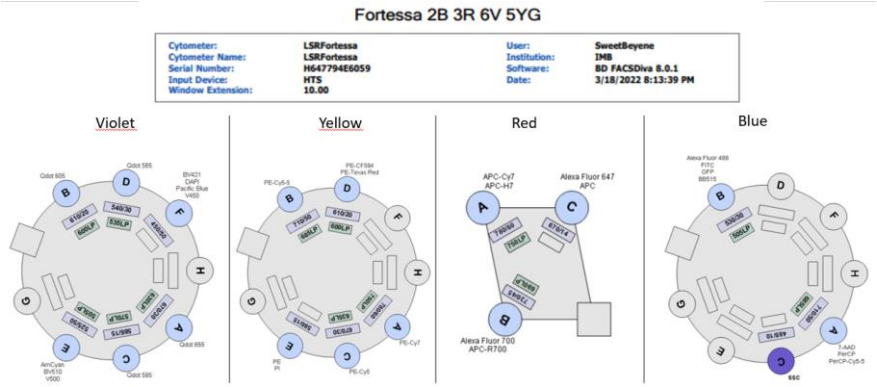

Figure 10. Fortessa configuration. *This image shows the filters and detectors that were used and the ones that were available on the flow cytometer LSRFortessa ™ used in this study. The red laser for example illustrates/demonstrated how multiple fluorophores can be detected by the sample detector. The system is set up to prevent the use of two fluorophores that can be detected by the same detector. This configuration is essential to know when planning to setup a panel. Figure taken from FACSDiva software.*

LSRFortessa ™ is equipped with four lasers: violet laser (405 nm), blue laser (488 nm), yellow/green laser (561 nm), and red laser (640 nm) and allows the use of up to 18 fluorochromes at the same time [52] (Figure 10). This is highly dependent on the selection of the appropriate fluorochromes and their filters. When running a multiparameter analysis, the most important part is to set up the appropriate compensation for the spectral overlap between the fluorochromes.

3.6.2 General procedure

The flow cytometer was always started 30 minutes prior to running the samples. This was done to allow the device system temperature to stabilize, since neglecting this could affect the results. Thereafter, the BD FACSDiva Software (RRID:SCR_001456) was started on the computer connected to the flow cytometer, this software contains tools that aid in data acquisition. Once the cytometer was warmed up and connected to the computer, the BD cytometer setup and Tracking (CS&T) software which is available within the BD FACSDiva software, was ran. CS&T was assessed by running a sample of CS&T beads, which generated a report showing the results and comparing them to the predefined baseline. This way one could check the state

of the cytometer. By doing this it is possible to eliminate device errors before samples were entered.

3.7 Panel setup

The first steps of designing the flow cytometry setup in this study were:

- Identifying the immune cells of interest and their surface markers
- Checking the filters available on the flow cytometer and then selecting the appropriate combination of fluorophores that can be used with as little overlap as possible; this was explored using a fluorescence spectra viewer
- Determine optimal antibody concentration by titrating
- Setting up compensation and checking for unspecific binding between antibodies and subtypes of interest using isotype controls
- Determine the gating strategy

For this study, two panels for the lymphocyte subtypes that were of interest were decided upon with Miltenyi Biotec Norden AB. Table 5 lists the setup for the CD8+ subtype panel (Panel 1) and Table 6 for the expanded lymphocyte panel (Panel 2) and viability stain for both panels.

Table 5 CD8+ subtype panel (Panel 1). *Information about the surface markers, their fluorophore conjugates and the fluorophore label used by the flow cytometer LSRFortessa™, as well as the lasers and filters used to detect the signal from the markers. The purpose lists what they are used to identify.*

Specificity	**Fluorophore**	**Purpose** [27]	**LSRFortessa ™ label**	**Laser**	**Filter**
CD3	VioBright R720	T Lineage	AlexaFluor 700	Red	725/40
CD8	APC-Vio770	T Lineage	APC-Cy7	Red	780/60
CD45Ra	VioGreen	Memory/effector	AmCyan	Violet	520/50
CCR7	PerCP-Vio700	Memory/effector	PerCP-Cy5-5	Blue	695/40
CD57	APC	Terminal differentiation	APC	Red	660/20
CD279 (PD-1)	VioBright B515	Exhaustion	AlexaFluor 488	Blue	530/30
CD39	VioBright V423	Non-bystander	Pacific Blue	Violet	450/40
CD103	PE-Vio770	Tissue resident	PE-Cy7	Yellow	780/60
CD95	PE	Marker for T_{SCM}	PE	Yellow	586/15
Viability	7-AAD	Live/Dead	PE-Cy5	Yellow	670/14

Table 6 Expanded lymphocyte panel (Panel 2). *Information about the surface markers, their fluorophore conjugates and the fluorophore label used by the flow cytometer LSRFortessa, and the lasers and filters used to detect the signal from them. The purpose lists what they are used to identify.*

Specificity	**Fluorophore**	**Purpose**[27]	**LSRFortessa ™ label**	**Laser**	**Filter**
CD3	VioBright R720	T Lineage	AlexaFluor 700	Red	725/40
CD19	APC-Vio770	B Lineage	APC-Cy7	Red	780/60
CD127	APC	Treg lineage	APC	Red	660/20
CD25	VioBright V423	Treg lineage	Pacific Blue	Violet	450/40
CD56	VioBright B515	Lineage	AlexaFluor 488	Blue	530/30
CD45RA	VioGreen	Memory/effector	AmCyan	Violet	520/50
CD27	PerCP-Vio700	Cytotoxicity	PerCP-Cy5-5	Blue	695/40
CD4	PE-Vio770	Lineage	PE-Cy7	Yellow	780/60
CD69	PE	Activation	PE	Yellow	586/15
Viability	7-AAD	Dead cells exclusion	PE-Cy5	Yellow	670/14

3.7.1 Titration

Antibody titration is imperative for panel optimization for identifying and separating populations and measuring expression levels of surface markers and various proteins. It can also help limit unspecific binding of the staining as well as save costly reagents. The antibody dilution that was recommended by the manufacturer was 1:50 per 10^6 cells. In order to ensure that the antibody concentration recommended by the manufacturer was optimal for this study, each antibody including the viability dye was titrated (1:50, 1:100, 1:200, 1:400 and 1:800).

This part of the study was conducted by the post.doctoral researcher in the group, Rodrigo Berzaghi. In summary, the optimal concentration was determined using the FlowJo software version 10.8.1_CL and by following the guide “FlowJo for antibody titrations: Separation Index and concatenation [53]”. In addition to visual assessment of the separation between the positive and negative population, the separation index (SI) provides a value that quantifies the separation. A higher value equals a better separation. A good separation can also help in minimizing spectral overlap, as using a higher concentration than needed would lead to false staining of the negative population and not necessarily provide better results.

3.7.1.1 General procedure

A PBMC cryotube was thawed as described in section 3.5.2. PBMCs were then aliquoted in eppendorf tubes at 1 x 10^6 cells/tube for a single stain experiment. The antibodies with their appropriate concentration were added to their respective tube with cells and incubated in the fridge for 15 minutes. The cells stained with viability stain were incubated in RT for 5 minutes. Following incubation, the cells were washed with MACS buffer, resuspended in 500 µl MACS buffer and transferred into flow cytometer tubes for analysis. The cells were analyzed using LSRFortessa^{TM}. Since these were single-stained cells, no compensation is necessary. Once the optimal concentration was determined, test samples with a cocktail of the antibodies for each panel was prepared and ran to check whether further adjustments were necessary.

3.7.2 Compensation

As aforementioned, compensation is a crucial step when running a multiparameter panel to minimize the effects of spectral overlap. Spectral overlap refers to the fluorescence of a dye being measured by more than one detector. If compensation is not performed, then one cannot be certain that when examining a graph with two parameters, the signals are in fact not false. After setting up the cytometer and prior to running the PBMC samples, compensation controls containing single stain are prepared and data is recorded. This data is added to the samples of interest by the software and the results are corrected when needed. However, to ensure that the compensation is as accurate as possible, meaning that the data are not being under- or overcompensated, isotype controls or fluorescence minus one (FMO) control were used [54]. Isotype controls are antibodies made for antigens that are not present in the cell population of interest and can therefore be used to check for levels of unspecific binding between the antibodies and cells in the sample of interest. The specificity of the antibodies used in this experiment were controlled using isotype controls.

3.7.2.1 General principle

Although fluorochromes are supposed to be detected by a specific channel, some may have a wide emission peak that spillover into different channels resulting in a spectral overlap. This can result in a false signal. When using few parameters, it can be possible to select fluorochromes that are far apart from each other to minimize the overlap. The main criteria that need to be followed to assure a proper compensation are: (I) compensation control must be brighter than or as bright as the fluorochrome used in the sample of interest, (II) the autofluorescence for the negative and positive populations must be the same, and (III) the

fluorochrome used for compensation must be the exact same to the fluorochrome used in the sample of interest.

3.7.2.2 General procedure

After setting up the panels, compensation was conducted using cells first, followed by using beads and isotype control. We finally settled on using beads and lot-specific antibodies as described here. Flow cytometry tubes of 5 mL were each labelled with the name of the fluorescent-labelled antibody. Compensation control samples are single-stained and therefore the tubes were filled with 100 µL MACS buffer along with one drop of MACS Comp Beads-anti-REA and one drop of MACS Comp Beads- Blank. Fluorochrome-conjugated REAfinity antibody was added to its respective tube at a concentration of 1:50. The tubes were then incubated for 15 minutes in the dark at 4ºC. Subsequently, 1 mL MACS buffer was added to each tube. An unstained blank control was also prepared to set up the autofluorescence as well as to serve as a compensation control for the viability dye.

Using the FACSDiva software, compensation was created, and the control samples were run. The PMT voltage was determined before recording the acquired data for each stain, using tool within the software, the compensation values were calculated. These values were then linked to the experiment prior to running the PBMC samples.

3.7.3 Gating strategy

Different lymphocytes and their subtypes bind different surface markers. After selecting the surface markers for the subtypes of interest, previous studies were consulted to identify the optimal gating strategy [55], [56]. After reviewing how the other studies gated these subtypes, the gating strategies shown in Figure 11 and Figure 12 were chosen. The former gating strategy will also be used in the future on white blood cells extracted from tumor cell samples from the same NSCLC patients [55].

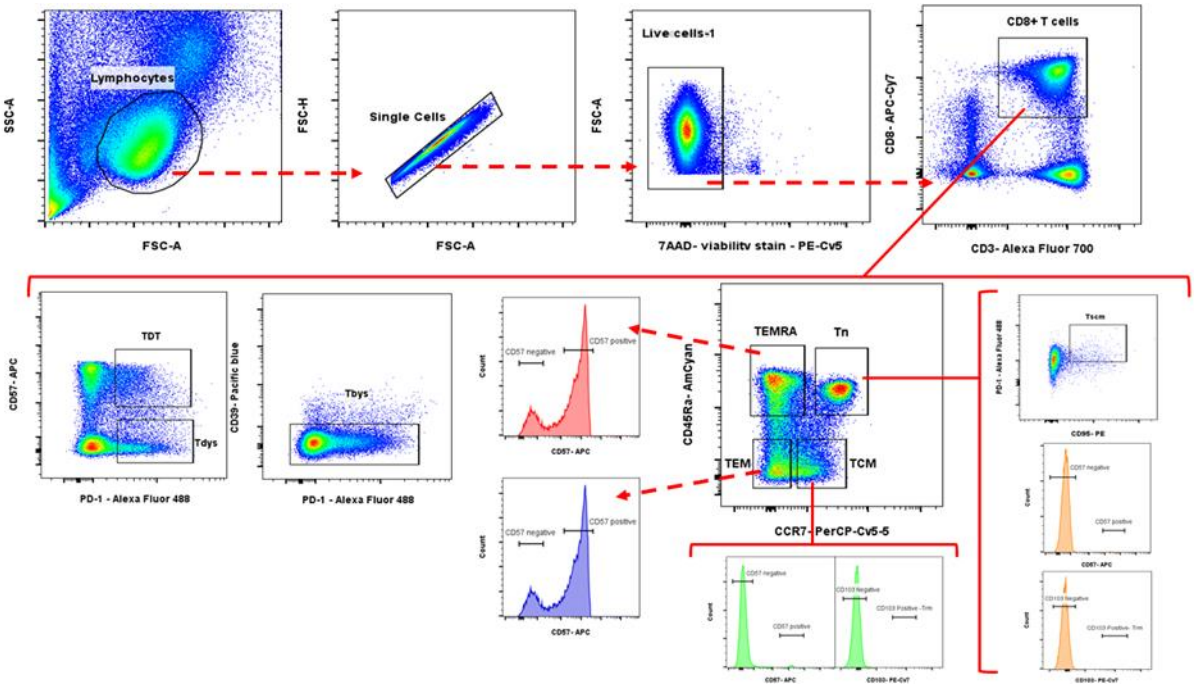

Figure 11. Gating strategy for the CD8+ subtype panel *Lymphocytes are gated based on the FSC-A and SSC-A, and single cells are selected using FSC-A and FSC-H. Live cells are selected based on their negative stain for 7AAD. Further, CD8+ T cells are gated on the live cells based on their positive stain for Alexa-Flour 700 and APC-Cy7. Terminally differentiated effector memory cells (T_{EMRA}), naïve T-cells (T_N), central memory T cell (T_{CM}) and effector memory T-cell (T_{EM}) are gated from the CD8+ T cells using the PerCP-Cy5-5 and AmCyan. The presence of tissue resident memory T-Cell (T_{RM}) and stem cell memory T-cell (T_{SCM}) is investigated on the subtype labelled T_N. Cells that are positive for PE & Alexa Fluor 488 are considered T_{SCM} while cells within the T_N & T_{CM} subtypes that stain positive for PE-Cy7 are classified as T_{RM}. Terminally differentiated dysfunctional T cells (T_{DT}) and dysfunctional T- cells (T_{dys}) are also gated using Alexa fluor 488 and APC on the CD8+ T cells. Finally, the number of bystander T cells (T_{bys}) within the CD8+ T cells population is gated using Alexa Fluor 488 and Pacific Blue.*

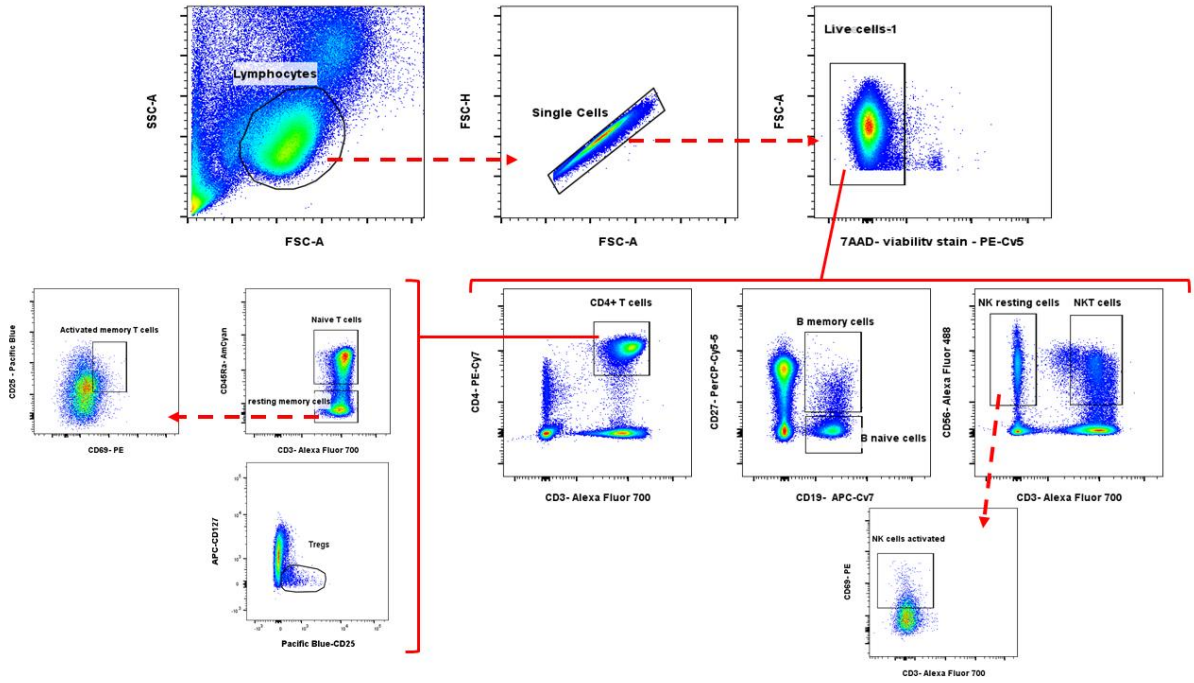

Figure 12. Gating strategy for the expanded lymphocyte panel. *Immune cells are gated based on the FSC-A and SSC-A, and single cells are selected using FSC-A and FSC-H. Live cells are selected based on their negative stain for 7AAD. From the live cells, CD4+ T cells, B cells and NK cells are gated based on their markers. CD4+ T cells are gated based on the CD3+CD4+ markers, and from them naïve T cells, memory cells and Tregs can be identified. Based on the expression of CD45RA, it can be distinguished between CD4+ naïve T cells (CD3+CD4+CD45RA+) and CD4+ memory cells (CD3+CD4+CD45RA-). CD4+ memory cells can be further divided into resting and activated when gating on CD3+CD4+CD45RA-, and further using CD69 and CD25 markers. Activated memory cells are CD25+ and CD69+ while resting memory cells express CD25 and CD69 at different levels . Tregs can be gated based on their positivity for CD25 marker and negativity for the surface marker CD127. B cells can be divided into naïve and memory cells using the markers CD19 and CD27, B naïve cells are CD19+CD27- while B memory cells are CD19+CD27+. NK cells and NK T cells can be gated on CD3 and CD56, NK cells are CD3-CD56+ while NK T cells are CD3+CD56+, activated NK cells can be gated from the NK cells using the marker CD69.*

3.8 Cell staining

The following cell staining procedure was used on both the frozen and fresh samples. As it is important to maintain a sterile environment to avoid contaminating the cells, all work was conducted inside a laminar fume hood. The samples were centrifuged at 1500 rpm for 10 minutes at 4ºC for all washing steps. Some of the fluorophore-conjugated antibodies were more sensitive to light exposure than others, and therefore were handled with minimal exposure to light. The flow cytometer LSRFortessa^{TM} was used to acquire the sample data no later than 1 hour following the staining procedure.

Following the quantification and viability assessment of the PBMCs, 1x10^{6} cells/ml of each donor samples were transferred into three eppendorf tubes. Two eppendorf tubes were labelled for each panel: CD8+ subtype panel (Panel 1), the expanded lymphocyte panel (Panel 2) and

one tube was used for an unstained sample. The eppendorf tubes were then centrifuged, and during that time antibody cocktails for the two panels were prepared. Using titration, the optimal antibody dilution was determined for panel 1. The second cocktail for panel 2 was prepared in the same manner with the antibodies at the dilution recommended by the manufacturer, and 50 µl of the cocktail mix was added to the respective samples. To the unstained samples, 50 µl MACS buffer was added. The tubes were then gently vortexed and incubated at 2 ºC for 15 minutes.

Excess antibody was washed away by adding MACS buffer to the tubes after the incubation. To be able to exclude dead cells from the analysis, 500 µl of 7AAD that was diluted 1:100 in MACS buffer was added to all the samples, with the exception of the unstained samples. The samples were then incubated at RT in the dark for 5 minutes before the excess 7AAD was washed off.

Subsequently, the pellets were resuspended in 500 µl MACS buffer and transferred into 5 ml flow cytometry tubes. The tubes were places on ice with minimal exposure to light awaiting analysis.

3.9 Data acquiring

The sample data was acquired using the LSRFortessa^{TM} and the software BD FACSDiva. The flow cytometer and the experiment was set up according to BD biosciences user guide [52]. Although the same fluorophores were used in both panels, they are conjugated to different antibodies. Therefore, the samples for panel 1 and panel 2 were run as separate experiments. After setting the compensation, the data from unstained samples for each donor were acquired before the data from the stained samples. To maximize the data output, approximately 250,000-300,000 events were recorded from the lymphocyte gate for each donor. After collecting the data from the fresh and frozen samples for all five healthy donors and the four NSCLC patient samples, the results were analyzed using the software FlowJo.

3.10 Statistics

Statistical analysis was performed using IBM SPSS Statistics version 28.0.1.1. The percentages of the various immune cell subtypes labelled with the CD8+ subtypes panel were calculated from the total number of live cells (7AAD negative) that were CD3+CD8+. The percentages of the different immune cell subtypes labelled with the expanded lymphocyte panel were calculated from the total number of live cells. In order to examine the statistical significance of

the differences between the fresh and frozen samples, we explored if our data met the assumptions for a paired t-test. A paired t-test has four assumptions: (I) the data must be continuous, (II) patients independent of one another, (III) variables must be normally distributed, and iv. variables should not contain outliers [57]. Our sample data were collected under different conditions (fresh vs frozen) and the patients were randomly chosen. Therefore, we conclude that our data met the first two assumptions. To check if our samples fulfilled the third and fourth assumptions we used the tools in SPSS check, and calculated the difference of fresh versus frozen samples for each subtype belonging to the healthy donors. The explore function was then used to check if the differences had a normal distribution and if they did not contain any outliers. A paired samples t-test was used to determine if the differences had statistical significance in the fresh versus frozen samples that met the assumptions while a non-parametric Wilcoxon signed-rank test was used in the samples that did not meet the assumptions. However, it should be noted that our study included small sample sizes and the results from the performed statistical analyses should be interpreted with caution. A bigger sample sizes are needed to be able to confirm these preliminary results.

4 Results

Two multi-parameter flow cytometry panels were established using blood samples from healthy donors and validated to examine the distribution of lymphocytes in blood from NSCLC patients. The first panel (Table 5) focuses on CD8+ lymphocytes and their subtypes while the second panel (Table 6) focuses on CD4+ lymphocytes, B cells, NK cells, NKT cells and Tregs. In addition, a viability stain 7AAD was used in both panels to exclude dead cells from analysis.

4.1 Antibody titration

As described in the method section 3.7.1, each antibody was titrated to the dilution that gave the best separation between positive and negative populations. The optimal dilution for both panels was determined to be 1:50 in MACS buffer. This corresponded to the manufacturer's recommendation. The results from the SI calculation based on the antibody titration are shown in Figures 13-14. The SI for all antibodies was highest at 1:50 dilution and therefore this dilution was used when staining the samples for both panels. Since the fluorophores in the expanded lymphocyte panel were the same as the fluorophores in the CD8+ subtype panel, the antibody titration was done once – for panel 1.

PBMCs from Health Donor						
SI / AB [ ]	1/50	1/100	1/200	1/400	1/800	Best [ ]
CD3	77.7	57.7	2.18	2.7	2.12	1/50
CD8	113	90.7	7.8	1.97	2.38	1/50
CD45RA	8.07	7.42	7.26	5.86	4.54	1/50 1/100
CCR7	x	4.75	1.94	2.01	2.94	1/50
CD39	34.6	26.6	18.1	13.6	9.2	1/50
CD57	11.26	10.71	10.49	9.26	8.22	1/50
PD-1	6.04	5.59	4.45	3.3	0.9	1/50
CD103	LP	LP	LP	LP	LP	1/50
CD95	LP	LP	LP	LP	LP	1/50
AB= Antibody; SI= Separation index; LP= Low population.						

Figure 13. Separation Index. *This figure shows the Separation index (SI) that was calculated for each antibody dilution (AB). The higher the Separation index value is the better the dilution is. Here we see that the 1:50 dilution is the most optimal, since it results in the highest SI. The SI for CD103 and CD96 markers is not shown, as there were not enough cell populations to do so. Image was obtained from Rodrigo Bergahzi, who conducted this experiment.*

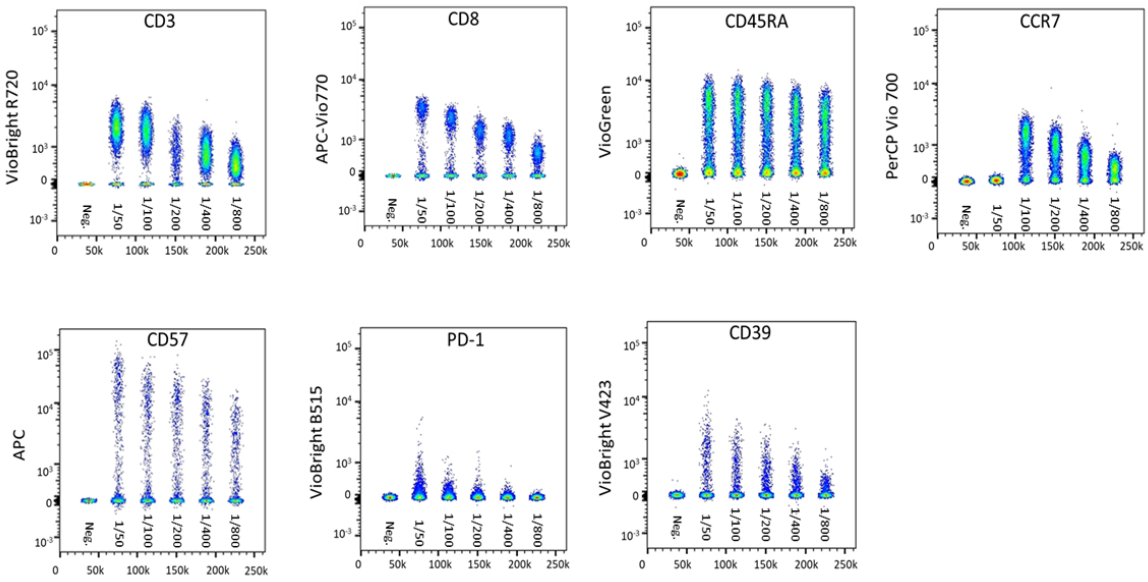

Figure 14. Antibody titration. *This figure shows the results, from which the separation index (SI) was calculated. Along the x-axis we have the dilution factor, and the y-axis shows the negative and positive population separation. We can see that at higher dilutions, the separation between the positive and negative population is too small and hard to distinguish. The separation gets better the lower the dilution is. This experiment was conducted by Rodrigo Bergahzi and image was obtained from him.*

The fluorescently-labelled antibody cocktail for each panel was prepared using the dilution determined during the titration to run multiple pilots. This was done to ensure that the panel setup will obtain desired results. This led to the discovery that one of the antibodies in panel 1 was a highly expressed marker that had been matched with a bright color. This resulted in a strong background signal in the PE-Cy5 channel, which was supposed to detect the viability dye 7-AAD (Figure 15). Figure 15 shows two samples from the same donor where A. is stained with the expanded lymphocyte panel and B. is stained with the CD8+ lymphocyte subtypes panel. Due to background staining, the sample stained with the CD8+ lymphocyte subtypes panel seems to have a higher percentage of dead cells compared to its counterpart (Figure 15A). The samples were from the same cryovial thawed and divided into two and treated in the exact way with the only exception being that the cells in the Figure 15A are stained with panel 2 antibody cocktail and in Figure 15B with panel 1 antibody cocktail.

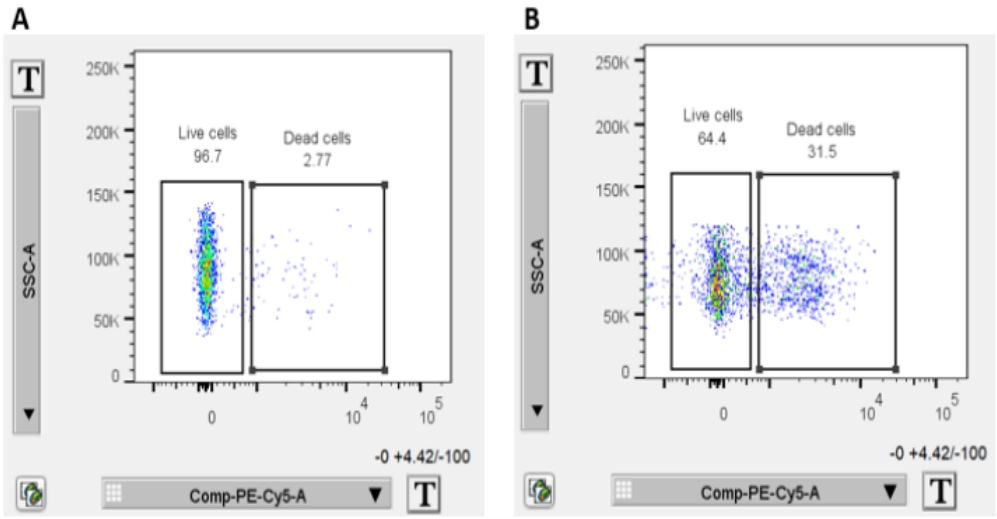

Figure 15. Background staining. *FlowJo image obtained by analyzing data from the same donor. The sample stained with the antibody cocktail for panel 2 (A) and the sample stained with the antibody cocktail panel 1 (B). A. The sample data shows that 96.7% of the cells that were stained with the antibodies for the extended lymphocyte panel were alive while 2.77% of them were dead. B. The sample data shows that 64.4 % of the cells that were stained with the antibodies for the CD8+ subtype panel were alive while 31,5% of them were dead.*

To determine the exact cause of the discrepancy between the two samples, single stained samples were prepared for all the antibodies in panel 1 and examined for their signal in the 7AAD channel for spillover. This showed that it was the antibody for the marker CD57 (APC) that had a strong signal spillover into the 7AAD channel (Figure 16). To further confirm this observation, the result was compared to the APC antibody signal in panel 2 (Figure 16C and Figure 16D). This showed that the APC in panel 1 had a much stronger signal compared to the APC in panel 2. The bottom of Figure 16D shows how the signal from APC gives a positive signal in the viability dye channel making it look like the sample has dead cells although 7AAD is not included. Based on these results, the APC labelled antibody in panel 1 was titrated again with the dilution 1/100, 1/200, and 1/300 (results not shown) and it was determined that 1/300 yielded the best results.

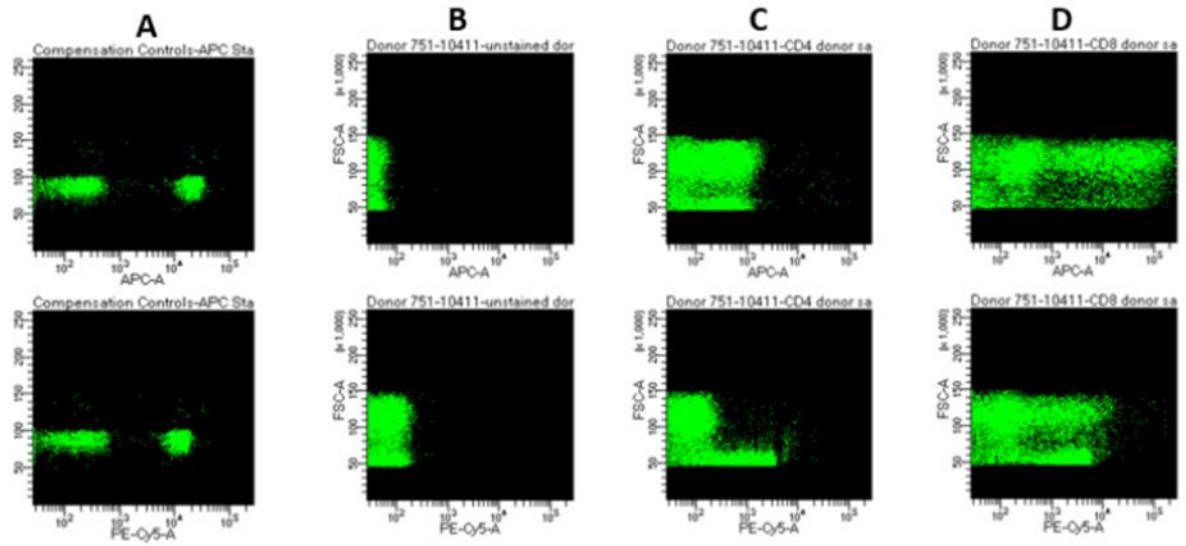

Figure 16. Single staining to determine spillover. All the antibodies were prepared as single stains (results not shown) and the single stain samples data was acquired using FACSDiva. The signal from each antibody was checked in each channel, and the CD57 – APC antibody's signal was detected in both APC and PE-Cy5 channels as shown in **A** in the upper and lower parts of the figure, respectively. PE-Cy5 is the channel that detects signals from 7AAD. **B**. This figure shows the autofluorescence of the cells in the unstained sample (used here for control). The APC antibody in panel 1 (**D**) was compared with the APC in panel 2 (**C**), and we can see that the signal from APC in panel 1 (**D**) had a strong background staining in the PE-Cy5 channel.

4.2 Compensation with beads

Optimal compensation was after several challenges (section 6) finally setup using commercially bought beads and the exact (lot-specific) antibodies used for the samples instead of isotype controls. The setup with isotype controls and beads resulted in an optimal compensation with negligible spillover from the various antibodies into the other channels (Figure 17).

Show All	Alexa Fluor 700-A	APC-Cy7-A	PerCP-Cy5-5-A	AmCyan-A	PE-A	Alexa Fluor 488-A	APC-A	PE-Cy7-A	Pacific Blue-A	PE-Cy5-A
Alexa Fluor 700-A	100	14.3796	4.5446	0.0105	0.011	0.0355	3.1073	2.6259	0.0053	1.0625
APC-Cy7-A	18.399	100	0.2569	0	0.0082	0	21.7671	21.2167	0	6.2248
PerCP-Cy5-5-A	15.8269	2.8658	100	0	0	0	4.1597	2.7719	0	7.6122
AmCyan-A	0.3315	0.1105	2.0253	100	0	0	0.1657	0.0578	5.0829	0.4049
PE-A	0.0109	0.0014	20.8071	0.015	100	1.0697	0.0389	0.9637	0	44.8099
Alexa Fluor 488-A	0.003	0.003	1.3668	0.3504	0.4881	100	0.0061	0.0032	0	0.2297
APC-A	20.7747	3.0474	0.6347	0	0.0356	0	100	0.7033	0	28.064
PE-Cy7-A	1.1657	8.4381	3.4686	0	1.5619	0.1662	0.203	100	0.0031	1.4154
Pacific Blue-A	0	0	0	12.0698	0.0358	0	0.0068	0.0501	100	0
PE-Cy5-A	3.2375	0	0	0	3.3898	0	1.6188	0	1.6187	100

Figure 17. Isotype control compensation. This table shows the compensation matrix generated by FACSDiva after setting up the compensation. It is obtained from FlowJo and shows how much the various antibodies spill over into the various channels. The smaller the value is, the better the analysis using the compensation will be. This compensation was made using beads and isotype controls.

The results from the lot-specific compensation yielded in a very similar result (Figure 18). However, although using isotype controls is cheaper, we used lot-specific compensation for all the experiments, because some of the antibodies were tandem fluorophores and they require it. This is because a variation in the conjugation between the antibodies can affect the spectral properties. The isotype control antibodies were then used to ensure that there was no unspecific binding between the fluorophore and the immune cells of interest (results not shown).

Show All	Alexa Fluor 700-A	APC-Cy7-A	PerCP-Cy5-5-A	AmCyan-A	PE-A	Alexa Fluor 488-A	APC-A	PE-Cy7-A	Pacific Blue-A	PE-Cy5-A
Alexa Fluor 700-A	100	14.2164	4.7102	0.0054	0.0285	0.0692	3.155	2.549	0	0.9637
APC-Cy7-A	21.3963	100	0.3632	0	0	0	34.8814	20.6404	0.0145	9.1766
PerCP-Cy5-5-A	15.5482	2.8083	100	0	0	0	4.174	2.5498	0	7.1825
AmCyan-A	0.0535	0	0	100	0	0	0	0	6.4449	0
PE-A	0	0	10.9113	0.007	100	0.5861	0.0189	0.4589	0	21.2322
Alexa Fluor 488-A	0	0	1.3127	0.3104	0.0283	100	0.0102	0	0	0.0142
APC-A	20.1531	2.9785	0.6721	0	0	0	100	0.6755	0	26.3969
PE-Cy7-A	1.2247	9.0188	3.6884	0	3.0679	0.1856	0.2021	100	0	1.2863
Pacific Blue-A	0.016	0	0	23.5016	0	0	0.1587	0.034	100	0
PE-Cy5-A	0	2.9402	8.6153	1.4189	7.6922	4.3076	7.3504	0	2.8376	100

Figure 18. Lot-specific compensation*. This table shows the compensation matrix generated by FACSDiva after setting up the compensation. It is obtained from FlowJo and shows how much the various antibodies spill over into the various channels. The smaller the value is, the better the analysis using the compensation will be. This compensation was made using beads and lot-specific antibodies. Lot-specific means that the same antibody from the same container was used in the compensation and in the sample.*

4.3 Phenotyping using CD8+ subtype panel

There were two reasons for running the flow cytometry panels on PBMCs from healthy donors: (I) Explore and establish the optimal protocols and their functionality and (II) Serve as a baseline control for NSCLC patient samples. After acquiring the data from running five fresh samples from healthy donors stained with panel 1, the data were analyzed and gated according to the predetermined strategy (Figure 11).

The results from Donor 1 - Donor 5 fresh samples are shown in Figures 19-21. After gating the live cells population, we used the gating as described in Table 1 and Figure 11 to identify the different subtypes. The same analysis was done on the frozen samples from Donors 1-5, the results are shown in Figures 22-24.

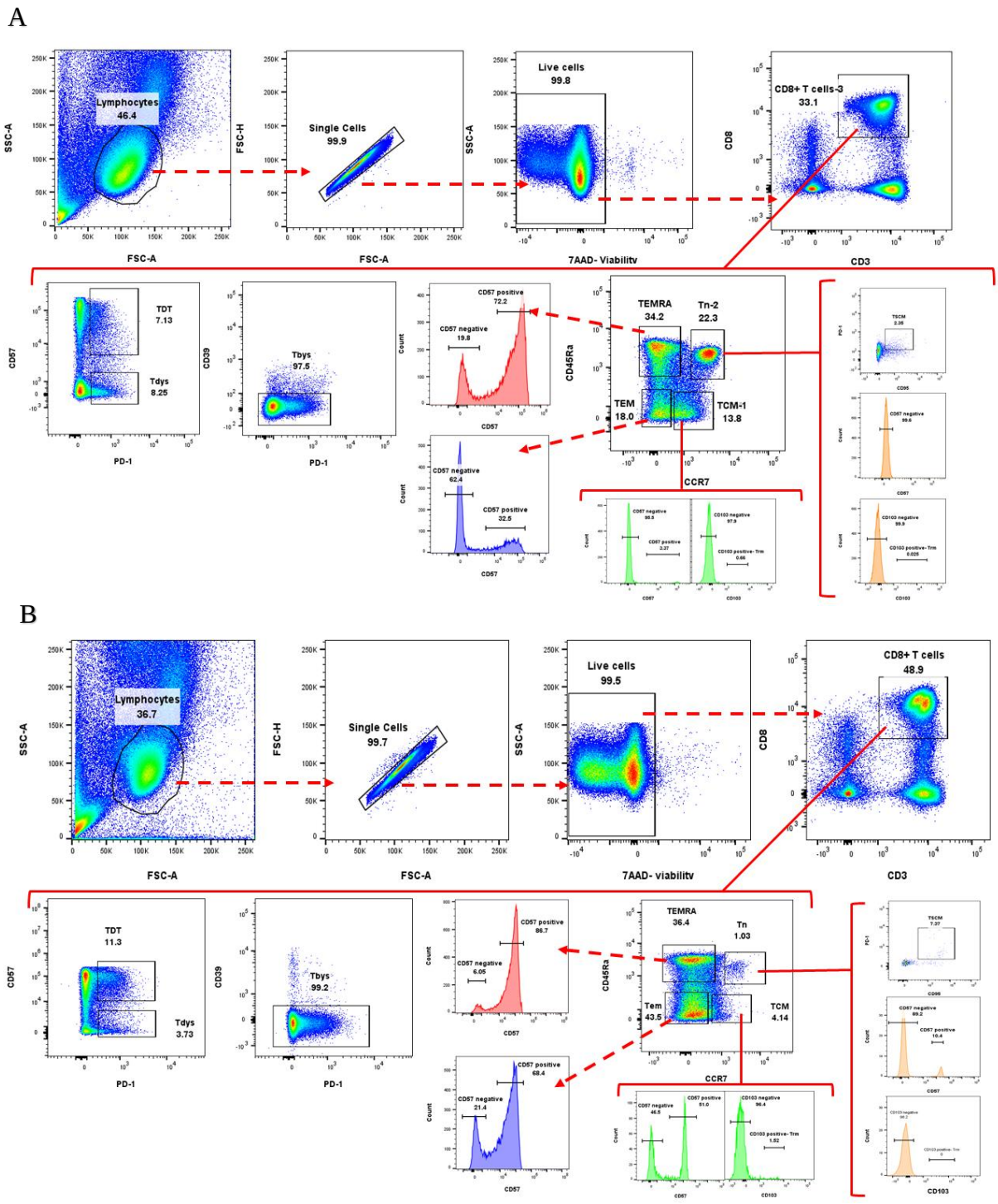

Figure 19. Analysis of fresh sample from Donor 1 (A) and Donor 2 (B) using CD8+ subtype panel. *Comprehensive surface marker screening in PBMCs from healthy donors. PBMCs were isolated using the density gradient Lymphoprep. The isolated PBMCs were then stained with an antibody cocktail mix (CD3, CD8, CD45RA, CCR7, CD57, CD279 (PD-1), CD39, CD103 and CD95). The sample was then analyzed according to the gating strategy demonstrated in Figure 11. The first gate selects lymphocytes eliminating monocytes, and cell debris. This is followed by gates to eliminate doublets and dead cells using 7AAD from the analysis. The channels Alexa fluor 700 (CD3) and APC-Cy7 (CD8) was used to identify the CD8+ T cell subtypes. Using the channels for CCR7 and CD45RA, T_N, T_{EM}, T_{CM} and T_{EMRA} were then identified from the CD8+ T cell subtypes.*

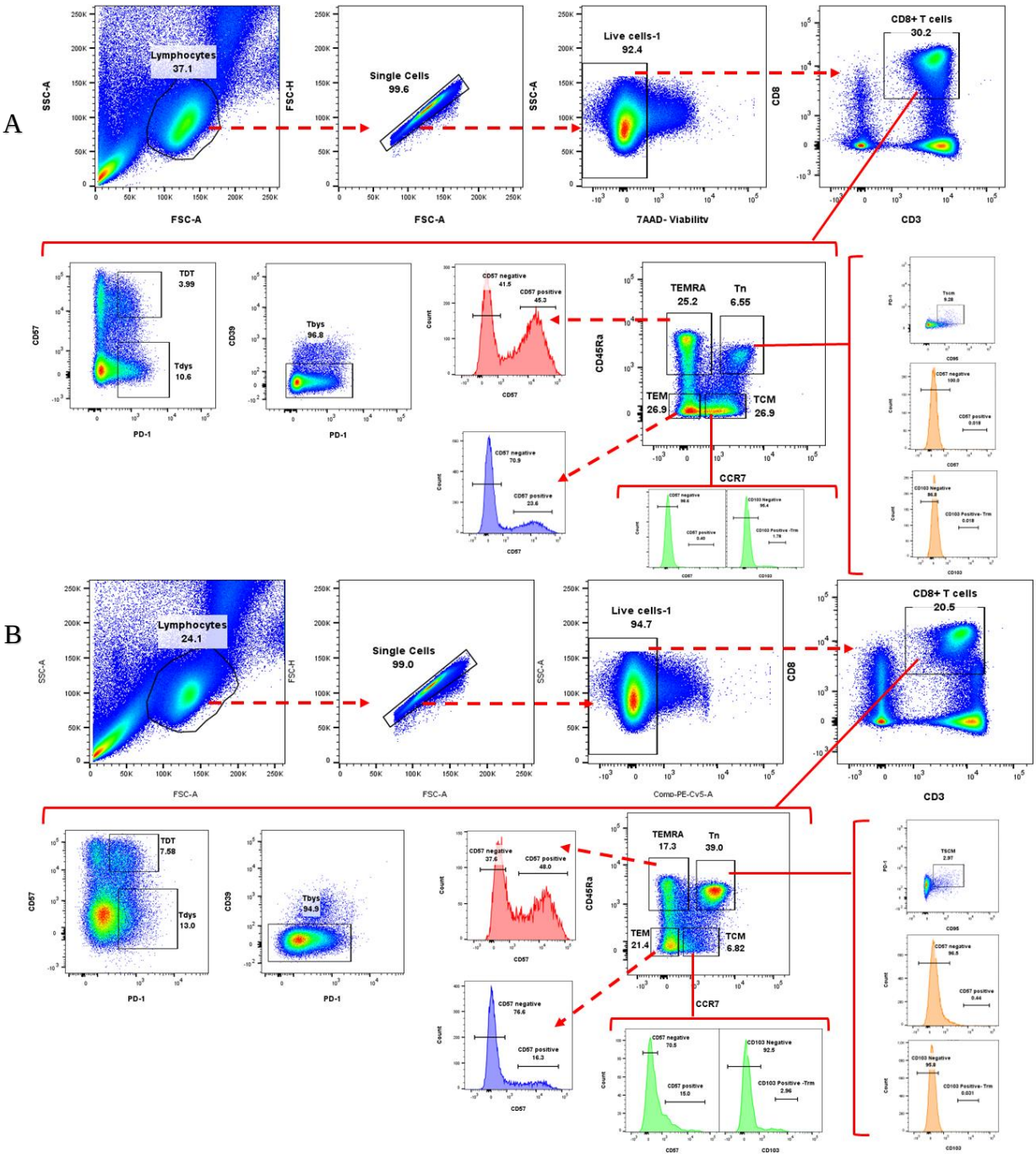

Figure 20. Analysis of fresh sample from Donor 3 (A) and Donor 4 (B) using CD8+ subtype panel. *Comprehensive surface marker screening in PBMCs from healthy donors. PBMCs were isolated using the density gradient Lymphoprep. The isolated PBMCs were then stained with an antibody cocktail mix (CD3, CD8, CD45RA, CCR7, CD57, CD279 (PD-1), CD39, CD103 and CD95). The sample was then analyzed according to the gating strategy demonstrated in Figure 11. The first gate selects lymphocytes eliminating monocytes, and cell debris. This is followed by gates to eliminate doublets and dead cells using 7AAD from the analysis. The channels Alexa fluor 700 (CD3) and APC-Cy7 (CD8) was used to identify the CD8+ T cell subtypes. Using the channels for CCR7 and CD45RA, T_N, T_{EM}, T_{CM} and T_{EMRA} were then identified from the CD8+ T cell subtypes.*

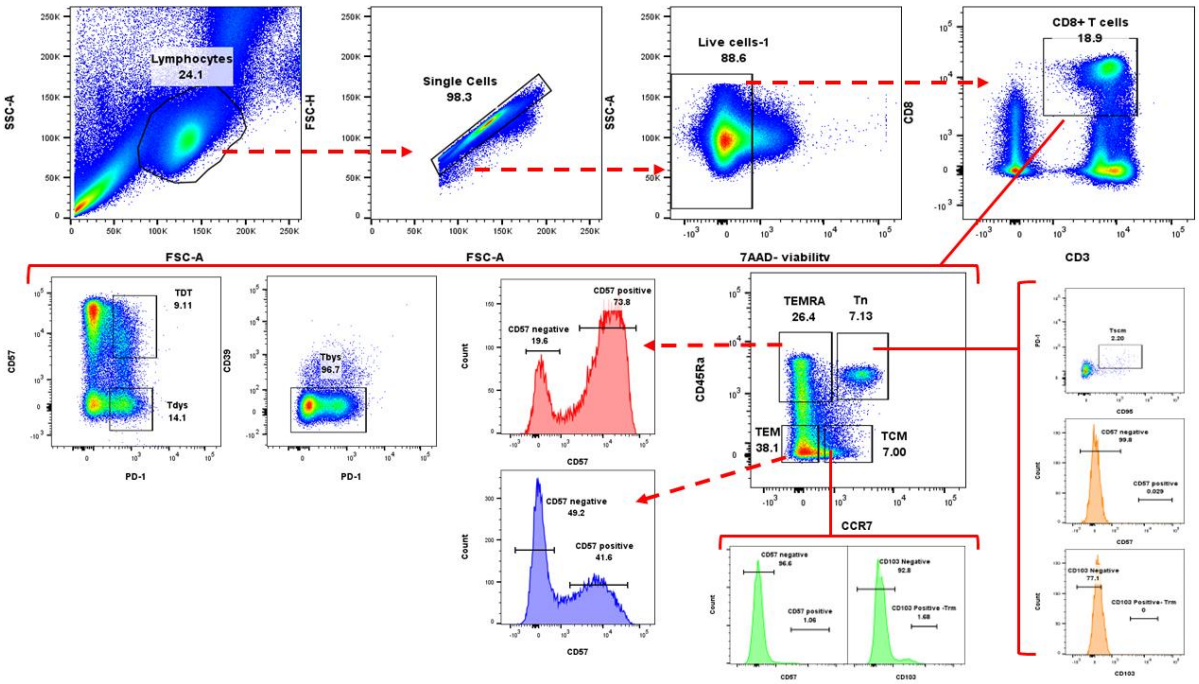

Figure 21. Analysis of fresh sample from Donor 5 using CD8+ subtype panel. Comprehensive surface marker screening in PBMCs from healthy donors. PBMCs were isolated using the density gradient Lymphoprep. The isolated PBMCs were then stained with an antibody cocktail mix (CD3, CD8, CD45RA, CCR7, CD57, CD279 (PD-1), CD39, CD103 and CD95). The sample was then analyzed according to the gating strategy demonstrated in Figure 11. The first gate selects lymphocytes eliminating monocytes, and cell debris. This is followed by gates to eliminate doublets and dead cells using 7AAD from the analysis. The channels Alexa fluor 700 (CD3) and APC-Cy7 (CD8) was used to identify the CD8+ T cell subtypes. Using the channels for CCR7 and CD45RA, T_N, T_{EM}, T_{CM} and T_{EMRA} were then identified from the CD8+ T cell subtypes.

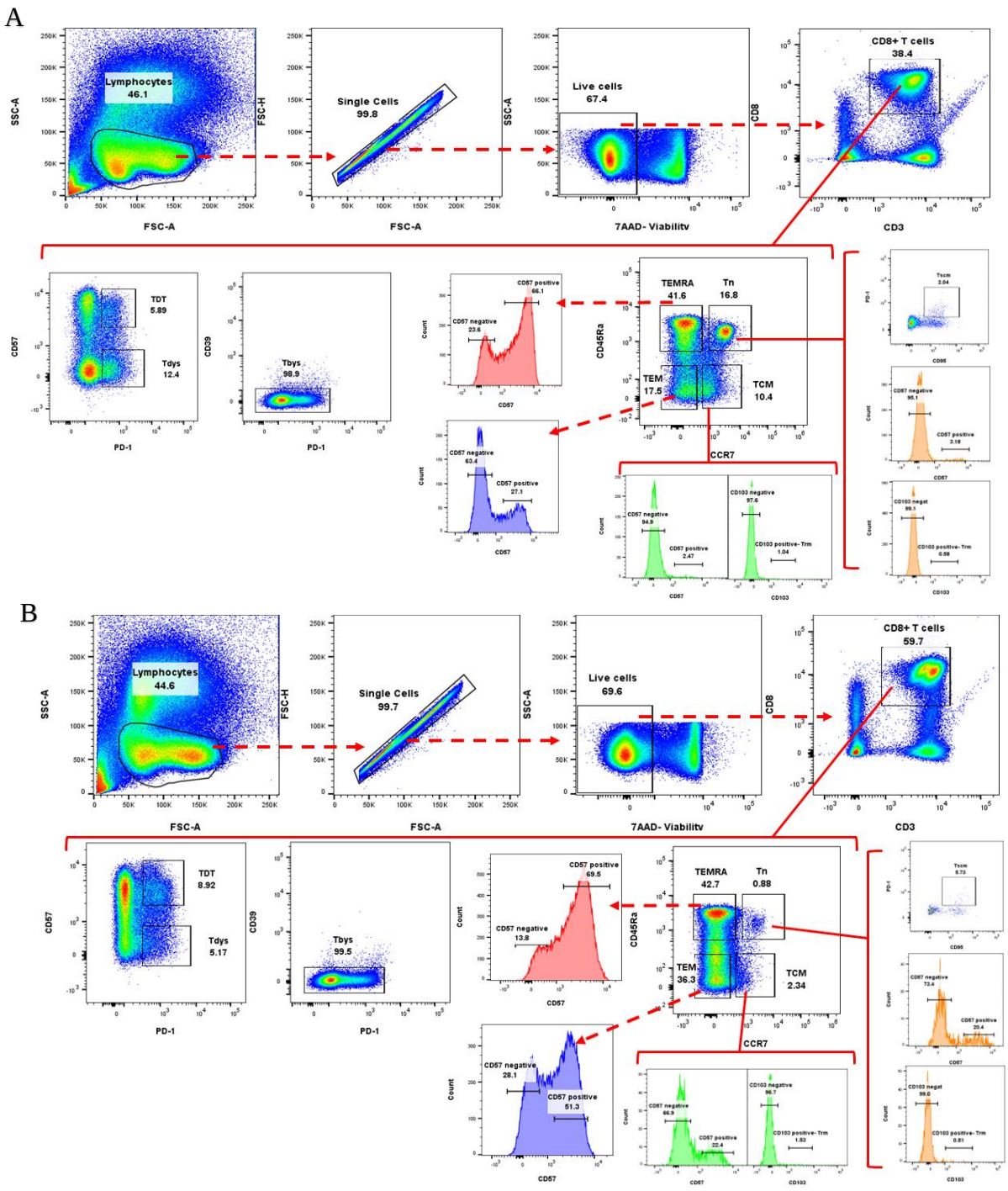

Figure 22. Analysis of frozen sample from Donor 1 (A) and Donor 2 (B) using CD8+ subtype panel. *Comprehensive surface marker screening in PBMCs from healthy donors. PBMCs were isolated using the density gradient Lymphoprep. The isolated PBMCs were then stained with an antibody cocktail mix (CD3, CD8, CD45RA, CCR7, CD57, CD279 (PD-1), CD39, CD103 and CD95). The sample was then analyzed according to the gating strategy demonstrated in Figure 11. The first gate selects lymphocytes eliminating monocytes, and cell debris. This is followed by gates to eliminate doublets and dead cells using 7AAD from the analysis. The channels Alexa fluor 700 (CD3) and APC-Cy7 (CD8) was used to identify the CD8+ T cell subtypes. Using the channels for CCR7 and CD45RA, T_N, T_{EM}, T_{CM} and T_{EMRA} were then identified from the CD8+ T cell subtypes.*

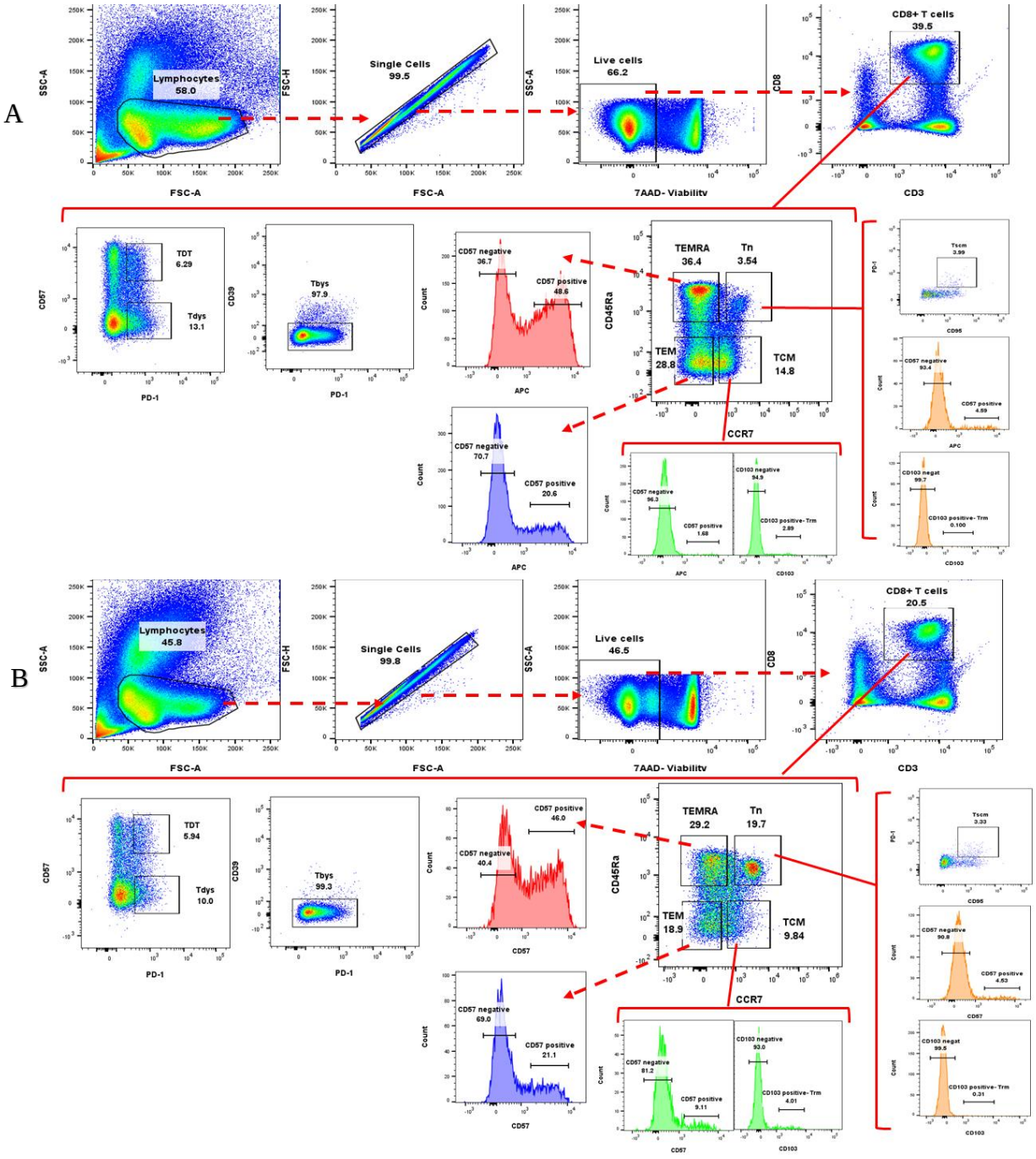

Figure 23. Analysis of frozen sample from Donor 3 (A) and Donor 4 (B) using CD8+ subtype panel. *Comprehensive surface marker screening in PBMCs from healthy donors. PBMCs were isolated using the density gradient Lymphoprep. The isolated PBMCs were then stained with an antibody cocktail mix (CD3, CD8, CD45RA, CCR7, CD57, CD279 (PD-1), CD39, CD103 and CD95). The sample was then analyzed according to the gating strategy demonstrated in Figure 11. The first gate selects lymphocytes eliminating monocytes, and cell debris. This is followed by gates to eliminate doublets and dead cells using 7AAD from the analysis. The channels Alexa fluor 700 (CD3) and APC-Cy7 (CD8) was used to identify the CD8+ T cell subtypes. Using the channels for CCR7 and CD45RA, T_N, T_{EM}, T_{CM} and T_{EMRA} were then identified from the CD8+ T cell subtypes.*

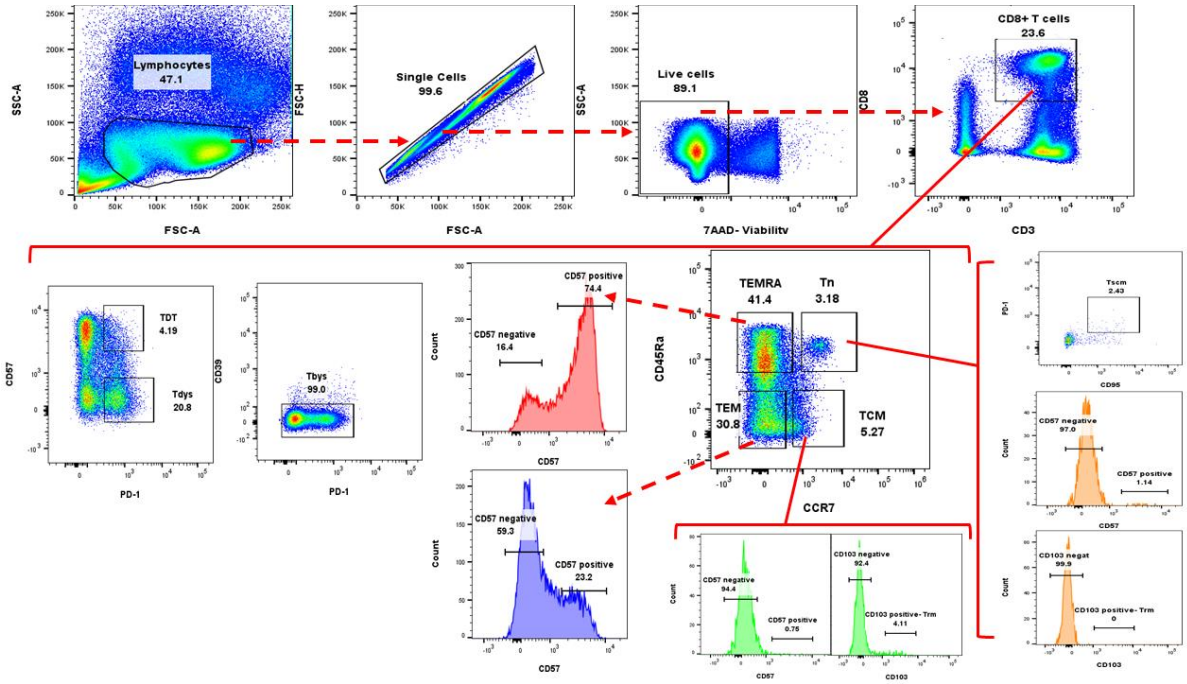

Figure 24. Analysis of frozen sample from Donor 3 (A) and Donor 4 (B) using CD8+ subtype panel. *Comprehensive surface marker screening in PBMCs from healthy donors. PBMCs were isolated using the density gradient Lymphoprep. The isolated PBMCs were then stained with an antibody cocktail mix (CD3, CD8, CD45RA, CCR7, CD57, CD279 (PD-1), CD39, CD103 and CD95). The sample was then analyzed according to the gating strategy demonstrated in Figure 11. The first gate selects lymphocytes eliminating monocytes, and cell debris. This is followed by gates to eliminate doublets and dead cells using 7AAD from the analysis. The channels Alexa fluor 700 (CD3) and APC-Cy7 (CD8) was used to identify the CD8+ T cell subtypes. Using the channels for CCR7 and CD45RA, T_N, T_{EM}, T_{CM} and T_{EMRA} were then identified from the CD8+ T cell subtypes.*

After gating the different CD8+ subtypes from the fresh and frozen samples, the counts were used to plot a graph (Figure 25). This was to provide a better overview, and to make it easier to assess the effects of cryopreservation on the samples. The raw data values can be found in Appendix II (Table A4). The graph shows that there is difference between the donors when using either fresh (red) or frozen (blue) samples.

The statistical analysis showed that only T_{EMRA} subtype had normal distribution and met all the assumptions for using a paired sample t-test. Paired sample t-test showed that the p-value for T_{EMRA} is p= 0.003 meaning that the difference between fresh and frozen is statistically significant. This is reflected in the graph (Figure 25), as we see that the T_{EMRA} subtype increased after cryopreservation. The subtypes T_N, T_{CM}, T_{EM}, T_{RM}, T_{dys}, T_{DT} and T_{bys} had normal distribution, but did not meet all the assumptions for a paired sample t-test as there were outliers. The T_{SCM} subtype did not have normal distribution. Therefore, the Wilcoxon signed-rank analysis was used for these subtypes, and it showed the following results: T_N p=0.043, T_{SCM} p=0.043, T_{CM} p=0.225, T_{EM} p=0.138, T_{dys} p=0.225, T_{DT} p=0.225, T_{bys} p=0.043. If the p-

value is greater than 0.05 then the difference was considered statistically insignificant, while if it was lower than 0.05 then it was considered statistically significant.

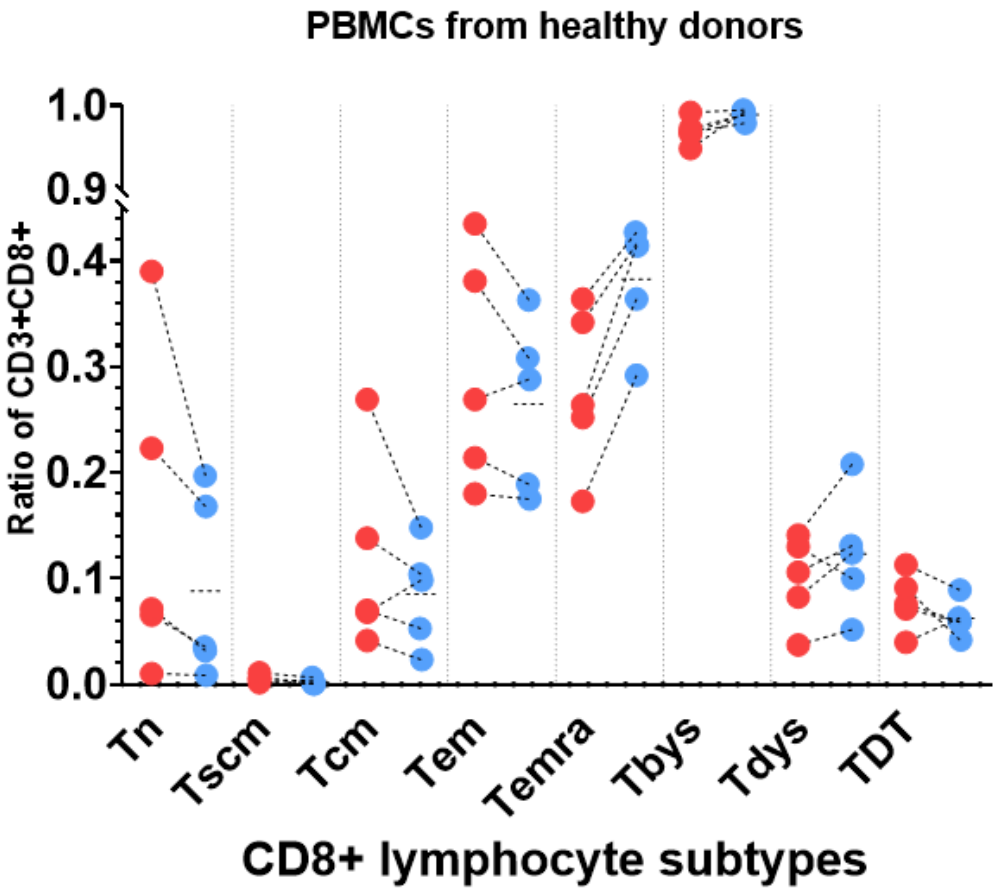

Figure 25. CD8+ T lymphocyte subtypes in Donors 1 – Donors 5. *The acquired data from analyzing the fresh and frozen samples from Donors 1 to Donors 5 are plotted. Fresh samples are shown in red and frozen samples are shown in blue. The lines between the red and blue points shows the subtypes before and after cryopreservation from the same donor (paired samples). The numbers are based on the subtypes/CD8 T cell ratio. Statistical calculations were performed with non-parametric Wilcoxon signed-rank analysis comparing fresh (red) and frozen (blue)The p-value for the subtypes is:* T_N *p=0.043,* T_{SCM} *p=0.043,* T_{CM} *p=0.225,* T_{EM} *p=0.138,* T_{bys} *p=0.043,* T_{dys} *p=0.225,* T_{DT} *p=0.225.* T_{EMRA} *had a normal distribution and therefore a paired sample t-test was run, the p= 0.003.*

4.4 Phenotyping using expanded lymphocyte panel

In addition to CD8+ lymphocytes, there are other lymphocytes subtypes that have a role in cancer, e.g., CD4+ T cells, T_{regs}, B cells, NK cells and NKT cells. These cells can be characterized and distinguished by their surface markers as described in Table 2. These subtypes were gated based on this characterization and according to the gating strategy shown in Figure 12. The results for the fresh samples from Donor 1-Donor 5 are shown in Figures 26-28, while the results for the frozen samples from Donor1- Donor 5 are shown in Figures 29-31.

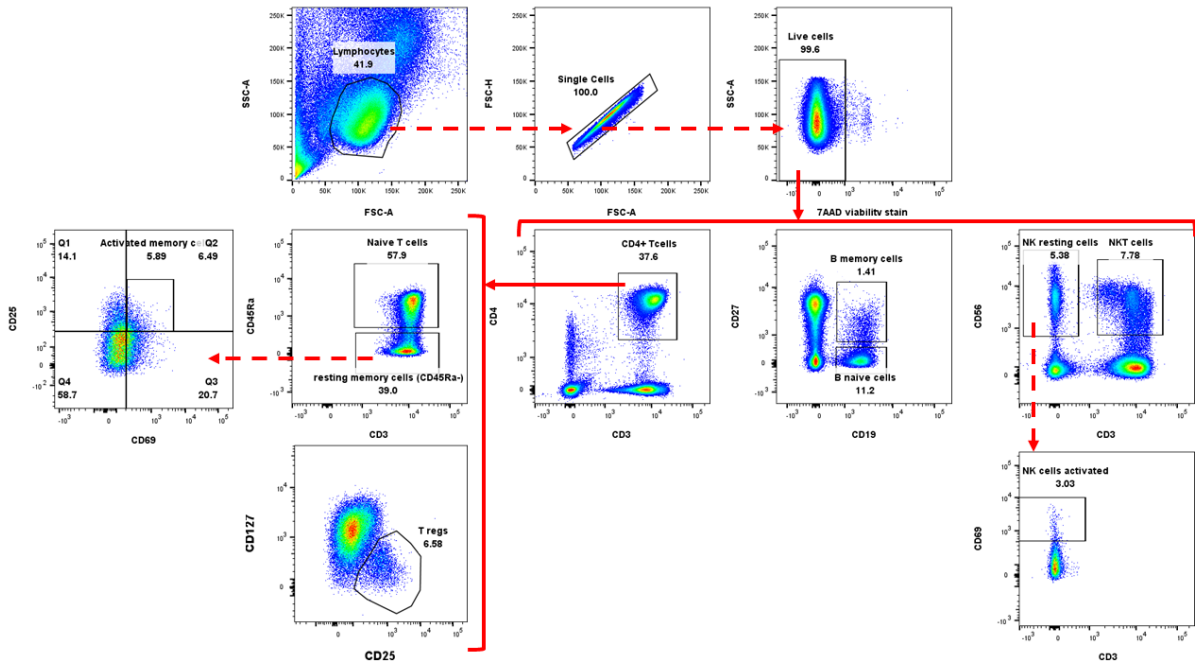

Figure 26. Analysis of fresh samples from Donor 1. *Immune cells are gated based on the FSC-A and SSC-A, and single cells are selected using FSC-A and FSC-H. Live cells are selected based on their negative stain for 7AAD. From the live cells, CD4+ T cells, B cells and NK cells are gated based on their markers. CD4+ T cells are gated based on the CD3+CD4+ markers, and from them naïve T cells, memory cells and Tregs can be identified. Based on the expression of CD45RA, it can be distinguished between CD4+ naïve T cells (CD3+CD4+CD45RA+) and CD4+ memory cells (CD3+CD4+CD45RA-). CD4+ memory cells can be further divided into resting and activated when gating on CD3+CD4+CD45RA-, and further using CD69 and CD25 markers. Activated memory cells are CD25+ and CD69+ while resting memory cells express CD25 and CD69 at different levels . Tregs can be gated based on their positivity for CD25 marker and negativity for the surface marker CD127. B cells can be divided into naïve and memory cells using the markers CD19 and CD27, B naïve cells are CD19+CD27- while B memory cells are CD19+CD27+. NK cells and NK T cells can be gated on CD3 and CD56, NK cells are CD3-CD56+ while NK T cells are CD3+CD56+, activated NK cells can be gated from the NK cells using the marker CD69.*

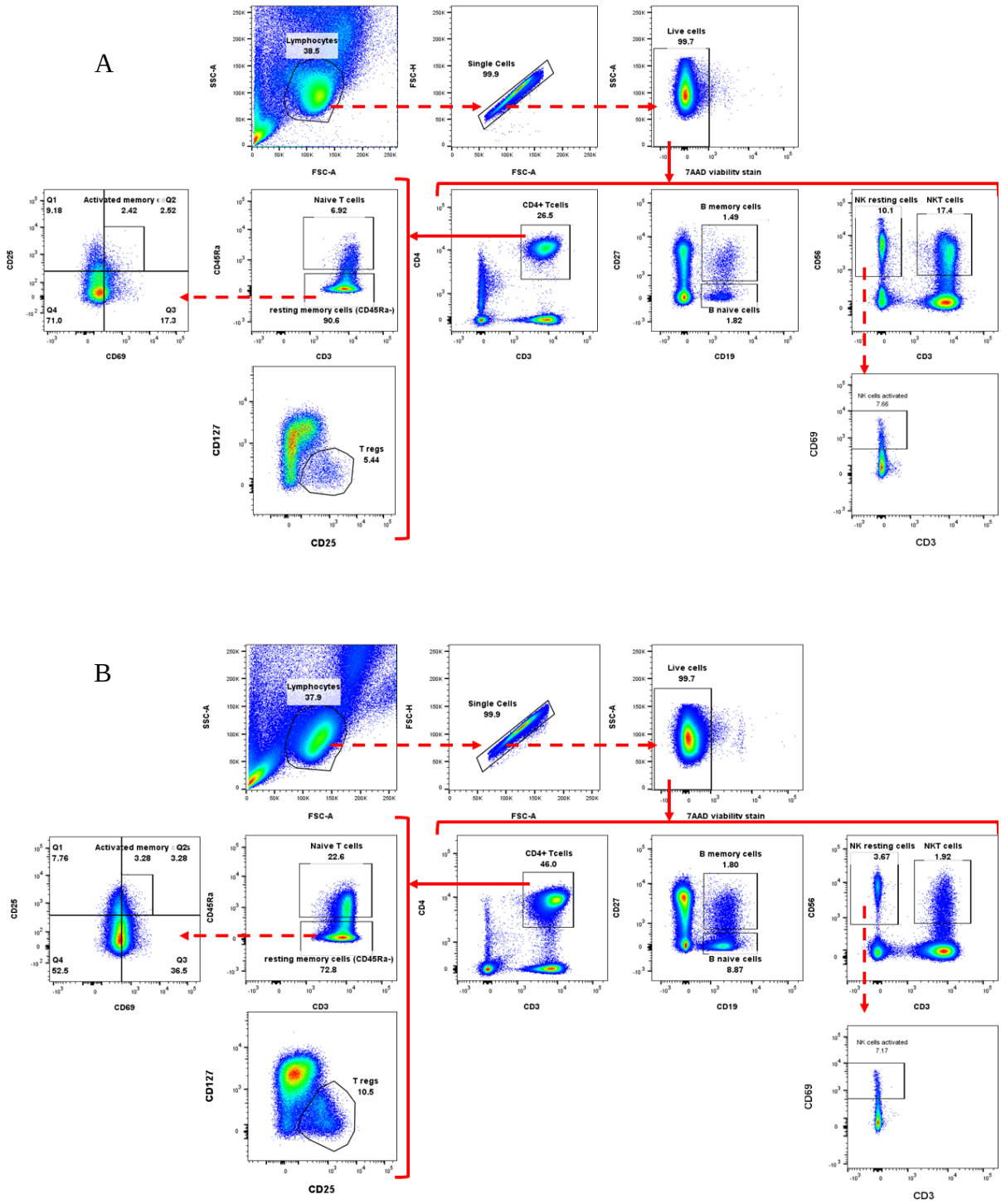

Figure 27. Analysis of fresh samples from Donor 2 (A) & Donor 3 (B). *Immune cells are gated based on the FSC-A and SSC-A, and single cells are selected using FSC-A and FSC-H. Live cells are selected based on their negative stain for 7AAD. From the live cells, CD4+ T cells, B cells and NK cells are gated based on their markers. CD4+ T cells are gated based on the CD3+CD4+ markers, and from them naïve T cells, memory cells and Tregs can be identified. Based on the expression of CD45RA, it can be distinguished between CD4+ naïve T cells (CD3+CD4+CD45RA+) and CD4+ memory cells (CD3+CD4+CD45RA-). CD4+ memory cells can be further divided into resting and activated when gating on CD3+CD4+CD45RA-, and further using CD69 and CD25 markers. Activated memory cells are CD25+ and CD69+ while resting memory cells express CD25 and CD69 at different levels . Tregs can be gated based on their positivity for CD25 marker and negativity for the surface marker CD127. B cells can be divided into naïve and memory cells using the markers CD19 and CD27, B naïve cells are CD19+CD27- while B memory cells are CD19+CD27+. NK cells and NK T cells can be gated on CD3 and CD56, NK cells are CD3-CD56+ while NK T cells are CD3+CD56+, activated NK cells can be gated from the NK cells using the marker CD69.*

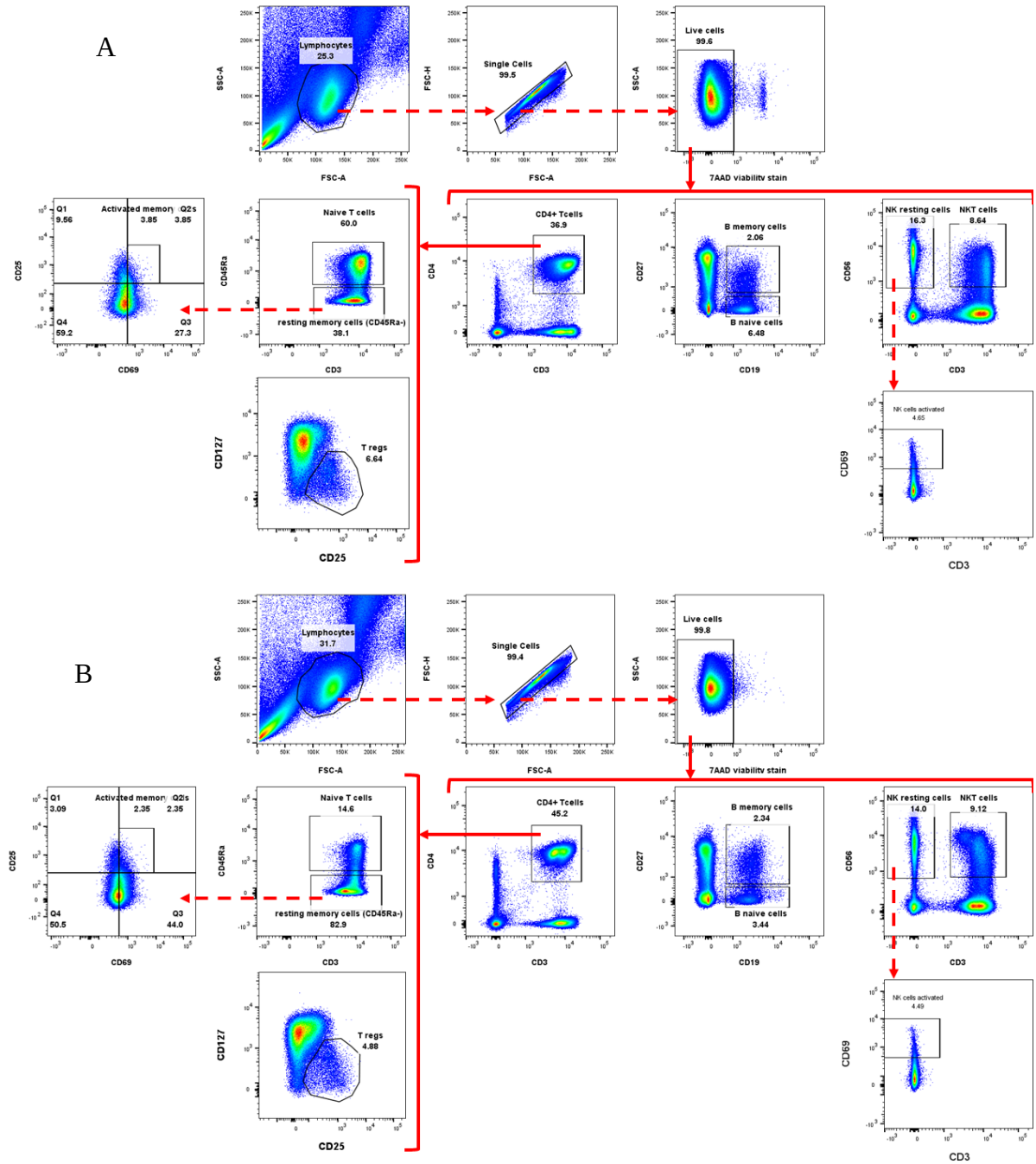

Figure 28. Analysis of fresh samples from Donor 4 (A) & Donor 5 (B). *Immune cells are gated based on the FSC-A and SSC-A, and single cells are selected using FSC-A and FSC-H. Live cells are selected based on their negative stain for 7AAD. From the live cells, CD4+ T cells, B cells and NK cells are gated based on their markers. CD4+ T cells are gated based on the CD3+CD4+ markers, and from them naïve T cells, memory cells and Tregs can be identified. Based on the expression of CD45RA, it can be distinguished between CD4+ naïve T cells (CD3+CD4+CD45RA+) and CD4+ memory cells (CD3+CD4+CD45RA-). CD4+ memory cells can be further divided into resting and activated when gating on CD3+CD4+CD45RA-, and further using CD69 and CD25 markers. Activated memory cells are CD25+ and CD69+ while resting memory cells express CD25 and CD69 at different levels . Tregs can be gated based on their positivity for CD25 marker and negativity for the surface marker CD127. B cells can be divided into naïve and memory cells using the markers CD19 and CD27, B naïve cells are CD19+CD27- while B memory cells are CD19+CD27+. NK cells and NK T cells can be gated on CD3 and CD56, NK cells are CD3-CD56+ while NK T cells are CD3+CD56+, activated NK cells can be gated from the NK cells using the marker CD69.*

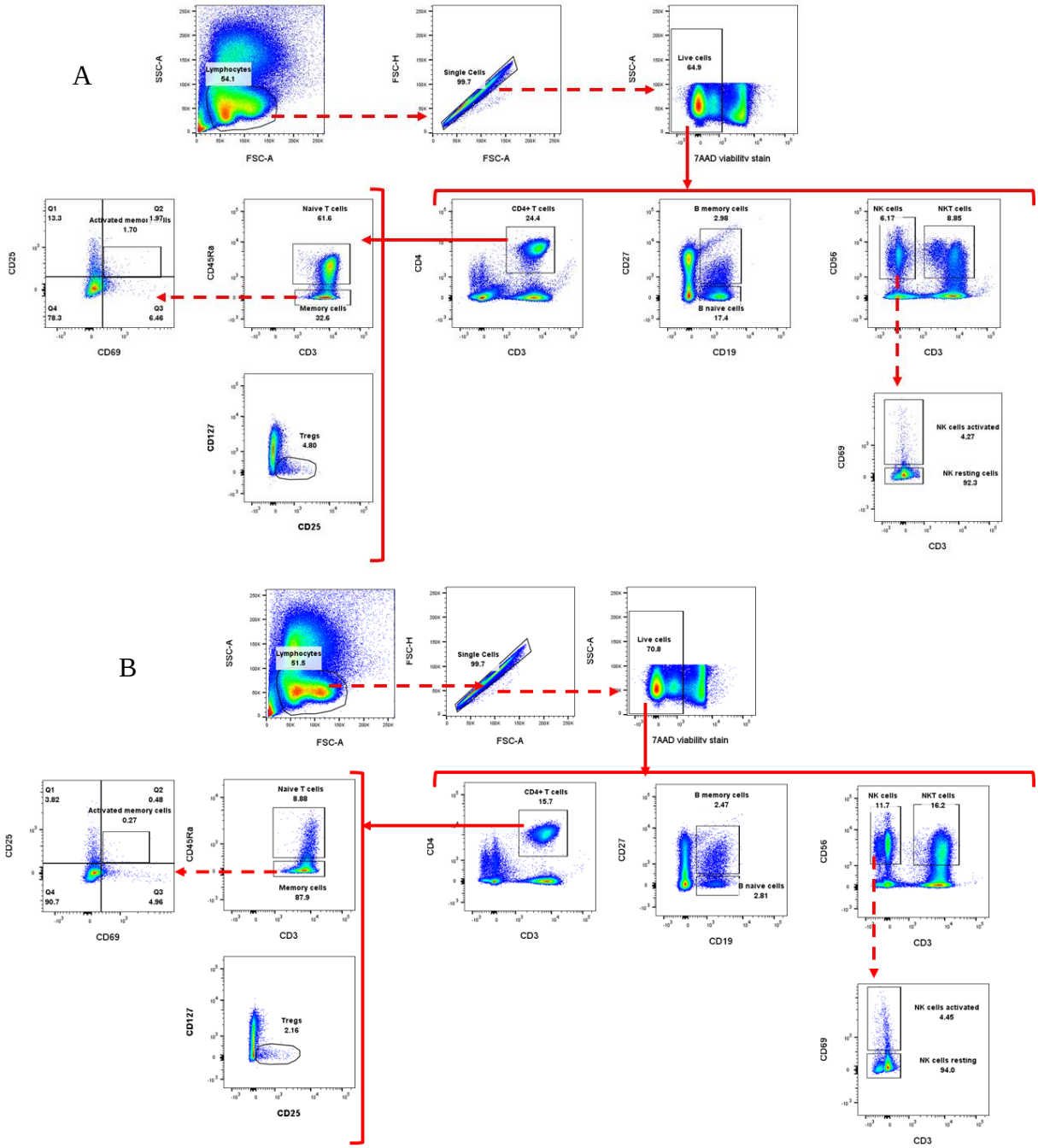

Figure 29. Analysis of frozen samples from Donor 1 (A) & Donor 2 (B). *Immune cells are gated based on the FSC-A and SSC-A, and single cells are selected using FSC-A and FSC-H. Live cells are selected based on their negative stain for 7AAD. From the live cells, CD4+ T cells, B cells and NK cells are gated based on their markers. CD4+ T cells are gated based on the CD3+CD4+ markers, and from them naïve T cells, memory cells and Tregs can be identified. Based on the expression of CD45RA, it can be distinguished between CD4+ naïve T cells (CD3+CD4+CD45RA+) and CD4+ memory cells (CD3+CD4+CD45RA-). CD4+ memory cells can be further divided into resting and activated when gating on CD3+CD4+CD45RA-, and further using CD69 and CD25 markers. Activated memory cells are CD25+ and CD69+ while resting memory cells express CD25 and CD69 at different levels . Tregs can be gated based on their positivity for CD25 marker and negativity for the surface marker CD127. B cells can be divided into naïve and memory cells using the markers CD19 and CD27, B naïve cells are CD19+CD27- while B memory cells are CD19+CD27+. NK cells and NK T cells can be gated on CD3 and CD56, NK cells are CD3-CD56+ while NK T cells are CD3+CD56+, activated NK cells can be gated from the NK cells using the marker CD69.*

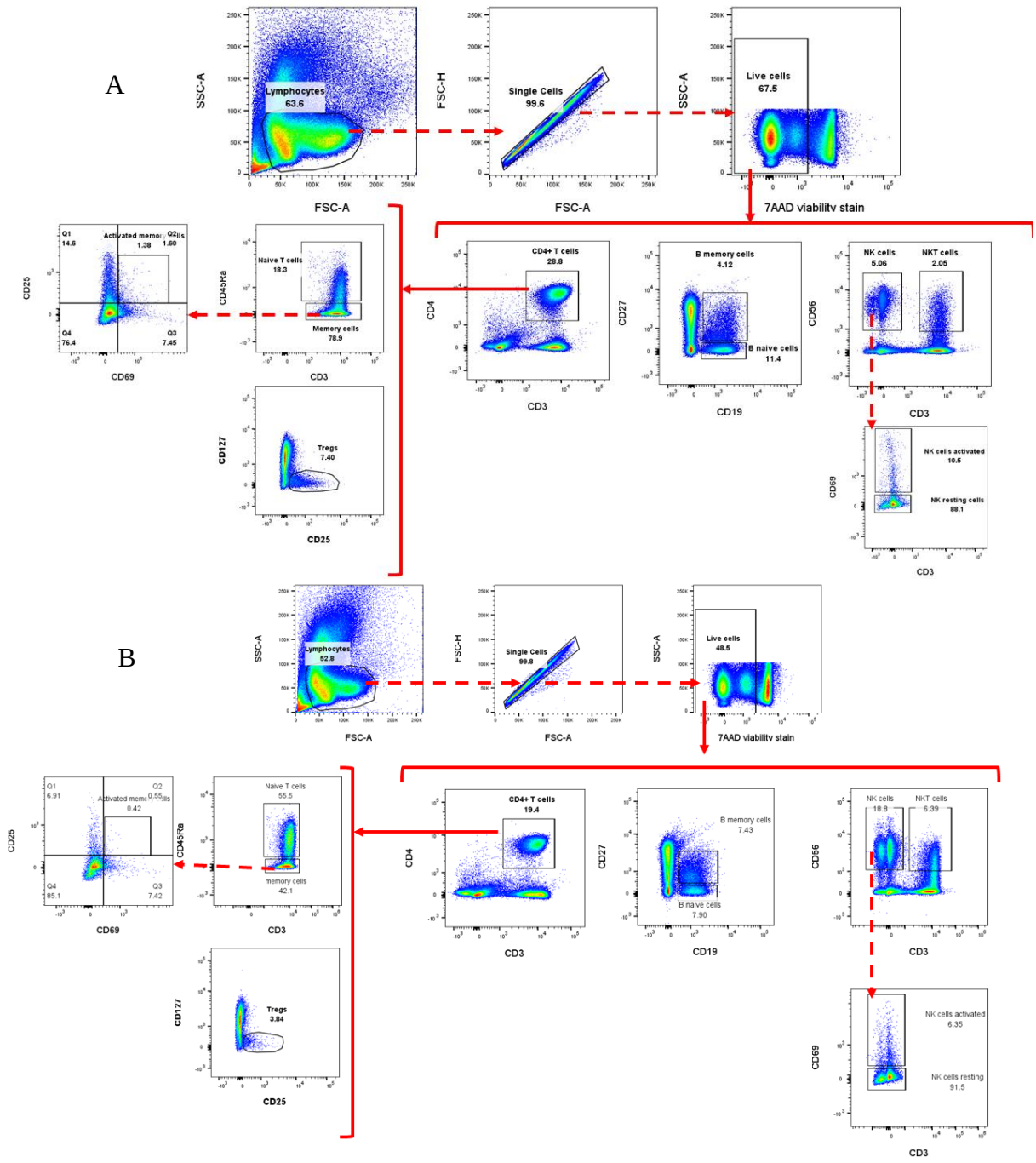

***Figure 30**. **Analysis of frozen samples from Donor 3 (A) & Donor 4 (B).** Immune cells are gated based on the FSC-A and SSC-A, and single cells are selected using FSC-A and FSC-H. Live cells are selected based on their negative stain for 7AAD. From the live cells, CD4+ T cells, B cells and NK cells are gated based on their markers. CD4+ T cells are gated based on the CD3+CD4+ markers, and from them naïve T cells, memory cells and Tregs can be identified. Based on the expression of CD45RA, it can be distinguished between CD4+ naïve T cells (CD3+CD4+CD45RA+) and CD4+ memory cells (CD3+CD4+CD45RA-). CD4+ memory cells can be further divided into resting and activated when gating on CD3+CD4+CD45RA-, and further using CD69 and CD25 markers. Activated memory cells are CD25+ and CD69+ while resting memory cells express CD25 and CD69 at different levels . Tregs can be gated based on their positivity for CD25 marker and negativity for the surface marker CD127. B cells can be divided into naïve and memory cells using the markers CD19 and CD27, B naïve cells are CD19+CD27- while B memory cells are CD19+CD27+. NK cells and NK T cells can be gated on CD3 and CD56, NK cells are CD3-CD56+ while NK T cells are CD3+CD56+, activated NK cells can be gated from the NK cells using the marker CD69.*

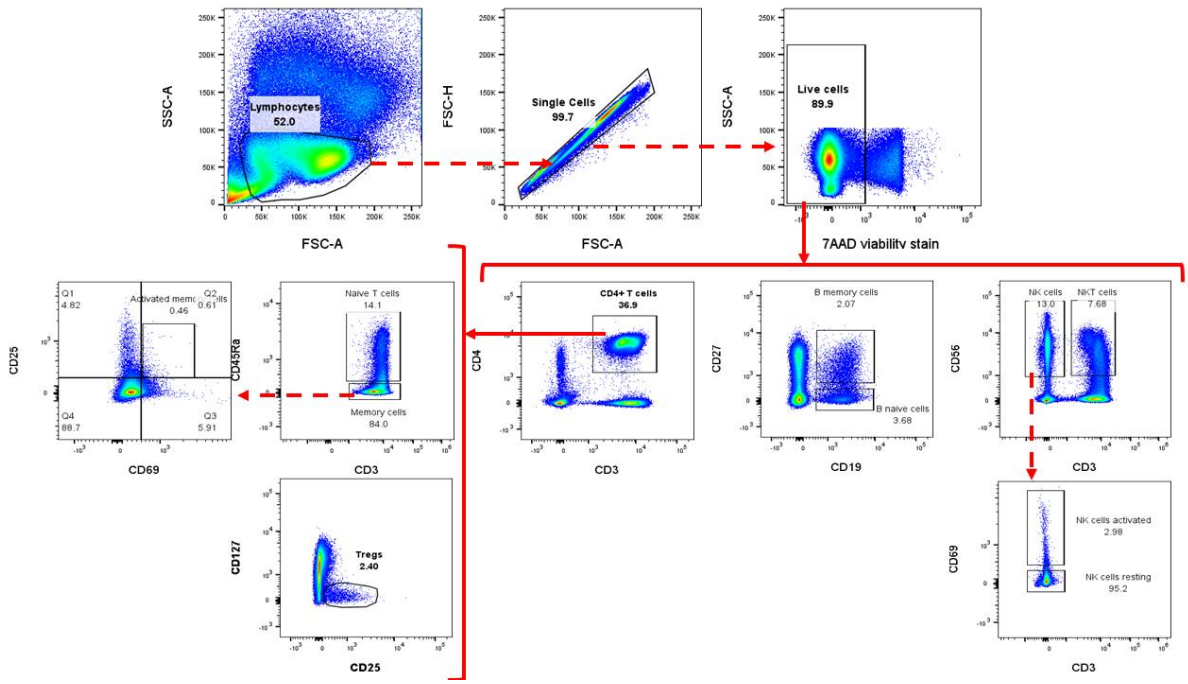

Figure 31. Analysis of frozen samples from Donor 5*. Immune cells are gated based on the FSC-A and SSC-A, and single cells are selected using FSC-A and FSC-H. Live cells are selected based on their negative stain for 7AAD. From the live cells, CD4+ T cells, B cells and NK cells are gated based on their markers. CD4+ T cells are gated based on the CD3+CD4+ markers, and from them naïve T cells, memory cells and Tregs can be identified. Based on the expression of CD45RA, it can be distinguished between CD4+ naïve T cells (CD3+CD4+CD45RA+) and CD4+ memory cells (CD3+CD4+CD45RA-). CD4+ memory cells can be further divided into resting and activated when gating on CD3+CD4+CD45RA-, and further using CD69 and CD25 markers. Activated memory cells are CD25+ and CD69+ while resting memory cells express CD25 and CD69 at different levels . Tregs can be gated based on their positivity for CD25 marker and negativity for the surface marker CD127. B cells can be divided into naïve and memory cells using the markers CD19 and CD27, B naïve cells are CD19+CD27- while B memory cells are CD19+CD27+. NK cells and NK T cells can be gated on CD3 and CD56, NK cells are CD3-CD56+ while NK T cells are CD3+CD56+, activated NK cells can be gated from the NK cells using the marker CD69.*

For a better overview, the percentage of each subtype was calculated to see the ratio that they make of the live cell population. These numbers are plotted in the graph shown in Figure 32. The red dots represent the lymphocyte subtypes from the fresh samples while the blue dots represent the subtypes from the frozen samples. We can see that the percentage of most subtypes decreased following cryopreservation.

Statistical analyses were conducted to examine if the differences between the fresh and frozen samples were statistically significant. We examined whether the subtypes met all the assumptions for a paired t-test including having a normal distribution. The subtypes that met all the assumptions were CD4+ T cells, T_N, activated memory T cells and NKT cells. Therefore, we used the paired t-test to calculate their p-values: CD4+ T cells p=0.055, T_N p=0.056, CD4+ activated memory T cells p=0.939 and NKT cells p=0.007. The remaining subtypes: CD4+ resting memory cells, T_{regs} , B_N, B_M, and NK cells did not meet all the assumptions for a paired

sample t-test. Therefore, the Wilcoxon signed-rank analysis was used, and it showed the following results: CD4+ resting memory cells p=0.097, T_{regs} p=0.043, B_N p=0.043, B_M p=0.043, NK resting cells p=0.5, and NK activated cells p= 0.686. If the p-value is greater than 0.05, then the difference was considered statistically insignificant. While if it was lower than 0.05, then it was considered statistically significant. The raw data values used to plot the graph shown in Figure 32. can be found in Appendix II (Table A5).

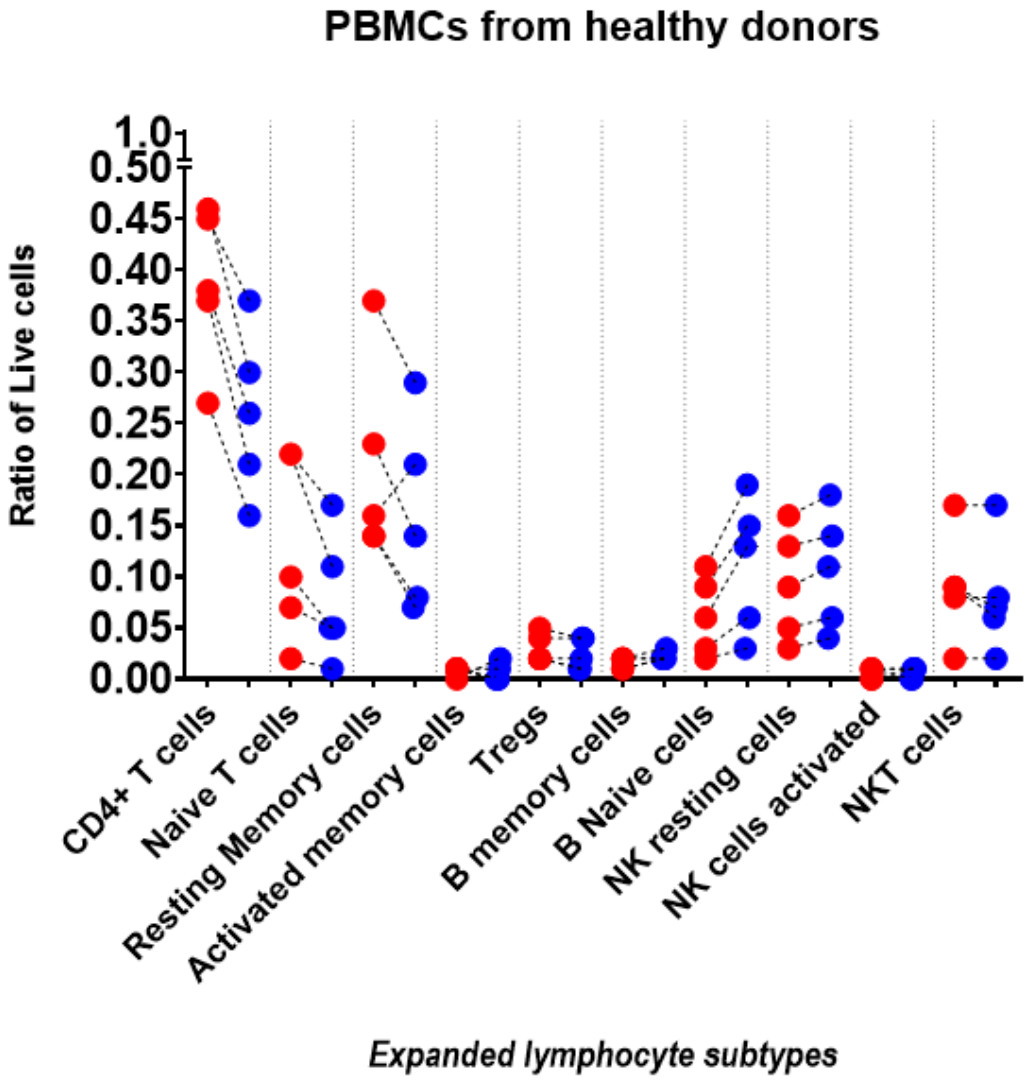

Figure 32. Expanded lymphocyte subtypes in Donors 1 – Donors 5. *The acquired data from analyzing the fresh and frozen samples from Donors 1 to Donors 5 are plotted. Fresh samples are shown in red and frozen samples are shown in blue. The lines between the red and blue points show the subtypes before and after cryopreservation from the same donors (paired samples). The numbers are based on the subtypes/Live cell ratio. Statistical calculations were performed with non-parametric Wilcoxon signed-rank analysis comparing fresh (red) and frozen (blue). The p-value for CD4+ resting memory cells p=0.097, T_{regs} p=0.043, B_N p=0.043, B_M p=0.043, NK resting cells p=0.5, and NK activated cells p= 0.686. Paired t-test was performed for the following subtypes meeting all the test assumption: CD4+ T cells p=0.055, T_N p=0.056, CD4+ activated memory T cells p=0.939 and NKT cells p=0.007.*

4.5 Pilot experiment on NSCLC patient samples

To validate the established protocol, we ran a pilot experiment on four NSCLC patient samples. Both panels were run, and the results gated and analyzed according to the surface marker characterizations (Table 5 and Table 6). The gating strategies shown Figure 11 and Figure 12.

4.5.1 CD8+ subtype panel (panel 1)

The gating results from running the CD8+ subtype panel on the randomly selected NSCLC patient samples (TNMI 30, 40, 58, and 95) are shown in Figures 33-36, respectively. Similarly to the healthy donor samples, there were high inter-patient variations in the distribution of the T_{EM} and T_{EMRA} subtypes (Figure 37). Since the number of patients included in this pilot is small and only done for methodological validation, a statistical analysis was not conducted.

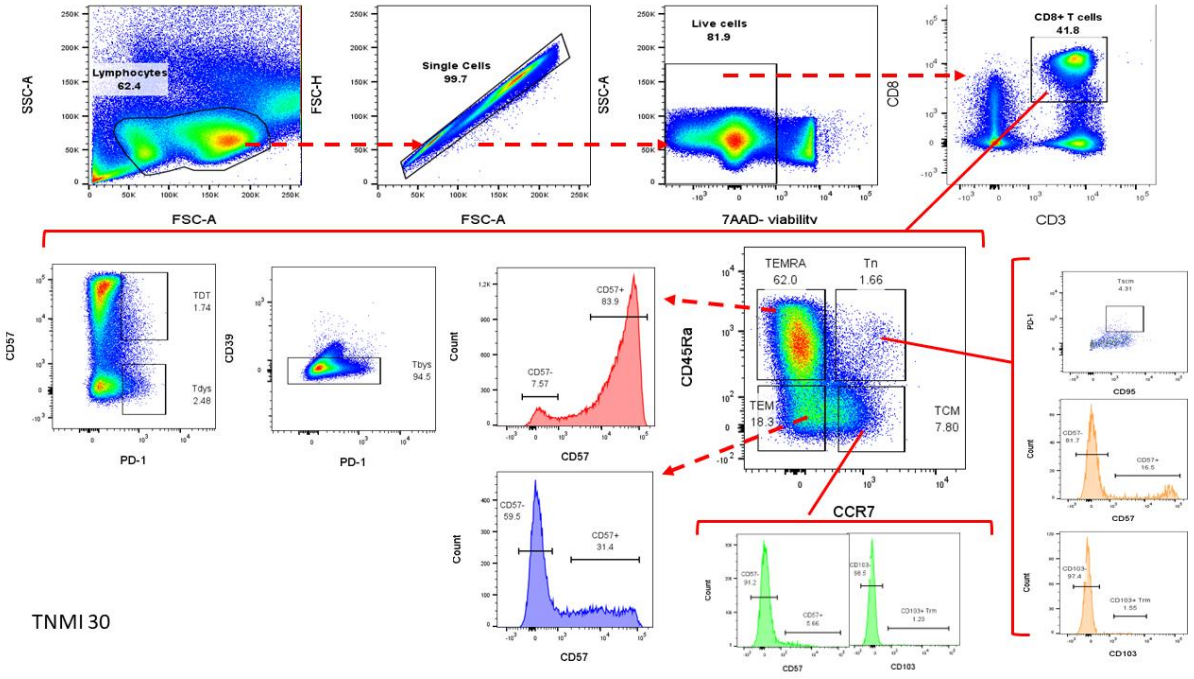

Figure 33. Gating results of a NSCLC patient TNMI 30 using panel 1. *The CD8+ subtype panel was run on a NSCLC patient sample. PBMCs were isolated using the density gradient medium Lymphoprep. The isolated PBMCs were then stained with an antibody cocktail mix (CD3, CD8, CD45RA, CCR7, CD57, CD279 (PD-1), CD39, CD103 and CD95). The sample was then analyzed according to the gating strategy demonstrated in Figure 11. The first gate selects lymphocytes eliminating monocytes, and cell debris. This is followed by gates to eliminate doublets and dead cells using 7AAD from the analysis.*

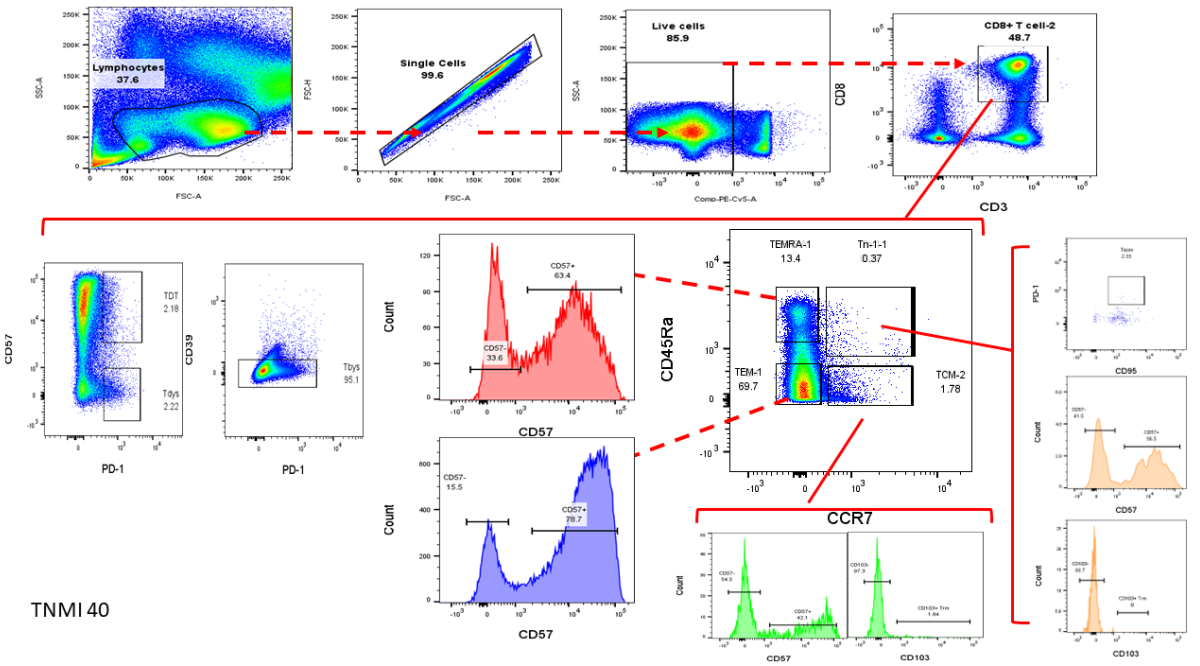

Figure 34. Gating results of a NSCLC patient TNMI 40 using panel 1. The CD8+ subtype panel was run on a NSCLC patient sample. PBMCs were isolated using the density gradient medium Lymphoprep. The isolated PBMCs were then stained with an antibody cocktail mix (CD3, CD8, CD45RA, CCR7, CD57, CD279 (PD-1), CD39, CD103 and CD95). The sample was then analyzed according to the gating strategy demonstrated in Figure 11. The first gate selects lymphocytes eliminating monocytes, and cell debris. This is followed by gates to eliminate doublets and dead cells using 7AAD from the analysis.

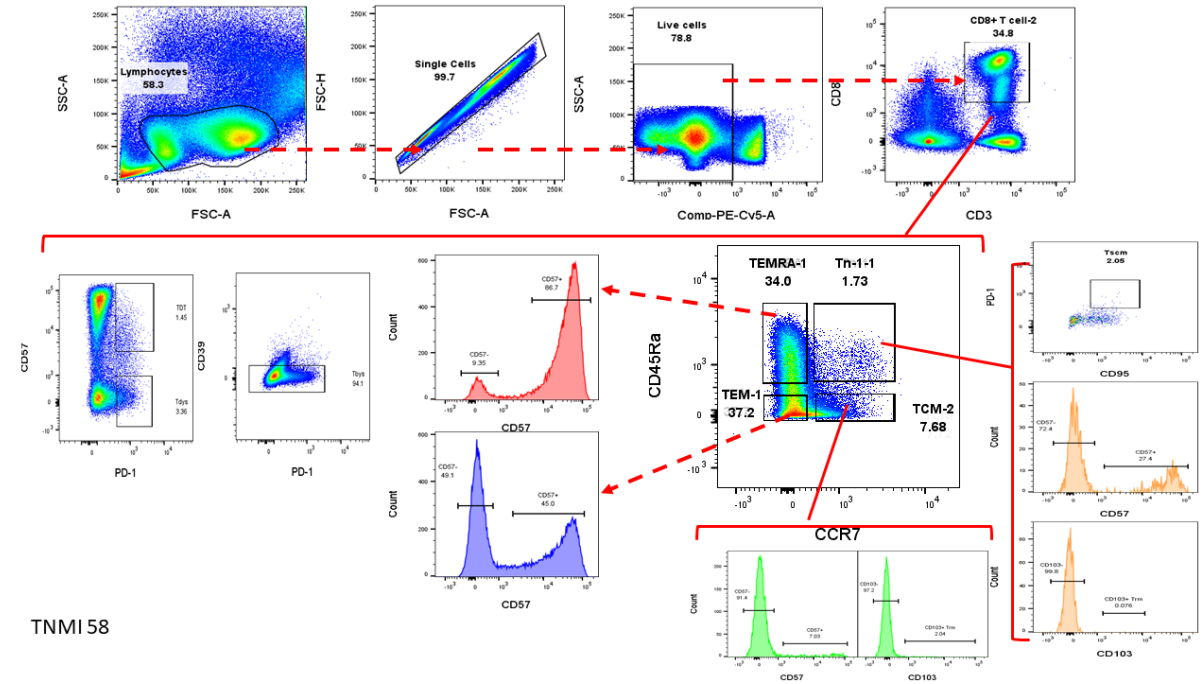

Figure 35. Gating results of a NSCLC patient TNMI 58 using panel 1. *The CD8+ subtype panel was run on a NSCLC patient sample. PBMCs were isolated using the density gradient medium Lymphoprep. The isolated PBMCs were then stained with an antibody cocktail mix (CD3, CD8, CD45RA, CCR7, CD57, CD279 (PD-1), CD39, CD103 and CD95). The sample was then analyzed according to the gating strategy demonstrated in Figure 11. The first gate selects lymphocytes eliminating monocytes, and cell debris. This is followed by gates to eliminate doublets and dead cells using 7AAD from the analysis.*

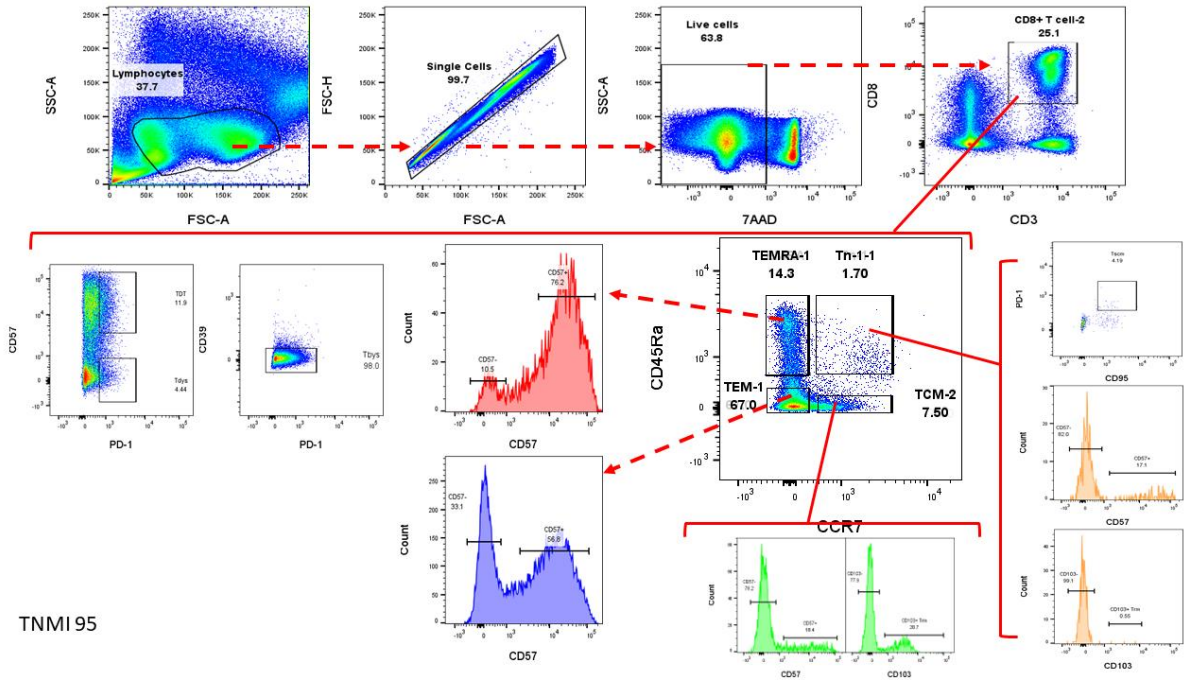

Figure 36. Gating results of a NSCLC patient TNMI 95 using panel 1. *The CD8+ subtype panel was run on a NSCLC patient sample. PBMCs were isolated using the density gradient medium Lymphoprep. The isolated PBMCs were then stained with an antibody cocktail mix (CD3, CD8, CD45RA, CCR7, CD57, CD279 (PD-1), CD39, CD103 and CD95). The sample was then analyzed according to the gating strategy demonstrated in Figure 11. The first gate selects lymphocytes eliminating monocytes, and cell debris. This is followed by gates to eliminate doublets and dead cells using 7AAD from the analysis.*

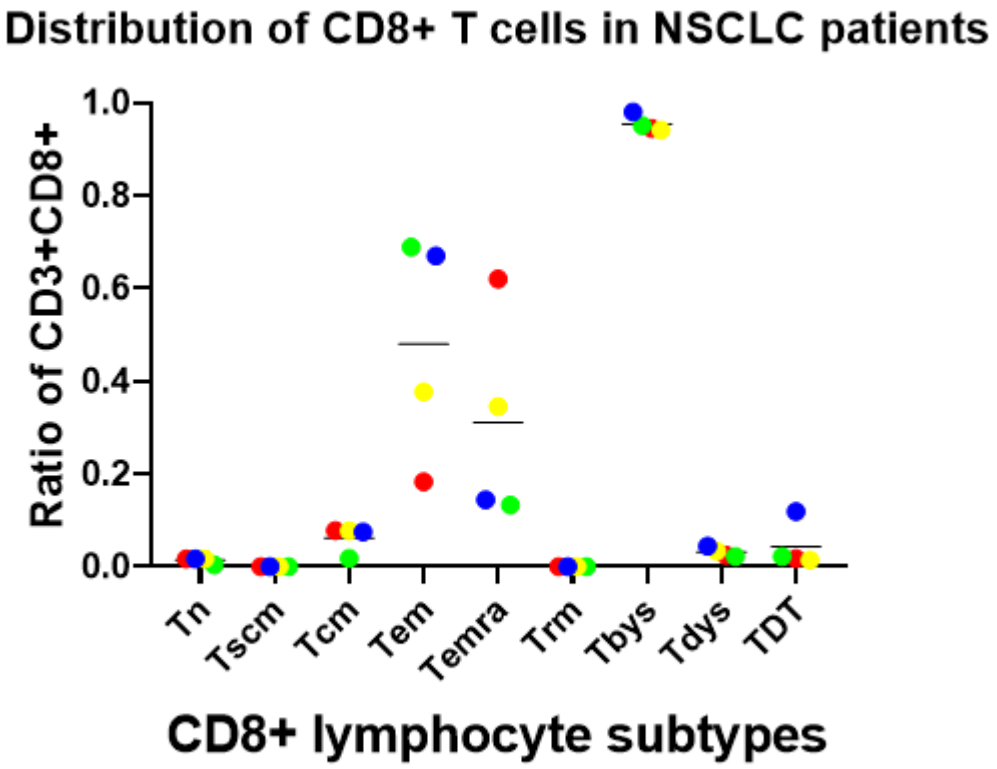

Figure 37. Distribution of CD8 + T cell subtypes in NSCLC patients*. Each point represents data from one patient, the patient's data are shown in different colors. Patient 1=red (age 85), patient 2= green (age 40), patient 3= purple (age 47), patient 4= blue(age 49). The different subtypes were calculated as a ratio of CD8+ T cells.*

4.5.2 Expanded lymphocyte panel (panel 2)

We also ran the second panel on the NSCLC patient samples to validate the established protocol. We chose the same NSCLC patient samples as for panel 1 (TNMI 30, 40, 58 and 95) and the gating results are shown in Figures 38-41, respectively. There were quite high inter-patient variations of the lymphocyte subtypes (Figure 42), similar to the healthy donor samples also when using this flow cytometry panel. Since the number of patients included in this pilot is small, a statistical analysis was not conducted.

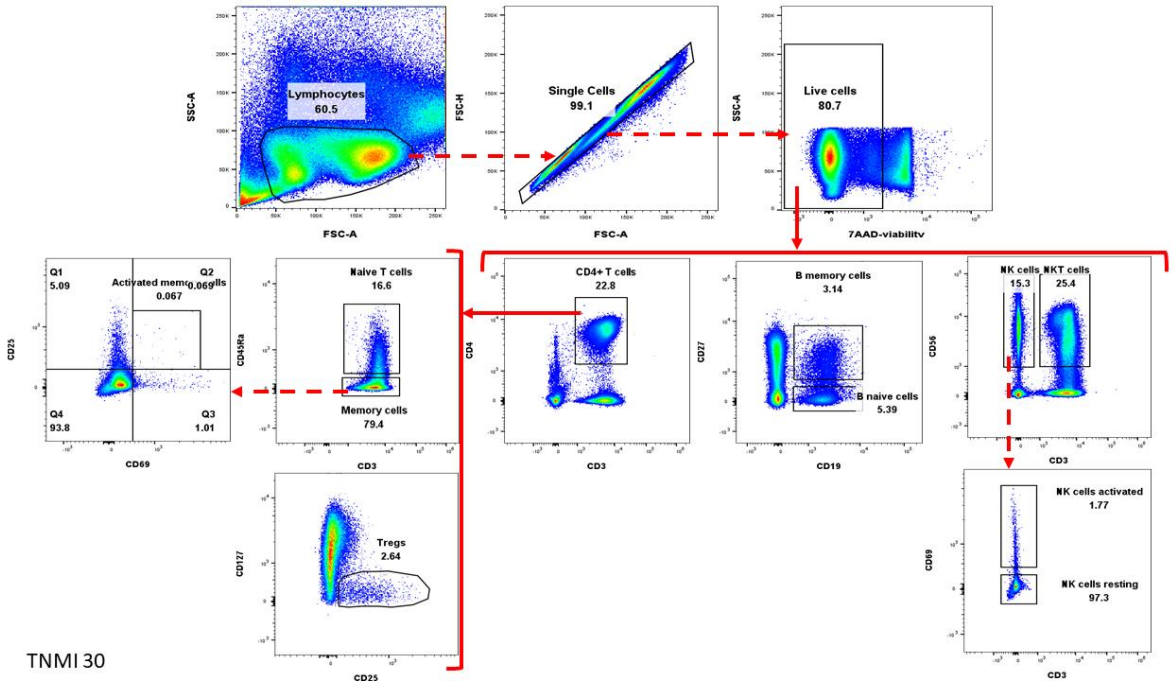

Figure 38. Gating results of a NSCLC patient TNMI 30 using panel 2*. Immune cells are gated based on the FSC-A and SSC-A, and single cells are selected using FSC-A and FSC-H. Live cells are selected based on their negative stain for 7AAD. From the live cells, CD4+ T cells, B cells and NK cells are gated based on their markers. CD4+ T cells are gated based on the CD3+CD4+ markers, and from them naïve T cells, memory cells and Tregs can be identified. Based on the expression of CD45RA, it can be distinguished between CD4+ naïve T cells (CD3+CD4+CD45RA+) and CD4+ memory cells (CD3+CD4+CD45RA-). CD4+ memory cells can be further divided into resting and activated when gating on CD3+CD4+CD45RA-, and further using CD69 and CD25 markers. Activated memory cells are CD25+ and CD69+ while resting memory cells express CD25 and CD69 at different levels . Tregs can be gated based on their positivity for CD25 marker and negativity for the surface marker CD127. B cells can be divided into naïve and memory cells using the markers CD19 and CD27, B naïve cells are CD19+CD27- while B memory cells are CD19+CD27+. NK cells and NK T cells can be gated on CD3 and CD56, NK cells are CD3-CD56.*

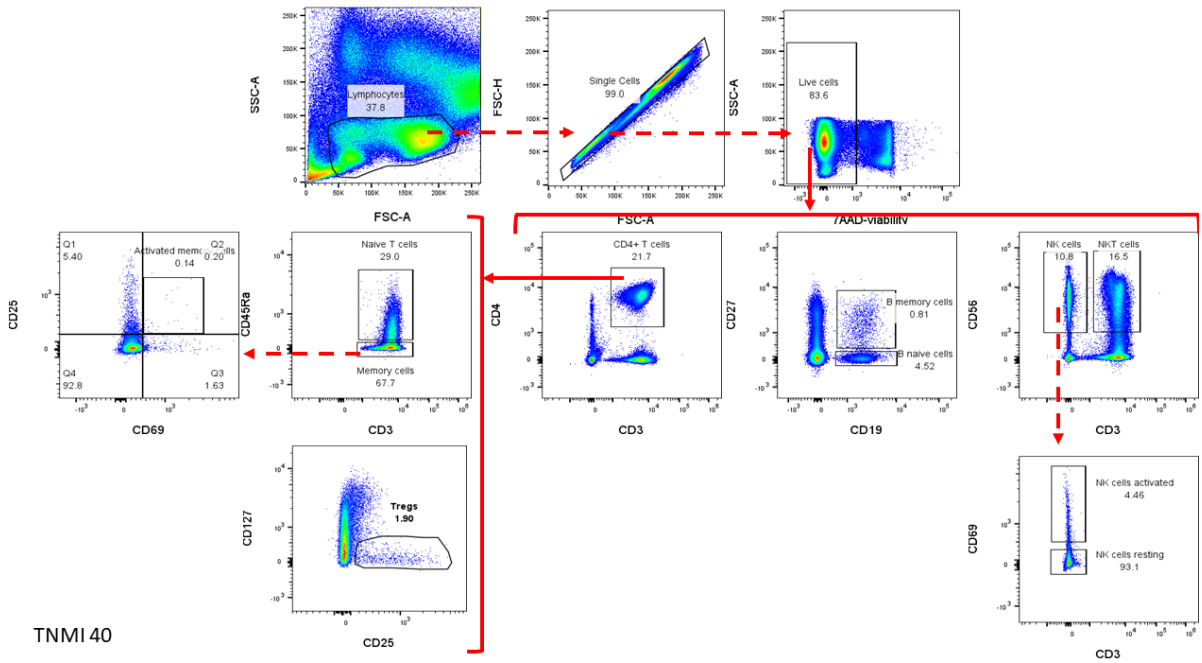

Figure 39. Gating results of a NSCLC patient TNMI 40 using panel 2. *Immune cells are gated based on the FSC-A and SSC-A, and single cells are selected using FSC-A and FSC-H. Live cells are selected based on their negative stain for 7AAD. From the live cells, CD4+ T cells, B cells and NK cells are gated based on their markers. CD4+ T cells are gated based on the CD3+CD4+ markers, and from them naïve T cells, memory cells and Tregs can be identified. Based on the expression of CD45RA, it can be distinguished between CD4+ naïve T cells (CD3+CD4+CD45RA+) and CD4+ memory cells (CD3+CD4+CD45RA-). CD4+ memory cells can be further divided into resting and activated when gating on CD3+CD4+CD45RA-, and further using CD69 and CD25 markers. Activated memory cells are CD25+ and CD69+ while resting memory cells express CD25 and CD69 at different levels . Tregs can be gated based on their positivity for CD25 marker and negativity for the surface marker CD127. B cells can be divided into naïve and memory cells using the markers CD19 and CD27, B naïve cells are CD19+CD27- while B memory cells are CD19+CD27+. NK cells and NK T cells can be gated on CD3 and CD56, NK cells are CD3-CD56.*

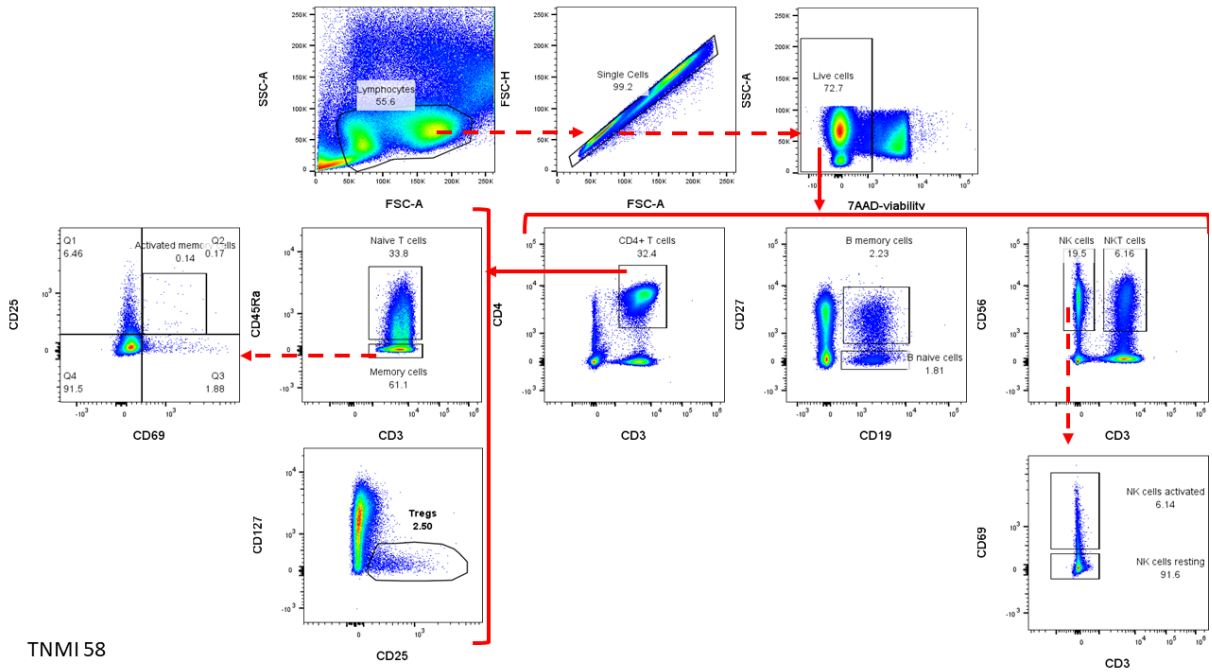

Figure 40. Gating results of a NSCLC patient TNMI 58 using panel 2. *Immune cells are gated based on the FSC-A and SSC-A, and single cells are selected using FSC-A and FSC-H. Live cells are selected based on their negative stain for 7AAD. From the live cells, CD4+ T cells, B cells and NK cells are gated based on their markers. CD4+ T cells are gated based on the CD3+CD4+ markers, and from them naïve T cells, memory cells and Tregs can be identified. Based on the expression of CD45RA, it can be distinguished between CD4+ naïve T cells (CD3+CD4+CD45RA+) and CD4+ memory cells (CD3+CD4+CD45RA-). CD4+ memory cells can be further divided into resting and activated when gating on CD3+CD4+CD45RA-, and further using CD69 and CD25 markers. Activated memory cells are CD25+ and CD69+ while resting memory cells express CD25 and CD69 at different levels . Tregs can be gated based on their positivity for CD25 marker and negativity for the surface marker CD127. B cells can be divided into naïve and memory cells using the markers CD19 and CD27, B naïve cells are CD19+CD27- while B memory cells are CD19+CD27+. NK cells and NK T cells can be gated on CD3 and CD56, NK cells are CD3-CD56.*

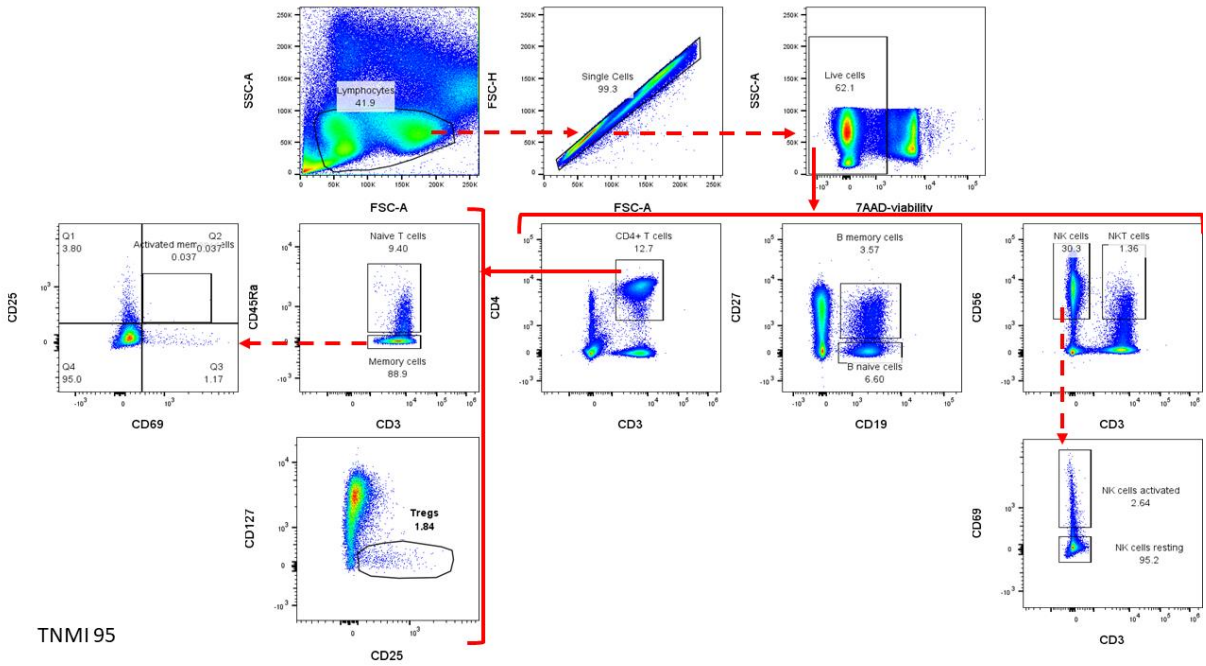

Figure 41. Gating results of a NSCLC patient TNMI 95 using panel 2. Immune cells are gated based on the FSC-A and SSC-A, and single cells are selected using FSC-A and FSC-H. Live cells are selected based on their negative stain for 7AAD. From the live cells, CD4+ T cells, B cells and NK cells are gated based on their markers. CD4+ T cells are gated based on the CD3+CD4+ markers, and from them naïve T cells, memory cells and Tregs can be identified. Based on the expression of CD45RA, it can be distinguished between CD4+ naïve T cells (CD3+CD4+CD45RA+) and CD4+ memory cells (CD3+CD4+CD45RA-). CD4+ memory cells can be further divided into resting and activated when gating on CD3+CD4+CD45RA-, and further using CD69 and CD25 markers. Activated memory cells are CD25+ and CD69+ while resting memory cells express CD25 and CD69 at different levels . Tregs can be gated based on their positivity for CD25 marker and negativity for the surface marker CD127. B cells can be divided into naïve and memory cells using the markers CD19 and CD27, B naïve cells are CD19+CD27- while B memory cells are CD19+CD27+. NK cells and NK T cells can be gated on CD3 and CD56, NK cells are CD3-CD56.

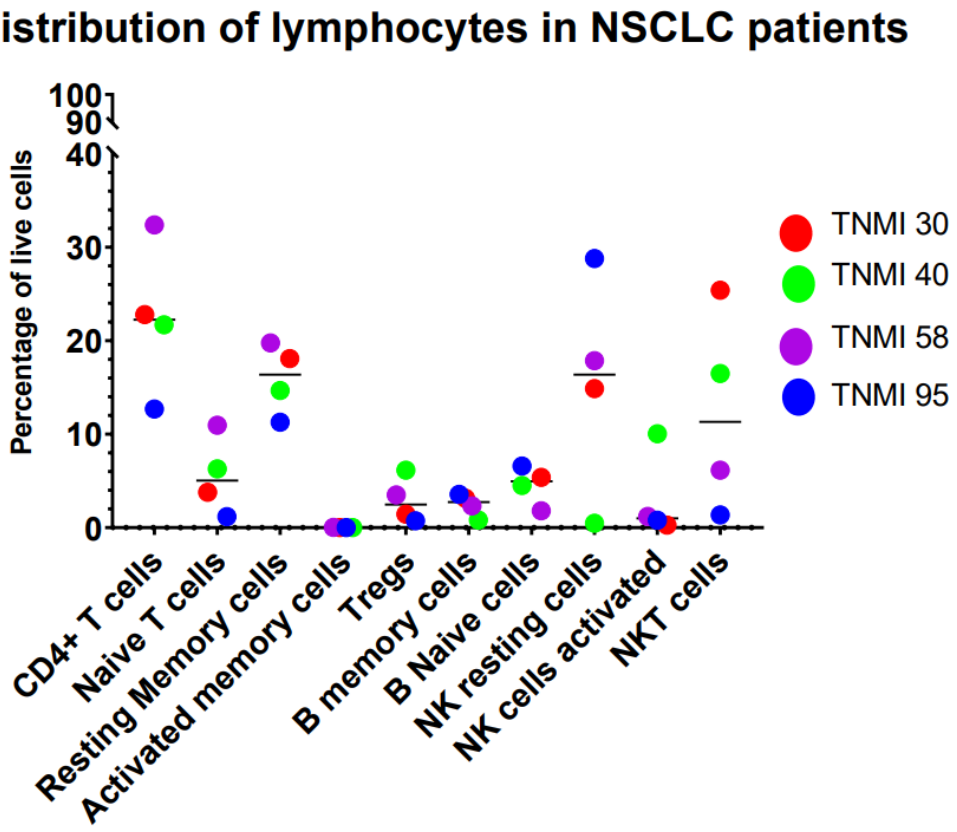

Figure 42. Expanded lymphocyte subtypes in PBMCs of four NSCLC patients. *Each point represents data from one patient, the patient's data are shown in different colors Patient 1=red (age 85), patient 2= green (age 40), patient 3= purple (age 47), patient 4= blue(age 49). The different subtypes were calculated as a ratio of the live cell population.*

4.6 Comparing healthy donor with NSCLC patient samples

The data from the frozen samples belonging to the healthy donors gated with panels 1 and 2 were compared with NSCLC patients' data. The CD8+ T lymphocyte subtypes in healthy donors (red) were compared to those NSCLC patients (green) (Figure 43). The graph shows that all the subtypes except for T_{CM} and T_{EM}, seem to be lower in NSCLC patients. However, the T_{EM} and T_{EMRA} subtypes seem to be higher in NSCLC patient samples.

Similarly, the expanded lymphocyte subtypes in healthy donors (red) were compared to those in NSCLC patients (green) (Figure 44). The graph shows that all the subtypes except Tregs, NK cells and NKT cells seem to be lower in NSCLC patient samples. However, the Tregs, NK cells and NKT cells seem to be higher in NSCLC patients. The patient size is too small to run a statistical analysis to examine the significance of the differences. It also has to be noted that age of the healthy donors and NSCLC patients, in addition to other relevant characteristics are

not taken into account in these graphs. Therefore, other patterns could be observed when a statistical analysis will be conducted, including more individuals and adjusting for relevant characteristics.

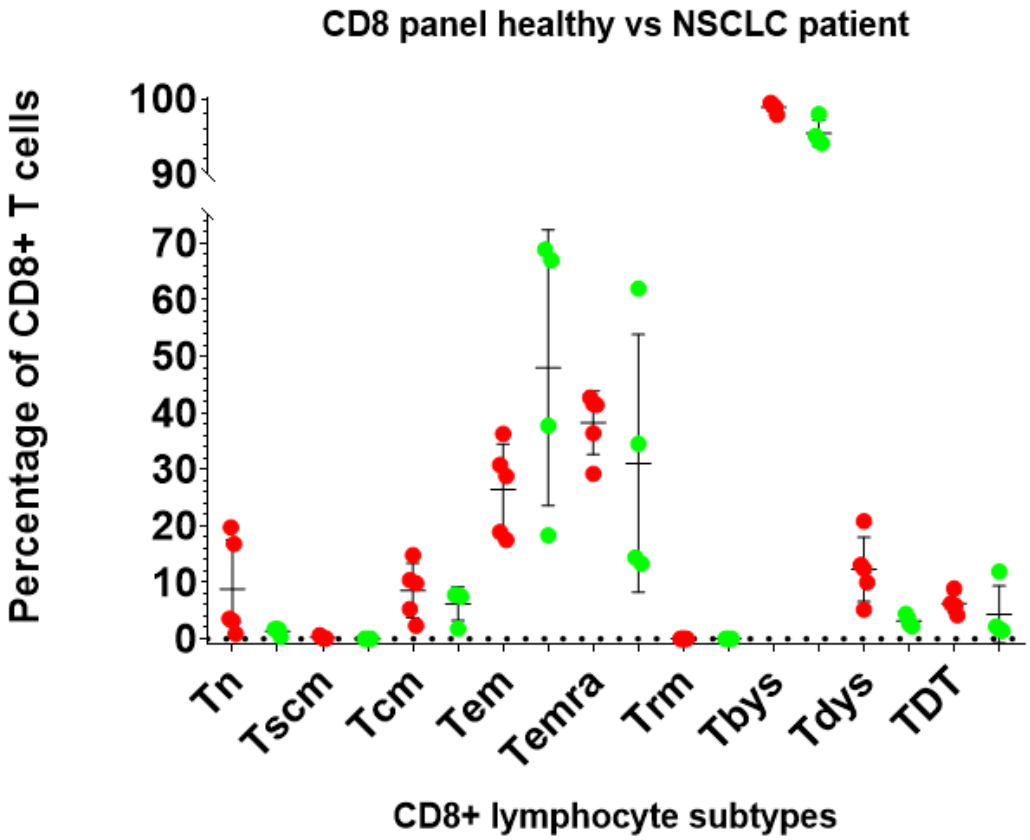

Figure 43. *CD8+ T lymphocyte subtypes in healthy donors (red) compared to NSCLC patients (green). The acquired data from analyzing the frozen samples from both healthy donors and NSCLC patients are plotted. It is shown that all the subtypes except for TEM , seem to have lower percentages of CD8+ T cells in NSCLC patients. However, the TEM and TEMRA subtypes seem to be higher in NSCLC patient samples compared to the healthy donors.*

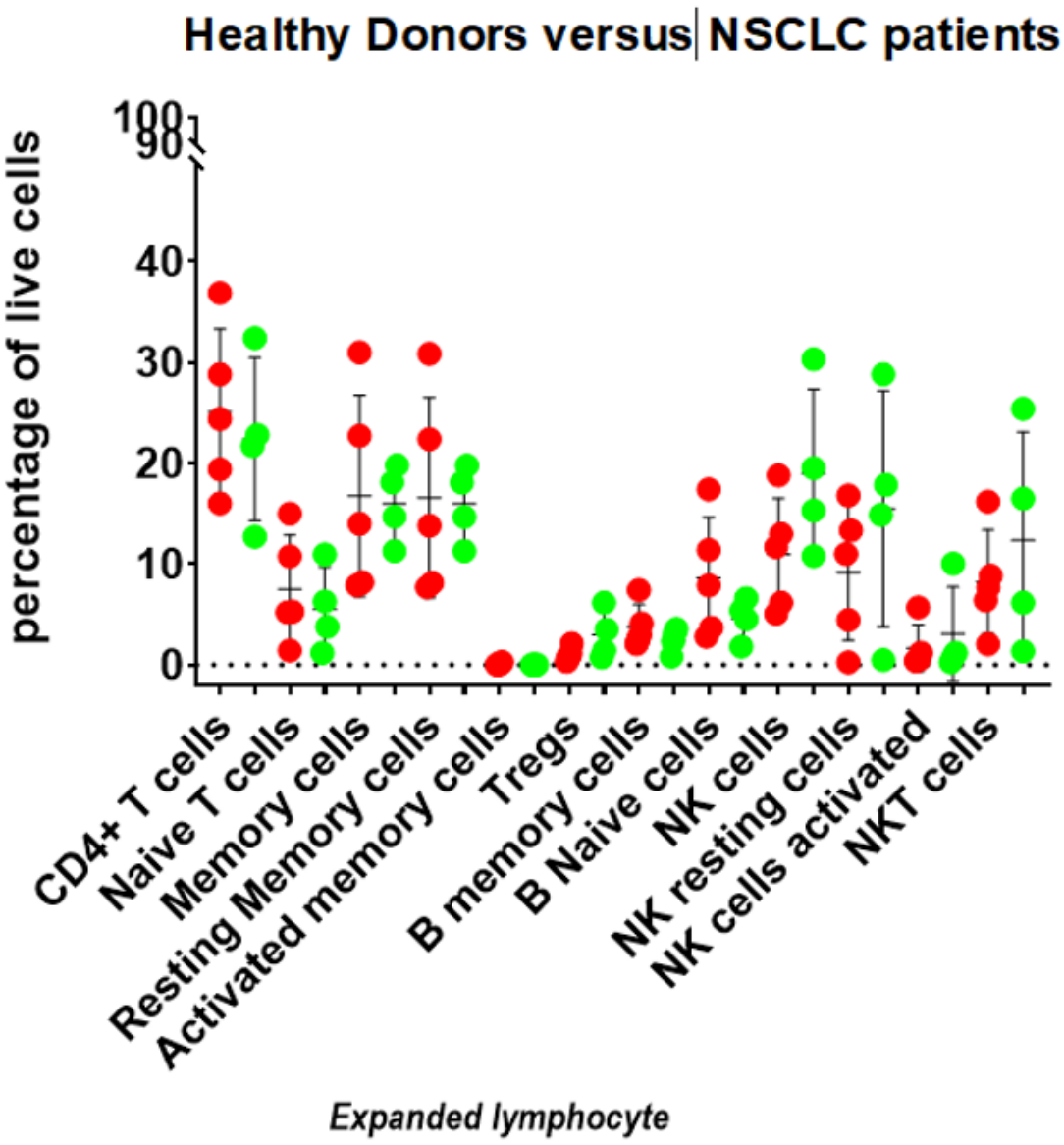

Figure 44. Expanded lymphocyte subtypes in healthy donors (red) compared to NSCLC patients (green). *The acquired data from analyzing the frozen samples from both frozen healthy and NSCLO patients were plotted. All the subtypes except for Tregs, NK cells and NKT cells seem to be lower in NSCLC patient samples. However, the Tregs, NK cells and NKT cells seem to be higher in NSCLC patients.*

5 Discussion

The aim of this thesis was to establish an advanced flow cytometry protocol to explore functional subtypes of lymphocytes in blood from resectable NSCLC patients. To do this, two panels were designed; each with markers for lymphocyte subtypes of interest, along with their matched fluorescently labelled antibodies. PBMCs from healthy donors served as test samples to establish the protocol, which was then validated on four NSCLC patient samples. Since the NSCLC patients' samples were cryopreserved, this study also explored the effects of cryopreservation on the various lymphocyte subtypes. Therefore, PBMCs from five healthy donors were isolated and divided into two batches. The first batch was stained and analyzed fresh. Meanwhile, the second batch was stained and analyzed after cryopreservation. In both cases, the two flow cytometry panels defined at the beginning of this study were used. The lymphocyte subtypes were gated based on the expression of the markers from the two panels. Subsequently, the results from the fresh samples were compared with the results from the frozen samples. The differences between the lymphocyte subtypes in the fresh and frozen samples were then examined using a paired sample t-test or a non-parametric Wilcoxon signed-rank test.

5.1 CD8+ T cell distribution in healthy donors

Characterizing the CD8+ T cell composition in PBMCs from healthy donors provided us with a baseline control for the PBMC samples from NSCLC patients. This protocol allowed us to divide CD8+ T cells into nine subtypes, identified by their surface expression of CD45RA, CCR7, CD57, PD-1, CD39, CD103 and CD95. It has previously been shown that neutrophils are the most abundant immune cells in NSCLC [58]. However, a more recent study showed that T cells are the most abundant immune cells in NSCLC tumors [38]. Our results showed that the proportions of each CD8+ T cell subtypes varied between healthy donors, but eight of the nine subtypess were found in all five healthy donors. The percentage of naïve CD8+ T cells in Donor 1 – Donor 5 ranged from 1.03% to 39% of the CD8+ T cells, which could be associated with the age of the donors. However, the donors in this study were anonymous, and therefore our statement cannot be confirmed. This speculation is supported by Koch et al. [56], who have documented that the CD8+ T cell subtypes distribution between healthy donors varied with age and specifically that the frequency of naïve CD8+ T cells decreased with age.

Similarly, there is possible age-associated increase in the percentage of CD8+ Temra cells, since the same donors who had a low CD8+ Tn population had an increased CD8+ Temra

population. This could suggest a correlation between the decrease of Tn cells and increase of Temra cells. The differences between the remaining subtypes seem to be attributed to inter-donor variations. Conversely, a consistency among the donors was the absence of CD8+ Trm. This result was expected, since these cells are long-lived memory T cells found exclusively in tissues, and do not circulate in blood like Tcm and Tem [59].

The results also identified the presence of Tdys and TDT CD8+ T cells in blood of healthy donors. As mentioned previously, dysfunctional T cells express PD-1, exhibit signs of proliferation defects, and lack inflammatory cytokine production [31]. T cells become exhausted or dysfunctional as a result of chronic stimulation of antigens [31]. Since the donors were otherwise believed to be healthy, and the samples were PBMCs from blood and not white blood cells from tumor tissue, the low percentage of CD8+ TDT and Tdys is expected.

5.2 Expanded lymphocyte distribution in healthy donors

The density of CD4+ T cells present in colorectal, renal, lung and breast cancer tissues had been shown to be related to prognosis [22], [60], [61]. Therefore, the expanded lymphocyte panel was also designed to characterize CD4+ T cells subtypes along with B cells, NK cells and NKT cells. As mentioned earlier, CD4+ T cells are important since they mediate cancer elimination through CD8+ T cells. Using the markers CD3, CD4, CD127, CD25, CD45RA, and CD69, the CD4+ T cells were sorted into naïve, memory, and regulatory T cells. The memory CD4+ T cells were then divided into resting and activated using the activation marker CD69. Our results showed that the subtypes in the expanded lymphocyte panel also had an inter-donor variation. Activated memory T cells, Tregs, B memory cells and activated NK cells constituted the lowest percentages of the live cells. The low number of Tregs present in the blood of these donors was not surprising, since studies state that Tregs are usually enriched in tumors, where their presence corresponds to poorer prognosis [27], [62]. NK cells are activated in response to infections and cancer [63], [64], and therefore this population is also not expected to be high in number, since these samples are from healthy donors.

5.3 Effects of cryopreservation

The ability to store isolated PBMCs and other cells is crucial when working with many samples or when there is a need to re-explore samples at a later point after isolation. This makes cryopreservation an indispensable procedure. Unfortunately, it is an aggressive procedure that may influence lymphocyte viability and their phenotype [65]. We therefore wanted to examine the effects of cryopreservation on the distribution of functional lymphocyte subtypes. This was

done by running the established protocol on freshly isolated PBMCs from healthy donors and then later on cryopreserved PBMCs from the same healthy donors. In this way, we could examine whether cryopreservation affected the viability of the PBMCs and the percentage of each subtype when compared to their fresh counterparts. The results showed that the quality and viability was affected, since the PBMCs viability decreased from almost 100% in fresh samples to values ranging between 50-80 % in the frozen samples. The percentages of the various lymphocyte subtypes were calculated and plotted in the graphs shown in Figures 25 and 32. The plots show that there were differences in the percentages of the lymphocyte subtypes in fresh vs frozen samples, and that and the statistical analysis showed that some of the differences were statistically significant while others were not. However, our sample size is too small to draw strong conclusions. The inter-donor variation is consistent with the results from a study by Li et al. [66], which showed that the proportion of all T cells was not affected by long term cryopreservation. However, the proportions of activated T cells, naïve T cells, central memory T cells, effector T cells and effector memory T cells were affected [67]. The study also showed that the duration of cryopreservation had an impact on CD8+ T cells [67]. The consequence of our results and the aforementioned studies is that when interpreting results from our future studies we need to be aware of the fact that our findings have a potential "cryobias".

5.4 CD8+ T cell distribution in NSCLC patients (pilot)

The nine distinct CD8+ T cell subtypes were identified in blood from NSCLC patients that were randomly selected for validating the protocol. The most abundant CD8+ T cell subtypes were Tem, Temra and Tbys. Comparison of the results from healthy donor samples with NSCLC patient samples showed that the naïve CD8+ T cell population was generally lower in the NSCLC patients. Similar to the results from the healthy donors, age seems to affect the number of naïve T cells in NSCLC patients [68]. The ages of the NSCLC patients included in this pilot ranged from 49 to 85 years old, with the youngest patient displaying the highest number of naïve CD8+ T cells. However, the naïve CD8+ T cell count could also have been affected by infections or diseases. A statistically significant trend in immune cell distribution between healthy donors and NSCLC patients was not determined. This is because the number of NSCLC patients included in this pilot is small and only done for methodological validation. However, the pilot does show that we can successfully gate the lymphocyte subtypes from panel 1 in NSCLC patient samples.

5.5 Expanded lymphocyte distribution in NSCLC patients (pilot)

We ran the expanded lymphocyte panel on the NSCLC patient samples and identified all the various subtypes of CD4+ T cells, B cells, NK cells and NKT cells. The most abundant subtype in NSCLC patients were CD4+ T cells, NK cells and NKT cells. The results show distribution of CD4+ T cell subtypes, B cells, NK cells and NKT cells similar to the healthy donor samples. However, a statistical significance of the differences between healthy donors and NSCLC patients could not be determined due to the small sample size. However, we did show that this protocol can be successfully used to analyze NSCLC patient samples using the panel 2.

6 Challenges and future direction

Several challenges were encountered while setting up the compensation for this study. Compensation was an integral part of establishing this advanced flow cytometry protocol. The first challenge with the compensation was determining the most appropriate component, i.e. whether to employ beads or cells. Cells were the primary candidates for compensation since they were already available, and it was thought that they reflect the staining of the donor sample population more accurately. In addition, cells were a cheaper alternative to beads. However, after conducting several pilot experiments with cells, it was discovered that the flow cytometer was not able to correctly distinguish overlapping colors. This was due to the lack of a bright enough signal for some of the surface markers and made compensation difficult using cells. A strong enough signal is crucial for compensation since the system must be able to distinguish between a true positive and a false positive signal. We attempted to resolve this by staining the cells at a higher antibody concentration but were unsuccessful. This was especially true for the markers of immune suppression i.e., PD-1, CD103 and CD39. These subtypes were not expected to be highly expressed in blood samples from healthy donors, therefore the samples were stimulated by Phytohemagglutinin P (PHA) [69]. PHA was expected to induce the proliferation of lymphocytes and thereby increase the number of cells expressing PD-1, CD103 and CD39. The compensation was then set up using the stimulated PBMCs, but the system was still unable to distinguish between positive and negative signals due to a low positive signal. Because of these setbacks, we therefore switched to beads. Beads are similar to cells and stain uniformly. However, the viability dye 7AAD cannot be used with beads. We therefore used beads for all the antibodies while cells were used for 7AAD. This presented a new challenge. Although we got strong enough signals from each antibody, there was a huge overlap between them and the viability dye. We tried to solve this by excluding 7AAD from the compensation setup but doing so prevented us from gating live cells from our sample analysis. We then changed the filter that detected 7AAD and by doing this we finally managed to setup a compensation. However, the spectral overlap values were still high. After several experiments, pilot runs and research it was discovered that unstained beads could be used instead of cells stained with 7-AAD, since we were only interested in live cells. Thus, we recommend that compensation for similar multiparameter protocols use beads instead of cells.

Multiple pilot experiments were conducted with samples from healthy donors to confirm the usability of this compensation setup. It was while gating the cell populations in FlowJo that a

new challenge presented itself spillover. One of the antibodies in panel 1 was a highly expressed surface marker conjugated to a bright fluorophore. To solve this issue, more pilots were run until we identified the antibody and then titrated it again. After identifying the optimal concentration for our panel, a new pilot was run, and the protocol confirmed.

As antibodies are expensive, we had ordered isotype control antibodies for compensation with beads. The use of isotype controls for compensation was later amended, as the antibodies used in the panels are tandem fluorochrome conjugates and require lot-specific compensation. Through several trail and errors, we have managed to continuously improve the study and learned first-hand the difficulty of setting up a complex flow cytometry study. Properly conducted, flow cytometry studies will from now on have my deepest respect and I will also be able to spot flaws in other studies more easily.

6.1 Future direction

Having established and validated this protocol, the future goal is to characterize presence and distribution of lymphocyte subtypes in blood and tumor tissue samples from NSCLC patients included in the TNM-I study. Then later on, use this data and explore the prognostic impact of the most interesting lymphocyte subtypes.

References

[1] M. He, J. Rosen, D. Mangiameli, and S. K. Libutti, 'Cancer development and progression', *Advances in experimental medicine and biology*, vol. 593, pp. 117–133, 2007, doi: 10.1007/978-0-387-39978-2_12.

[2] D. Hanahan, 'Hallmarks of Cancer: New Dimensions', *Cancer Discovery*, vol. 12, no. 1, pp. 31–46, Jan. 2022, doi: 10.1158/2159-8290.CD-21-1059.

[3] H. C. Pitot, 'The Molecular Biology of Carcinogenesis', 1993.

[4] H. Sung *et al.*, 'Global Cancer Statistics 2020: GLOBOCAN Estimates of Incidence and Mortality Worldwide for 36 Cancers in 185 Countries', *CA: A Cancer Journal for Clinicians*, vol. 71, no. 3, pp. 209–249, May 2021, doi: 10.3322/CAAC.21660.

[5] 'Cancer in Norway 2021'. https://www.kreftregisteret.no/Generelt/Rapporter/Cancer-in-Norway/cancer-in-norway-2021/ (accessed Jul. 23, 2022).

[6] 'Lungekreft'. https://www.kreftregisteret.no/Temasider/kreftformer/Lungekreft/ (accessed Aug. 04, 2022).

[7] R. L. Siegel, K. D. Miller, and A. Jemal, 'Cancer statistics, 2018', *CA: A Cancer Journal for Clinicians*, vol. 68, no. 1, pp. 7–30, Jan. 2018, doi: 10.3322/CAAC.21442.

[8] C. M. Rudin, E. Brambilla, C. Faivre-Finn, and J. Sage, 'Small-cell lung cancer', *Nature reviews. Disease primers*, vol. 7, no. 1, p. 3, Jan. 2021, doi: 10.1038/S41572-020-00235-0.

[9] S. S. Hecht, 'Progress and Challenges in Selected Areas of Tobacco Carcinogenesis', *Chemical research in toxicology*, vol. 21, no. 1, p. 160, Jan. 2008, doi: 10.1021/TX7002068.

[10] A. Risch and C. Plass, 'Lung cancer epigenetics and genetics', *International journal of cancer*, vol. 123, no. 1, pp. 1–7, Jul. 2008, doi: 10.1002/IJC.23605.

[11] U. Testa, G. Castelli, and E. Pelosi, 'Lung Cancers: Molecular Characterization, Clonal Heterogeneity and Evolution, and Cancer Stem Cells', *Cancers*, vol. 10, no. 8, Aug. 2018, doi: 10.3390/CANCERS10080248.

[12] W. D. Travis *et al.*, 'The 2015 World Health Organization Classification of Lung Tumors: Impact of Genetic, Clinical and Radiologic Advances Since the 2004 Classification', *Journal of Thoracic Oncology*, vol. 10, no. 9, pp. 1243–1260, Sep. 2015, doi: 10.1097/JTO.0000000000000630.

[13] 'Nasjonalt handlingsprogram med retningslinjer for diagnostikk, behandling og oppfølging av lungekreft, mesoteliom og thymom Nasjonal faglig retningslinje', Accessed: Jul. 08, 2022. [Online]. Available: www.helsedirektoratet.no

[14] A. G. Nicholson *et al.*, 'The 2021 WHO Classification of Lung Tumors: Impact of Advances Since 2015', *Journal of Thoracic Oncology*, vol. 17, no. 3, pp. 362–387, Mar. 2022, doi: 10.1016/J.JTHO.2021.11.003.

[15] X. Sha, G. Gong, Q. Qiu, J. Duan, D. Li, and Y. Yin, 'Identifying pathological subtypes of non-small-cell lung cancer by using the radiomic features of 18 F-fluorodeoxyglucose positron emission computed tomography', *Translational Cancer Research*, vol. 8, no. 5, pp. 1741–1749, 2019, doi: 10.21037/31738.

[16] Y. R. Zhao, X. Xie, H. J. De Koning, W. P. Mali, R. Vliegenthart, and M. Oudkerk, 'NELSON lung cancer screening study', *Cancer Imaging*, vol. 11, no. 1A, p. S79, 2011, doi: 10.1102/1470-7330.2011.9020.

[17] 'Lung cancer screenings to begin in Norway - Norwegian Cancer Society'. https://kreftforeningen.no/en/lung-cancer-screenings-to-begin-in-norway/ (accessed Jul. 23, 2022).

[18] P. Goldstraw *et al.*, 'The IASLC Lung Cancer Staging Project: Proposals for Revision of the TNM Stage Groupings in the Forthcoming (Eighth) Edition of the TNM Classification for Lung Cancer', *Journal of Thoracic Oncology*, vol. 11, no. 1, pp. 39–51, Jan. 2016, doi: 10.1016/J.JTHO.2015.09.009.

[19] E. E. Graves, A. Maity, and Q. T. Le, 'The Tumor Microenvironment in Non-Small Cell Lung Cancer', *Seminars in radiation oncology*, vol. 20, no. 3, p. 156, Jul. 2010, doi: 10.1016/J.SEMRADONC.2010.01.003.

[20] D. Hanahan and R. A. Weinberg, 'Hallmarks of Cancer: The Next Generation', *Cell*, vol. 144, no. 5, pp. 646–674, Mar. 2011, doi: 10.1016/J.CELL.2011.02.013.
[21] S. H. Kim *et al.*, 'Prognostic impact of CD8 and programmed death-ligand 1 expression in patients with resectable non-small cell lung cancer', *British Journal of Cancer 2019 120:5*, vol. 120, no. 5, pp. 547–554, Feb. 2019, doi: 10.1038/s41416-019-0398-5.
[22] T. Kuwahara *et al.*, 'Intratumoural-infiltrating CD4 + and FOXP3 + T cells as strong positive predictive markers for the prognosis of resectable colorectal cancer', *British Journal of Cancer*, vol. 121, no. 8, pp. 659–665, Oct. 2019, doi: 10.1038/S41416-019-0559-6.
[23] A. K. Abbas, A. H. Lichtman, and S. Pillai, 'Introduction to the immune system Nomenclature, General Properties and Components', in *Basic Immunology Functions and Disorders of the Immune system*, Sixth Edit., Elsevier Inc., 2020, pp. 1–72.
[24] R. M. Bremnes *et al.*, 'The Role of Tumor-Infiltrating Immune Cells and Chronic Inflammation at the Tumor Site on Cancer Development, Progression, and Prognosis: Emphasis on Non-small Cell Lung Cancer', *Journal of Thoracic Oncology*, vol. 6, no. 4, pp. 824–833, Apr. 2011, doi: 10.1097/JTO.0B013E3182037B76.
[25] S. M. Hald *et al.*, 'CD4/CD8 co-expression shows independent prognostic impact in resected non-small cell lung cancer patients treated with adjuvant radiotherapy', *Lung Cancer*, vol. 80, no. 2, pp. 209–215, May 2013, doi: 10.1016/J.LUNGCAN.2012.12.026.
[26] J. S. O'Donnell, M. W. L. Teng, and M. J. Smyth, 'Cancer immunoediting and resistance to T cell-based immunotherapy', *Nature Reviews Clinical Oncology 2018 16:3*, vol. 16, no. 3, pp. 151–167, Dec. 2018, doi: 10.1038/s41571-018-0142-8.
[27] S. Holmberg-Thyden, K. Grønbæk, A. O. Gang, D. El Fassi, and S. R. Hadrup, 'A user's guide to multicolor flow cytometry panels for comprehensive immune profiling', *Analytical biochemistry*, vol. 627, Aug. 2021, doi: 10.1016/J.AB.2021.114210.
[28] N. R. Maimela, S. Liu, and Y. Zhang, 'Fates of CD8+ T cells in Tumor Microenvironment', *Computational and Structural Biotechnology Journal*, vol. 17, pp. 1–13, Jan. 2019, doi: 10.1016/J.CSBJ.2018.11.004.
[29] X. Zheng, Y. Hu, and C. Yao, 'The paradoxical role of tumor-infiltrating immune cells in lung cancer', *Intractable & Rare Diseases Research*, vol. 6, no. 4, p. 234, 2017, doi: 10.5582/IRDR.2017.01059.
[30] K. E. De Visser, A. Eichten, and L. M. Coussens, 'Paradoxical roles of the immune system during cancer development', *Nature Reviews Cancer 2006 6:1*, vol. 6, no. 1, pp. 24–37, Jan. 2006, doi: 10.1038/nrc1782.
[31] L. Apetoh *et al.*, 'Consensus nomenclature for CD8 + T cell phenotypes in cancer', *Oncoimmunology*, vol. 4, no. 4, 2015, doi: 10.1080/2162402X.2014.998538.
[32] A. M. van der Leun, D. S. Thommen, and T. N. Schumacher, 'CD8+ T cell states in human cancer: insights from single-cell analysis', *Nature Reviews Cancer 2020 20:4*, vol. 20, no. 4, pp. 218–232, Feb. 2020, doi: 10.1038/s41568-019-0235-4.
[33] D. Bruni, H. K. Angell, and J. Galon, 'The immune contexture and Immunoscore in cancer prognosis and therapeutic efficacy', *Nature Reviews Cancer 2020 20:11*, vol. 20, no. 11, pp. 662–680, Aug. 2020, doi: 10.1038/s41568-020-0285-7.
[34] J. Galon *et al.*, 'Towards the introduction of the "Immunoscore" in the classification of malignant tumours', *The Journal of pathology*, vol. 232, no. 2, pp. 199–209, Jan. 2014, doi: 10.1002/PATH.4287.
[35] R. Remark *et al.*, 'Characteristics and clinical impacts of the immune environments in colorectal and renal cell carcinoma lung metastases: influence of tumor origin', *Clinical cancer research : an official journal of the American Association for Cancer Research*, vol. 19, no. 15, pp. 4079–4091, Aug. 2013, doi: 10.1158/1078-0432.CCR-12-3847.
[36] H. Jian *et al.*, 'Th1 high in tumor microenvironment is an indicator of poor prognosis for patients with NSCLC', *Oncotarget*, vol. 8, no. 8, pp. 13116–13125, Jan. 2017, doi: 10.18632/ONCOTARGET.14471.
[37] J. L. Reading, F. Gálvez-Cancino, C. Swanton, A. Lladser, K. S. Peggs, and S. A. Quezada, 'The function and dysfunction of memory CD8+ T cells in tumor immunity', *Immunological*

Reviews, vol. 283, no. 1, pp. 194–212, May 2018, doi: 10.1111/IMR.12657.
[38] B. Stankovic *et al.*, 'Immune Cell Composition in Human Non-small Cell Lung Cancer', *Frontiers in immunology*, vol. 9, p. 3101, 2018, doi: 10.3389/FIMMU.2018.03101/BIBTEX.
[39] A. M. van der Leun, D. S. Thommen, and T. N. Schumacher, 'CD8+ T cell states in human cancer: insights from single-cell analysis', *Nature Reviews Cancer 2020 20:4*, vol. 20, no. 4, pp. 218–232, Feb. 2020, doi: 10.1038/s41568-019-0235-4.
[40] P. K. Gupta *et al.*, 'CD39 Expression Identifies Terminally Exhausted CD8+ T Cells', *PLoS Pathogens*, vol. 11, no. 10, 2015, doi: 10.1371/JOURNAL.PPAT.1005177.
[41] F. P. Canale *et al.*, 'CD39 expression defines cell exhaustion in tumor-infiltrating CD8+ T cells', *Cancer Research*, vol. 78, no. 1, pp. 115–128, Jan. 2018, doi: 10.1158/0008-5472.CAN-16-2684/657753/AM/CD39-EXPRESSION-DEFINES-CELL-EXHAUSTION-IN-TUMOR.
[42] Y. Simoni *et al.*, 'Bystander CD8 + T cells are abundant and phenotypically distinct in human tumour infiltrates', *Nature*, vol. 557, no. 7706, pp. 575–579, May 2018, doi: 10.1038/S41586-018-0130-2.
[43] E. Ghorani *et al.*, 'The T cell differentiation landscape is shaped by tumour mutations in lung cancer', *Nature cancer*, vol. 1, no. 5, p. 546, May 2020, doi: 10.1038/S43018-020-0066-Y.
[44] G. J. Yuen, E. Demissie, and S. Pillai, 'B lymphocytes and cancer: a love-hate relationship', *Trends in cancer*, vol. 2, no. 12, p. 747, Dec. 2016, doi: 10.1016/J.TRECAN.2016.10.010.
[45] A. Adan, G. Alizada, Y. Kiraz, Y. Baran, and A. Nalbant, 'Flow cytometry: basic principles and applications', *https://doi.org/10.3109/07388551.2015.1128876*, vol. 37, no. 2, pp. 163–176, Feb. 2016, doi: 10.3109/07388551.2015.1128876.
[46] S. M. Manohar, P. Shah, and A. Nair, 'Flow cytometry: principles, applications and recent advances', *https://doi.org/10.4155/bio-2020-0267*, vol. 13, no. 3, pp. 185–202, Feb. 2021, doi: 10.4155/BIO-2020-0267.
[47] Z. Maciorowski, P. K. Chattopadhyay, and P. Jain, 'Basic Multicolor Flow Cytometry', *Current protocols in immunology*, vol. 117, pp. 5.4.1-5.4.38, Apr. 2017, doi: 10.1002/CPIM.26.
[48] S. Technologies Inc, 'BR27104_LYMPHOPREP ™ Density Gradient Medium', 2018.
[49] C. Riedhammer, D. Halbritter, and R. Weissert, 'Peripheral blood mononuclear cells: Isolation, freezing, thawing, and culture', *Methods in Molecular Biology*, vol. 1304, pp. 53–61, 2015, doi: 10.1007/7651_2014_99/FIGURES/2.
[50] W. Strober, 'Trypan Blue Exclusion Test of Cell Viability', *Current Protocols in Immunology*, vol. 21, no. 1, p. A.3B.1-A.3B.2, Mar. 1997, doi: 10.1002/0471142735.IMA03BS21.
[51] A. Adan, G. Alizada, Y. Kiraz, Y. Baran, and A. Nalbant, 'Flow cytometry: basic principles and applications', *Critical Reviews in Biotechnology*, vol. 37, no. 2, pp. 163–176, 2017, doi: 10.3109/07388551.2015.1128876.
[52] Becton, 'For Research Use Only BD LSRFortessa™ X-20 Cell Analyzer User's Guide', 2020.
[53] D. Sheerar, 'FlowJo for Antibody Titrations: Separation Index and Concatenation', Accessed: Jul. 23, 2022. [Online]. Available: http://www.uwhealth.org/flowlab
[54] M. Roederer, 'Spectral Compensation for Flow Cytometry: Visualization Artifacts, Limitations, and Caveats', 2001, doi: 10.1002/1097-0320.
[55] L. Jachimowicz, M. Lei, P. Ye, Y. Lu, and G. Guenther, 'Comprehensive Analysis of T Cell Status Following Activation Using a 16-Color Immunophenotyping Panel'.
[56] S. Koch, A. Larbi, E. Derhovanessian, D. Özcelik, E. Naumova, and G. Pawelec, 'Multiparameter flow cytometric analysis of CD4 and CD8 T cell subsets in young and old people', *Immunity & Ageing : I & A*, vol. 5, p. 6, Jul. 2008, doi: 10.1186/1742-4933-5-6.
[57] 'Paired Sample T-Test - Statistics Solutions'. https://www.statisticssolutions.com/free-resources/directory-of-statistical-analyses/paired-sample-t-test/ (accessed Aug. 13, 2022).
[58] J. Kargl *et al.*, 'Neutrophils dominate the immune cell composition in non-small cell lung cancer', *Nature Communications 2017 8:1*, vol. 8, no. 1, pp. 1–11, Feb. 2017, doi: 10.1038/ncomms14381.

[59] J. M. Schenkel and D. Masopust, 'Tissue-Resident Memory T Cells', *Immunity*, vol. 41, no. 6, p. 886, Dec. 2014, doi: 10.1016/J.IMMUNI.2014.12.007.
[60] R. Droeser *et al.*, 'Differential pattern and prognostic significance of CD4+, FOXP3+ and IL-17+ tumor infiltrating lymphocytes in ductal and lobular breast cancers', *BMC cancer*, vol. 12, Apr. 2012, doi: 10.1186/1471-2407-12-134.
[61] P. A. McArdle, K. Canna, D. C. McMillan, A. H. McNicol, R. Campbell, and M. A. Underwood, 'The relationship between T-lymphocyte subset infiltration and survival in patients with prostate cancer', *British journal of cancer*, vol. 91, no. 3, pp. 541–543, Aug. 2004, doi: 10.1038/SJ.BJC.6601943.
[62] B. J. Chen, J. W. Zhao, D. H. Zhang, A. H. Zheng, and G. Q. Wu, 'Immunotherapy of Cancer by Targeting Regulatory T cells', *International Immunopharmacology*, vol. 104, p. 108469, Mar. 2022, doi: 10.1016/J.INTIMP.2021.108469.
[63] B. Farhood, M. Najafi, and K. Mortezaee, 'CD8+ cytotoxic T lymphocytes in cancer immunotherapy: A review', *Journal of Cellular Physiology*, vol. 234, no. 6, pp. 8509–8521, Jun. 2019, doi: 10.1002/JCP.27782.
[64] S. Nair and M. V. Dhodapkar, 'Natural killer T cells in cancer immunotherapy', *Frontiers in Immunology*, vol. 8, no. SEP, p. 1178, Sep. 2017, doi: 10.3389/FIMMU.2017.01178/BIBTEX.
[65] O. Ticha, L. Moos, and I. Bekeredjian-Ding, 'Effects of long-term cryopreservation of PBMC on recovery of B cell subpopulations', *Journal of immunological methods*, vol. 495, Aug. 2021, doi: 10.1016/J.JIM.2021.113081.
[66] S. R. Panch *et al.*, 'Effect of Cryopreservation on Autologous Chimeric Antigen Receptor T Cell Characteristics', *Molecular therapy : the journal of the American Society of Gene Therapy*, vol. 27, no. 7, pp. 1275–1285, Jul. 2019, doi: 10.1016/J.YMTHE.2019.05.015.
[67] B. Li *et al.*, 'Comprehensive evaluation of the effects of long-term cryopreservation on peripheral blood mononuclear cells using flow cytometry', *BMC Immunology 2022 23:1*, vol. 23, no. 1, pp. 1–14, Jun. 2022, doi: 10.1186/S12865-022-00505-4.
[68] M. Li *et al.*, 'Age related human T cell subset evolution and senescence', *Immunity and Ageing*, vol. 16, no. 1, pp. 1–7, Sep. 2019, doi: 10.1186/S12979-019-0165-8/TABLES/1.
[69] D. E. Campbell *et al.*, 'Cryopreservation decreases receptor PD-1 and ligand PD-L1 coinhibitory expression on peripheral blood mononuclear cell-derived T cells and monocytes', *Clinical and Vaccine Immunology*, vol. 16, no. 11, pp. 1648–1653, Nov. 2009, doi: 10.1128/CVI.00259-09.

Appendix I

Table 1A Reagents

Name	Catalog number	Lot number	Supplier	Origin
Dimethyl Sulfoxide (DMSO)	D4540	BCCD1104	Sigma-Aldrich	USA
Lymphoprep™	-	00418	Serumwerk Bernburg	Norway
Roswell Park Memorial Institute (RPMI)	R8758	RNBK4917	Sigma-Aldrich	UK
Fetal Bovine Serum (FBS)	S0115	-	Biochrom	Germany
Penicillin-Streptomycin	15140122	-	Thermo Fisher	USA
MACS BSA Stock Solution	130-091-376	5180820196	Miltenyi Biotec	Germany
autoMACS™ Rinsing Solution	130-091-222	7210400057	Miltenyi Biotec	Germany
Red Blood Cell Lysis Buffer	11814389001	48356700	Roche	Germany
Phytohemagglutinin-L (PHA-L) Solution (500x)	00-4977-93	2115359	Invitrogen	USA
Trypan Blue (0.4%)	T8154	RNBJ2266	Sigma-Aldrich	UK
Dulbecco's Phosphate Buffer Saline (DPBS)	D8537	RNBK4896	Sigma-Aldrich	UK

Table A2 Antibodies Panel 1 Cd8+ subtypes

Specificity	Clone	Fluorophore	Vendor	Catalog number
CD3	REA613	VioBright R720	Miltenyi Biotec	130-127-377
CD8	REA734	APC-Vio770	Miltenyi Biotec	130-110-681
CD45Ra	REA562	VioGreen	Miltenyi Biotec	130-113-369
CCR7	REA546	PerCP-Vio700	Miltenyi Biotec	130-120-469
CD57	REA769	APC	Miltenyi Biotec	130-111-811
CD279 (PD-1)	REA1165	VioBright B515	Miltenyi Biotec	130-120-386
CD39	REA739	VioBright V423	Miltenyi Biotec	130-127-194
CD103	REA803	PE-Vio770	Miltenyi Biotec	130-111-834
CD95	REA738	PE	Miltenyi Biotec	130-113-004
Viability	7-AAD Staining Solution	7-AAD	Miltenyi Biotec	130-111-568

Table A3 Antibodies Panel 2: Expanded lymphocytes

Specificity	Clone	Fluorophore	Vendor	Catalog number
CD3	REA613	VioBright R720	Miltenyi Biotec	130-127-377
CD19	REA675	APC-Vio770	Miltenyi Biotec	130-113-643
CD127	REA614	APC	Miltenyi Biotec	130-113-413
CD25	REA945	VioBright V423	Miltenyi Biotec	130-126-613
CD56	REA196	VioBright B515	Miltenyi Biotec	130-114-552
CD45RA	REA562	VioGreen	Miltenyi Biotec	130-113-369
CD27	REA499	PerCP-Vio700	Miltenyi Biotec	130-120-037
CD4	REA623	PE-Vio770	Miltenyi Biotec	130-113-227
CD69	FN50	PE	Miltenyi Biotec	130-113-524

Appendix II

Table A4. Data used to plot graph (Figure 25). CD8+ T lymphocyte phenotypes in Donors 1 – Donors 5. The acquired data from analyzing the fresh and frozen samples from Donors 1 to Donors 5 are plotted. The numbers are based on the subtypess/CD8 T cell ratio.

	Fresh										Frozen									
Donors	Tn	Tscm	Tcm	Tem	Temra	Trm	Tbys	Tdys	TDT	Tn	Tscm	Tcm	Tem	Temra	Trm	Tbys	Tdys	TDT	Tn	Tscm	Tcm
1	22,30 %	0,50 %	13,80 %	18,00 %	34,20 %	0,00 %	97,30 %	8,25 %	7,13 %	16,80 %	0,34 %	10,40 %	17,50 %	41,60 %	0,00 %	98,90 %	12,40 %	5,89 %	22,30 %	0,50 %	13,80 %	18,00 %	34,20 %	0,00 %
2	1,03 %	0,16 %	4,14 %	43,50 %	36,40 %	0,00 %	99,20 %	3,73 %	11,30 %	0,88 %	0,05 %	2,34 %	36,30 %	42,70 %	0,00 %	99,50 %	5,17 %	8,92 %	1,03 %	0,16 %	4,14 %	43,50 %	36,40 %	0,00 %
3	6,55 %	0,60 %	26,90 %	26,90 %	25,20 %	0,00 %	96,80 %	10,60 %	3,99 %	3,54 %	0,14 %	14,80 %	28,80 %	36,40 %	0,00 %	97,90 %	13,10 %	6,29 %	6,55 %	0,60 %	26,90 %	26,90 %	25,20 %	0,00 %
4	39,00 %	1,10 %	6,82 %	21,40 %	17,30 %	0,00 %	94,90 %	13,00 %	7,58 %	19,70 %	0,65 %	9,84 %	18,90 %	29,20 %	0,00 %	99,30 %	10,00 %	5,94 %	39,00 %	1,10 %	6,82 %	21,40 %	17,30 %	0,00 %
5	7,13 %	0,20 %	7,00 %	38,10 %	26,40 %	0,00 %	96,70 %	14,10 %	9,11 %	3,18 %	0,08 %	5,27 %	30,80 %	41,40 %	0,00 %	99,00 %	20,80 %	4,19 %	7,13 %	0,20 %	7,00 %	38,10 %	26,40 %	0,00 %

Table A5. Data used to plot graph (Figure 32). Expanded lymphocytes subtypes healthy in Donors 1 – Donors 5. The acquired data from analyzing the fresh and frozen samples from Donors 1 to Donors 5 are plotted based on these numbers The numbers are based on the subtypess/live cells ratio.

	Fresh											Frozen									
Donors	CD4+ T	Naive T	Memory	Resting	Activated	Tregs	B	B Naive	NK cells	NK	NK cells	NKT cells	CD4+ T	Naive T	Memory	Resting	Activated	Tregs	B	B Naive	NK cells	NK	NK cells	NKT cells
1	38,00 %	22,00 %	15,00 %	14,00 %	1,00 %	2,00 %	1,00 %	11,00 %	5,00 %	5,00 %	0,00 %	8,00 %	24,40 %	15,00 %	7,90 %	7,70 %	0,13 %	1,36 %	2,98 %	17,40 %	6,17 %	0,26 %	5,69 %	8,85 %
2	27,00 %	2,00 %	24,00 %	23,00 %	1,00 %	4,00 %	1,00 %	2,00 %	10,00 %	9,00 %	1,00 %	17,00 %	16,00 %	1,42 %	14,00 %	13,80 %	0,04 %	2,85 %	2,47 %	2,81 %	11,70 %	11,00 %	0,52 %	16,20 %
3	46,00 %	10,00 %	16,00 %	16,00 %	1,00 %	5,00 %	2,00 %	9,00 %	4,00 %	3,00 %	0,00 %	2,00 %	28,80 %	5,27 %	22,70 %	22,38 %	0,31 %	5,44 %	4,10 %	11,40 %	5,06 %	4,46 %	0,53 %	2,05 %
4	37,00 %	22,00 %	14,00 %	14,00 %	1,00 %	2,00 %	2,00 %	6,00 %	16,00 %	16,00 %	1,00 %	9,00 %	19,40 %	10,77 %	8,17 %	8,13 %	0,03 %	1,56 %	7,43 %	7,90 %	18,80 %	16,80 %	1,19 %	6,39 %
5	45,00 %	7,00 %	37,00 %	37,00 %	0,00 %	2,00 %	2,00 %	3,00 %	14,00 %	13,00 %	1,00 %	9,00 %	36,90 %	5,20 %	30,99 %	30,84 %	0,14 %	2,47 %	2,07 %	3,68 %	13,00 %	13,33 %	0,39 %	7,68 %

Appendix III

Table A6. Data used to plot graph (Figure 37). CD8+ subtypes in NSCLC patients (30,40,58 and 95).

P.	Tn	Tscm	Tcm	Tem	Temra	Trm	Tbys	Tdys	TDT
30	1,66 %	0,00 %	7,80 %	18,30 %	62,00 %	0,00 %	94,50 %	2,48 %	1,74 %
40	0,37 %	0,00 %	1,77 %	68,90 %	13,30 %	0,00 %	95,10 %	2,22 %	2,18 %
58	1,69 %	0,00 %	7,72 %	37,70 %	34,50 %	0,00 %	94,10 %	3,36 %	1,45 %
95	1,70 %	0,00 %	7,50 %	67,00 %	14,40 %	0,00 %	98,00 %	4,44 %	11,90 %

Table A7. Data used to plot graph (Figure 42). Expanded lymphocyte subtypes in NSCLC patients (30,40,58 and 95).

P.	CD4+ T cells	Naive T cells	Memory cells	Resting Memory cells	Activated memory cells	Tregs	B memory cells	B Naive cells	NK cells	NK resting cells	NK cells activated	NKT cells
30	0,23	0,04	0,18	0,18	0,00	0,01	0,03	0,05	0,15	0,15	0,00	0,25
40	0,22	0,06	0,15	0,15	0,00	0,06	0,01	0,05	0,11	0,00	0,10	0,17
58	0,32	0,11	0,20	0,20	0,00	0,03	0,02	0,02	0,20	0,18	0,01	0,06
95	0,13	0,01	0,11	0,11	0,00	0,01	0,04	0,07	0,30	0,29	0,01	0,01